3

PNL-2850 Pt 4

UC-48

Pacific Northwest Laboratory Annual Report for 1978 to the DOE Assistant Secretary for Environment

Part 4 Physical Sciences February 1979

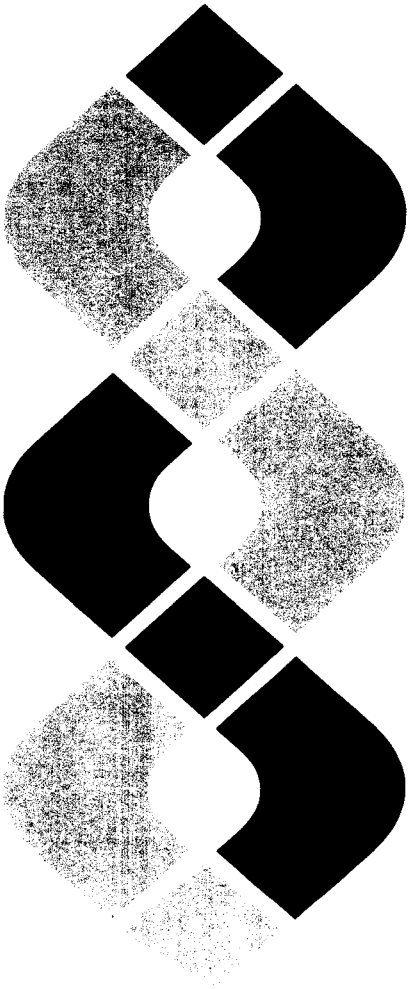

Prepared for the U.S. Department of Energy
under Contract EY-76-C-06-1830

Pacific Northwest Laboratory
Operated for the U.S. Department of Energy
by Battelle Memorial Institute

Battelle

PNL-2850

NOTICE

PACIFIC NORTHWEST LABORATORY
operated by
BATTELLE
for the
UNITED STATES DEPARTMENT OF ENERGY
Under Contract EY-76-C-06-1830

Printed in the United States of America
Available from
National Technical Information Service
United States Department of Commerce
5285 Port Royal Road
Springfield, Virginia 22151

Price: Printed Copy $____*; Microfiche $3.00

*Pages	NTIS Selling Price
001-025	$4.00
026-050	$4.50
051-075	$5.25
076-100	$6.00
101-125	$6.50
126-150	$7.25
151-175	$8.00
176-200	$9.00
201-225	$9.25
226-250	$9.50
251-275	$10.75
276-300	$11.00

PNL-2850 PT4
UC-48

Pacific Northwest Laboratory Annual Report for 1978 to the DOE Assistant Secretary for Environment

Part 4 Physical Sciences

J. M. Nielsen and Staff Members
of Pacific Northwest Laboratory

February 1979

Prepared for
the U.S. Department of Energy
under Contract EY-76-C-06-1830

Pacific Northwest Laboratory
Richland, Washington 99352

PREFACE

The 1978 Annual Report from Pacific Northwest Laboratory (PNL) to the DOE Assistant Secretary for Environment is the first report covering a full year's work under the Department of Energy since it came into existence on October 1, 1977. Most of the research conducted during this period and described in this report was begun under the Energy Research and Development Administration or its predecessor agency, the Atomic Energy Commission. However, several new projects have enhanced the PNL emphasis on environment, health and safety research in the area of synthetic fuels. Preliminary reports on these efforts are spread throughout the five parts of this annual report.

The five parts of the report are oriented to particular segments of our program. Parts 1-4 report on research performed for the DOE Office of Health and Environmental Research. Part 5 reports progress on all other research performed for the Assistant Secretary for Environment including the Office of Technology Impacts and the Office of Environmental Compliance and Overview.

Each part consists of project reports authored by scientists from several PNL research departments, reflecting the interdisciplinary nature of the research effort. Parts 1-4 are organized primarily by energy technology, although it is recognized that much of the research performed at PNL is applicable to more than one energy technology.

The parts of the 1978 Annual Report are:

Part 1: Biomedical Sciences		
	Program Manager - W. R. Wiley	D. L. Felton, Editor
Part 2: Ecological Sciences		
	Program Manager - B. E. Vaughan	B. E. Vaughan, Report Coordinator
		C. H. Connally, Editor
Part 3: Atmospheric Sciences		
	Program Manager - C. L. Simpson	R. L. Drake, Report Coordinator
		P. R. Partch/C. M. Gilchrist, Editors
Part 4: Physical Sciences		
	Program Manager - J. M. Nielsen	J. M. Nielsen, Report Coordinator
		J. S. Burlison, Editor

Part 5: Environmental Assessment, Control,
Health and Safety.

Program Managers - N. E. Carter
D. B. Cearlock
D. L. Hessel
S. Marks — W. J. Bair, Report Coordinator
C. M. Unruh — R. W. Baalman, Editor

Activities of the scientists whose work is described in this annual report are broader in scope than the articles indicate. PNL staff have responded to numerous requests from DOE during the year for planning, for service on various task groups, and for special assistance.

Credit for this annual report goes to many scientists who performed the research and wrote the individual project reports, to the program managers who directed the research and coordinated the technical progress reports, to the editors who edited the individual project reports and assembled the five parts, and to Dr. Ray Baalman, editor in chief, who directed the total effort.

W. J. Bair, Manager
S. Marks, Associate Manager
Environment, Health and Safety Research Program

Previous Reports in this Series:

Annual Report for	
1951	W-25021, HW-25709
1952	HW-27814, HW-28636
1953	HW-30437, HW-30464
1954	HW-30306, HW-33128, HW-35905, HW-35917
1955	HW-39558, HW-41315, HW-41500
1956	HW-47500
1957	HW-53500
1958	HW-59500
1959	HW-63824, HW-65500
1960	HW-69500, HW-70050
1961	HW-72500, HW-73337
1962	HW-76000, HW-77609
1963	HW-80500, HW-81746
1964	BNWL-122
1965	BNWL-280, BNWL-235, Vol. 1-4, BNWL-36I
1966	BNWL-480, Vol. 1, BNWL-481, Vol. 2, Pt 1-4
1967	BNWL-714, Vol. 1, BNWL-715, Vol. 2, Pt 1-4
1968	BNWL-1050, Vol. 1, Pt. 1-2, BNWL-1051, Vol. 2, Pt. 1-3
1969	BNWL-1306, Vol. 1, Pt. 1-2, BNWL-1307, Vol. 2, Pt. 1-3
1970	BNWL-1550, Vol. 1, Pt. 1-2, BNWL-1551, Vol. 2, Pt. 1-2
1971	BNWL-1650, Vol. 1, Pt. 1-2, BNWL-1651, Vol. 2, Pt. 1-2
1972	BNWL-1750, Vol. 1, Pt. 1-2, BNWL-1751, Vol. 2, Pt. 1-2
1973	BNWL-1850, Pt. 1-4
1974	BNWL-1950, Pt. 1-4
1975	BNWL-2000, Pt. 1-4
1976	BNWL-2100, Pt. 1-5
1977	PNL-2500, Pt. 1-5

FOREWORD

Part 4 of the Pacific Northwest Laboratory Annual Report for 1978 to the Assistant Secretary for Environment, DOE, includes those programs funded under the title "Physical and Technological Programs." The 189 program studies reports are grouped under the most directly applicable energy technology heading. Each energy technology section is introduced by a divider page which indicates the 189s reported in that section. These reports only briefly indicate progress made during 1978, so for details the reader should contact the principal investigators named or examine the publications cited.

CONTENTS

1.0 Coal

• Reaction Kinetics of Combustion Products

The goal of the Reaction Kinetics of Combustion Products program is to determine the conditions, mechanism, and chemical reactions that control the identity and concentrations of emissions from coal combustion processes. The first two years of this program have emphasized the characterization of fly ash and the development of a model for its formation. The model successfully rationalizes the large enrichments observed for many trace elements in fly ash emitted from coal-fired steam plants. Mass spectrometric techniques have been developed for the study of the high temperature kinetics relevant to coal combustion, with specific emphasis on techniques which will allow investigation of the mechanism and rates of formation for toxic and carcinogenic organic compounds.

Formation of Fly Ash During Coal Combustion

R. D. Smith and J. A. Campbell

It has been established that the smaller fly-ash particles formed during coal combustion show significant enrichments of several volatile trace elements. The accepted mechanism for trace element enrichment during fly-ash formation involves the volatilization of these elements during combustion, followed by condensation or adsorption over the available matrix material, which is composed primarily of the nonvolatile oxides of Al, Mg, and Si. The larger surface-to-volume ratio of the smaller particle should then lead to a trace element concentration inversely related to the particle diameter (Campbell, Smith, and Davis 1978). In our work, we found that fly-ash surfaces were enriched in several trace elements, which supports this mechanism for the larger particles.

The particles in the 0.1 to 1.0 μm size range, which are most important from an environmental viewpoint, have received little study because of extreme experimental complications. The smaller particles, which show the highest concentrations of several potentially toxic trace metals, are not efficiently collected by pollution control devices. These particles have the highest atmospheric mobilities and are deposited preferentially in the pulmonary and bronchial regions of the respiratory system.

During the past year, the emphasis of this program has centered upon characterizing the submicron particles and obtaining a better understanding of their formation mechanism. In addition, nearly complete elemental analyses (66 elements) have been obtained by x-ray fluorescence and instrumental neutron activation for several size fractions in the 0.1 to 1.0 μm size range; the submicron particles have also been subjected to analysis by surface techniques: (Campbell et al. 1978) photoelectron spectroscopy, Auger spectroscopy, and electron microprobe techniques. These studies have revealed a wealth of new information concerning the composition and formation of submicron particles during coal combustion.

One of the most significant findings has been that the concentration of a given trace element does not continue to increase throughout the submicron size range, as predicted by all previous models (Davison et al. 1974). Instead, the concentration becomes nearly independent of particle size in the submicron size range, as shown by the results in Figure 1.1 for six elements.

We were able to determine the most likely mechanism for formation of the submicron particles by using the following combination of techniques:

- elemental analyses as a function of particle size
- electron mapping studies of the heterogeneity of the submicron particles
- surface/depth profiling using photoelectron spectroscopy and a sputtering technique.

This mechanism postulates the "bursting" of larger molten particles during heating and rapid gas (CO_2, SO_2, and H_2O) release. The large numbers of very small liquid particles formed in this manner then coagulate and form

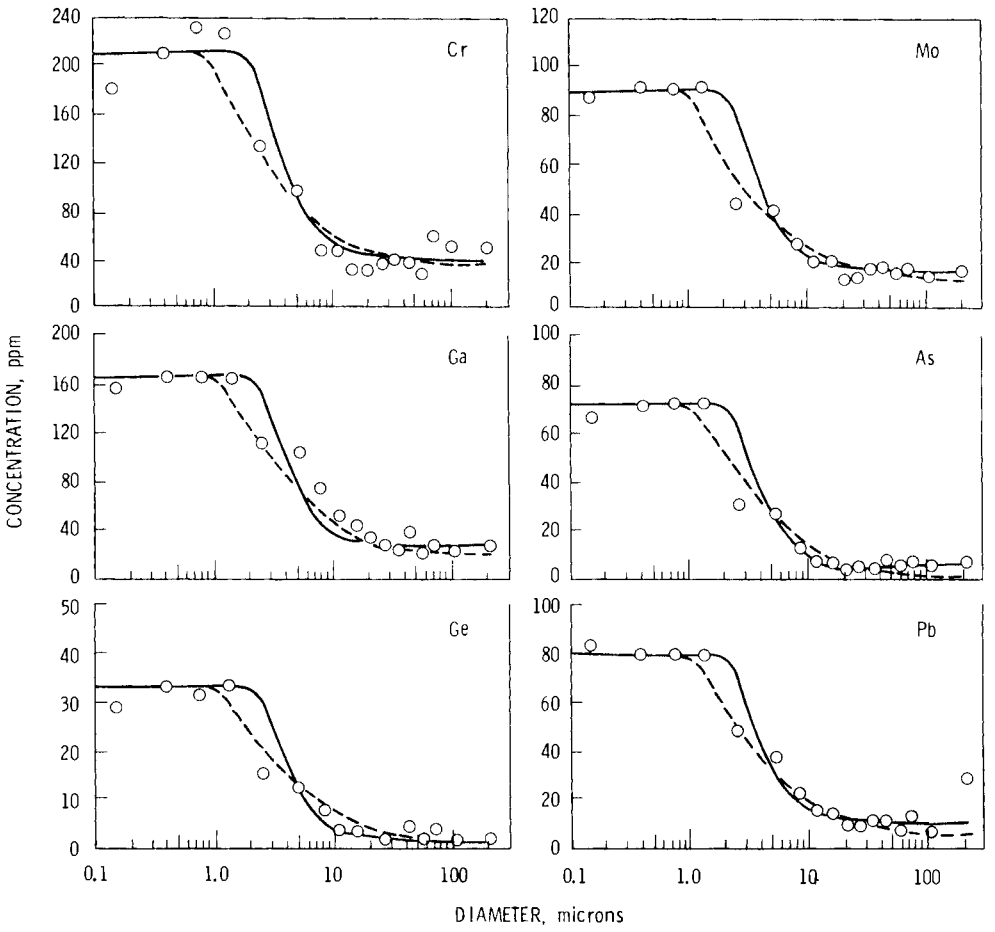

FIGURE 1.1. Concentration Dependence Upon Particle Size for Six Elements in Finely-Sized Fly Ash. Each of these elements is apparently volatilized to a considerable extent during coal combustion. The solid and dashed lines represent the best fits to two simple models developed in this work.

particles in the 0.1 to 1.0 μm size range. The concentrations of volatilized trace elements in these particles are expected to be independent of particle size in the submicron size range, consistent with results presented in Figure 1.1.

If this mechanism is correct, the implications for the control of particulate emissions from coal-fired plants will be far-reaching. For example, it may be possible to greatly reduce the quantity of submicron particles formed by limiting the maximum combustion temperatures or decreasing residence time in the high temperature region. Because the submicron particles are the least efficiently collected and have the highest concentrations of trace elements, the emissions of potentially toxic trace elements could, therefore, be greatly reduced.

High Temperature Reactions Related to Coal Combustion

R. D. Smith

The mutagenic and/or carcinogenic organic compounds emitted from combustion facilities can be generated from two sources: 1) breakdown products of complex fuels such as coal, and 2) formation from reactions of smaller organic molecules. A more complete understanding of the temperature dependence of the major reaction pathways (formation, decomposition by pyrolysis, and oxidation) could lead to the prediction of the nature and concentration of the organic pollutants from combustion processes. The construction of a model for these chemical processes may also suggest combustion parameters designed to minimize the emission of the organic pollutants.

These studies employ the high temperature mass spectrometer system shown in Figure 1.2.

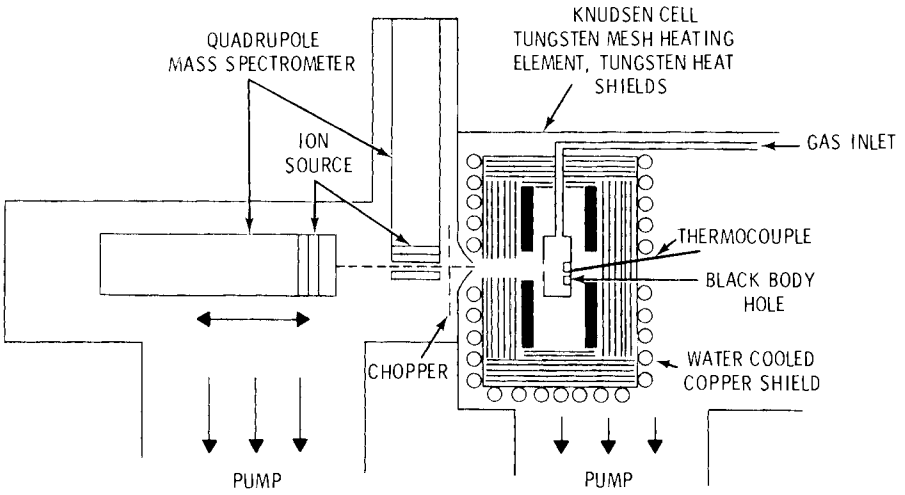

FIGURE 1.2. Schematic of the High-Temperature Knudsen Cell-Modulated Molecular Beam Mass Spectrometer Constructed for the Study of High-Temperature Reactions Related to Coal Combustion.

Samples of complex fuels (coal) and combustion products (fly ash) are placed in the high temperature Knudsen cell, and the vapor phase species are examined as a function of temperature either in a vacuum or in the presence of any gas. Simple fuels and model compounds can also be introduced directly into the high temperature region using the gas inlet.

In many cases, the rate constants for the relevant unimolecular and bimolecular reactions can be deduced. An example of the type of information that may be obtained from such studies is illustrated in Figure 1.3. This figure gives the concentrations of the major species (excluding hydrogen) as a function of temperature formed upon pyrolysis of toluene at a pressure of approximately 10^{-2} torr. The ability to unambiguously measure both radical and molecular concentrations over a large temperature range (up to 3000°C) and pressure range (10^{-5} to 10 torr), as well as to measure the relevant rate constants, is immensely helpful in understanding these reactions. For instance, toluene pyrolysis at 1250°C and 10^{-2} to 10^{-1} torr pressure produces large concentrations of higher molecular weight products. Anthracene, benzopyrene, and a number of carcinogenic compounds are observed under these conditions. Because these products are also known to be trace products of nearly all combustion processes, knowledge of these reaction pathways is an important step in understanding the formation of these products in combustion processes.

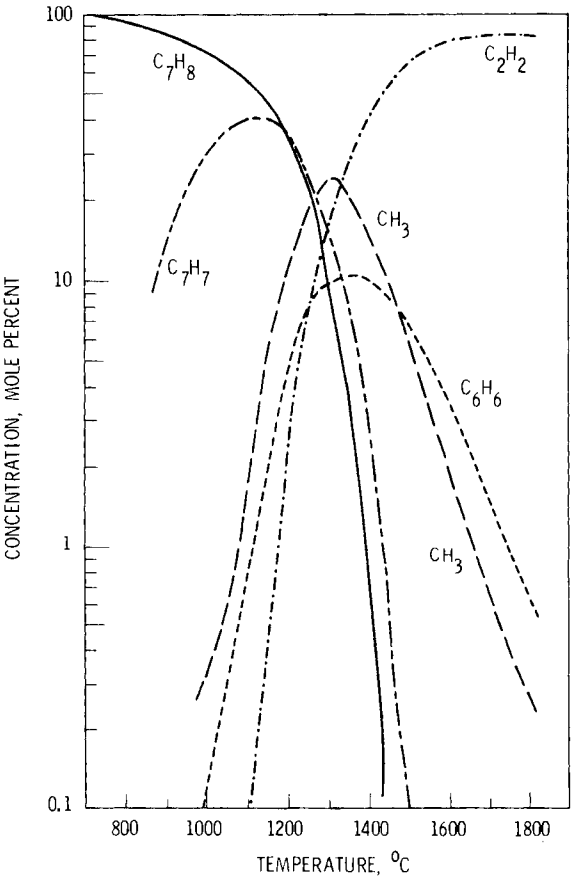

FIGURE 1.3. Concentration as a Function of Temperature for the Major Products of Toluene Pyrolysis at a Pressure of Approximately 10^{-2} torr. These results were obtained in a tungsten Knudsen cell having a 2-mm diameter orifice.

Pollutant Transformation in the Atmosphere

D. R. Kalkwarf and S. R. Garcia

Coal-fired power plants emit polynuclear aromatics and other undesirable organic

compounds. The purpose of this study is to measure the chemical transformation rates of these compounds as they are transported through the atmosphere. This information is needed to more accurately assess the potential environmental impact of coal-fired plants.

A procedure has been developed to assay coal fly ash for polynuclear aromatic hydrocarbons (PAHs) that are produced during combustion. The process consists of extracting the PAHs into dichloromethane, concentrating the extract under vacuum at room temperature, and using a liquid-crystal column packing [1.5% N,N'-bis (p-phenylbenzylidene) α, α' bi-p-toluidine on Supelcoport] in a gas chromatograph to separate the components. The PAHs were identified by their retention times, which were reproducible to within 5% on the column. The amounts present were evaluated by comparing peak areas of sample components and prepared standards. Detection levels for the initial group of 9 PAHs (see Table 1.1) were ≤0.5 ng of injected compound. Extraction efficiencies were determined on spiked 50 mg PAH/100 mg fly-ash samples and found to be in the 90-100% range except for anthracene, whose recovery was found to be in the 60-70% range.

glass-fiber filters* and cellulose mats.** Prior to use, the glass-fiber filters were heated to 400°C to remove trace organic matter and were individually packaged in aluminum foil. Following sample collection, these filters were resealed in foil and stored either on dry ice or in a freezer until they were extracted. The cellulose mats were assayed for calcium by energy dispersive x-ray fluorescence analysis to measure the density of fly-ash particles in the plume at the various sampling sites.

The results of the field-sample assays are shown in Table 1.1. Quantities are expressed as nanograms of PAH (or calcium) per cubic meter of plume air. No PAHs were detected in the samples taken upwind from the stacks, indicating that the samples were not contaminated with helicopter exhaust products. Only four PAHs were found in measurable quantities: fluoranthene, pyrene, benzo(e)pyrene, and benzo(a)pyrene. The latter compound is of particular interest because it is a recognized carcinogen. Generally, the concentrations of fly-ash-bound PAHs decreased with distance downwind from the stacks; however, as shown by the calcium concentrations, the

TABLE 1.1. Concentrations of Fly Ash-Bound Polynuclear Aromatic Hydrocarbons in the Atmosphere at Various Distances Downwind from the Colstrip Stacks.

		Compound, ng/m³									
Date	Distance, km	Fluoranthene	Pyrene	Benzo[e]-pyrene	Benzo[a]-pyrene	Anthracene	Triphenylene	Benzo[a] anthracene	Chrysene	Perylene	Calcium
July 15	-2[a]	<0.5	<0.5	<0.5	<0.5	<0.8	<0.4	<0.8	<0.4	<0.4	
	2	290	450	12	3.7	<1.0	<0.5	<1.0	<0.5	<0.6	2900
	8	150	230	5	<0.7	<1.0	<0.5	<1.1	<0.6	<0.7	1230
	16	20	10	<0.5	1.3	<0.8	<0.5	<1.0	<0.5	<0.6	900
July 16	8	150	190	2.3	30	<1.2	<0.6	<1.2	<0.6	<0.7	1550
	32	103	110	1.7	12	<1.1	<0.5	<1.1	<0.5	<0.6	1330
July 17	2	360	290	21	19	<1.9	<0.9	<2.0	<0.9	<1.4	6260
	8	110	80	10	8.5	<1.4	<0.6	<1.4	<0.6	<1.0	2480
	24	1.1	14	<1.2	<1.1	<1.7	<0.8	<1.8	<0.8	<1.3	1110

[a]Sample taken upwind from stacks

This procedure was used to assay samples of airborne particulates collected during power production near the Colstrip, Montana power plant. The goals of the study were to identify PAHs bound to the emitted fly-ash particles and to determine PAH-degradation rates in air as a function of distance from the power plant. Samples were collected with high volume air-filtering equipment mounted on a helicopter. The plume was traversed at right angles to the wind direction, and time in the plume was detected by real-time monitors for ozone and condensation nuclei. Fly-ash samples were collected simultaneously on both

density of fly ash also decreased with distance because of particle dispersion.

To assess the loss of PAHs by chemical degradation, PAH concentrations were divided by the calcium concentrations for each sampling site in order to normalize the values to unit plume density. Because calcium is not expected to degrade chemically in the

* Whatman GF/B
** International Paper Co. 1478

atmosphere, these concentration ratios should have changed with distance along the plume only if chemical degradation had occurred. Figure 1.4 shows that each of the identified compounds appeared to degrade with distance in a roughly exponential manner. Because of the limited amount of data, the distances shown to achieve half degradation should be regarded as only qualitatively accurate. Nevertheless, they do demonstrate that chemical degradation of PAHs does occur in the atmosphere and that on a sunny day much of the change occurs within 20 km of the source.

The photolysis of benzo(a)pyrene adsorbed on fly ash was also studied under controlled laboratory conditions. Aqueous slurries of washed fly ash were dried on glass microscope slides to form cohesive layers of fly ash, 0.25 mm thick. Samples of benzo(a)pyrene were distributed uniformly over portions of these layers and then exposed to bright sunlight while the temperature was maintained in the 30-40°C range. Assays of the fly ash after exposure indicated that benzo(a)pyrene degraded at the rate of 20% hr^{-1}.

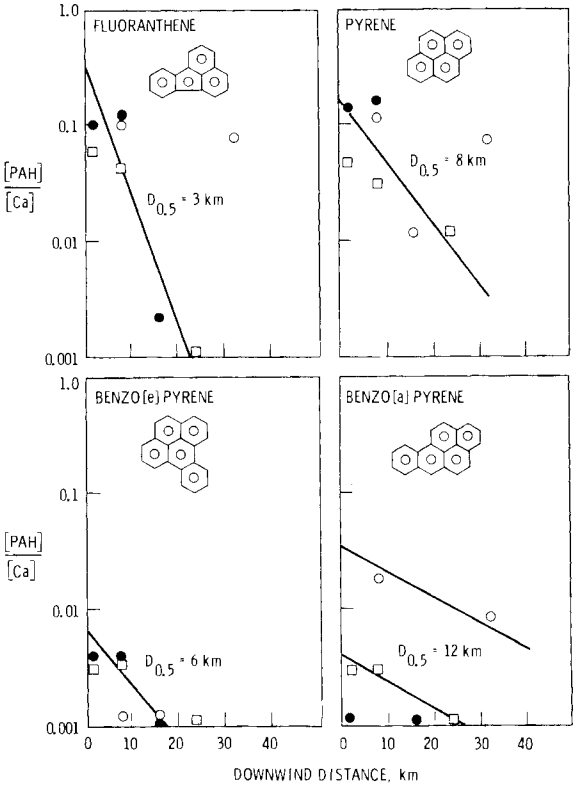

FIGURE 1.4. Degradation of Polynuclear Aromatic Hydrocarbons (PAHs) with Distance from Colstrip Stacks on July 15 (●), July 16 (○) and July 17 (■). [PAH/Ca] ratios used to adjust data to constant plume density.

2.0 Fission

• Radiation Physics

The Radiation Physics Program is concerned with the investigation of basic mechanisms of energy deposition by fast charged particles and the subsequent transport and degradation of that energy as it leads to the formation of chemically active molecular species. Energy deposition is studied through the measurement of interaction cross-sections that, when compared to theory, provide insight into the mechanisms of energy deposition in biologically significant matter. These measurements also provide the necessary data base for energy transport studies. Our effort in energy transport and degradation combines the use of Monte Carlo calculations and theoretical investigation of condensed-phase chemical kinetics. Monte Carlo calculations provide detailed information on the initial formation of the particle track, and the theoretical investigation provides the link between initial energy deposition and the final observation of chemically active molecular species. Time-resolved measurements of fluorescence from liquid systems excited by irradiation with pulsed beams of fast charged particles and ultraviolet light provide definitive tests of the theoretical results. Understanding the energy deposition mechanisms and how energy is subsequently converted to chemically active species is of direct value for correlating dose-response relationships to quantifiable chemical and physical processes.

• Initial Interaction Processes

Ionization by Helium Ions and Alpha Particles

L. H. Toburen, W. E. Wilson and
R. J. Popowich*

The radiation effects on biological matter strongly depend on how energy is initially deposited by the radiation field. For fast charged particles with energies greater than about 100 keV/amu, the principal means of energy loss is ionization of the stopping media (Miller and Green 1973, and Wilson 1972). The radiochemical and biological effectiveness of fast charged particles, therefore, is closely related to the energy and spatial distributions of secondary electrons generated in the path of the moving ion. An understanding of energy deposition by alpha particles and helium ions is particularly important in assessing the radiation effects associated with the decay of radioactive elements such as plutonium, which may be encountered as an airborne contaminant at various stages of the nuclear reactor fuel cycle.

During the past year, we completed an extensive analysis of our measurements of differential cross-sections for ionization of argon and water vapor by He^+ and He^{++} ions. Ion energies from 0.3 MeV (0.075 MeV/amu) to 2 MeV (0.5 MeV/amu) were investigated and compared with equal velocity proton results where available. Of particular interest were the applicability of Z^2 scaling and the effects of projectile structure on the ionization processes. A detailed description of this work has recently been prepared for publication (Toburen and Wilson in press, and Toburen, Wilson, and Popowich in press).

An example of the cross-section surfaces generated by the measurements of energy and angular distributions of ionization electrons is shown in Figure 2.1a for ionization of water vapor by 1.2 MeV ions. In this illustration, the log of $\varepsilon\sigma(\varepsilon, \theta)$ is plotted in units of 10^{-20} cm^2/sr as a function of

*Present address: Dept of Energy,
1333 Broadway, Oakland, CA.

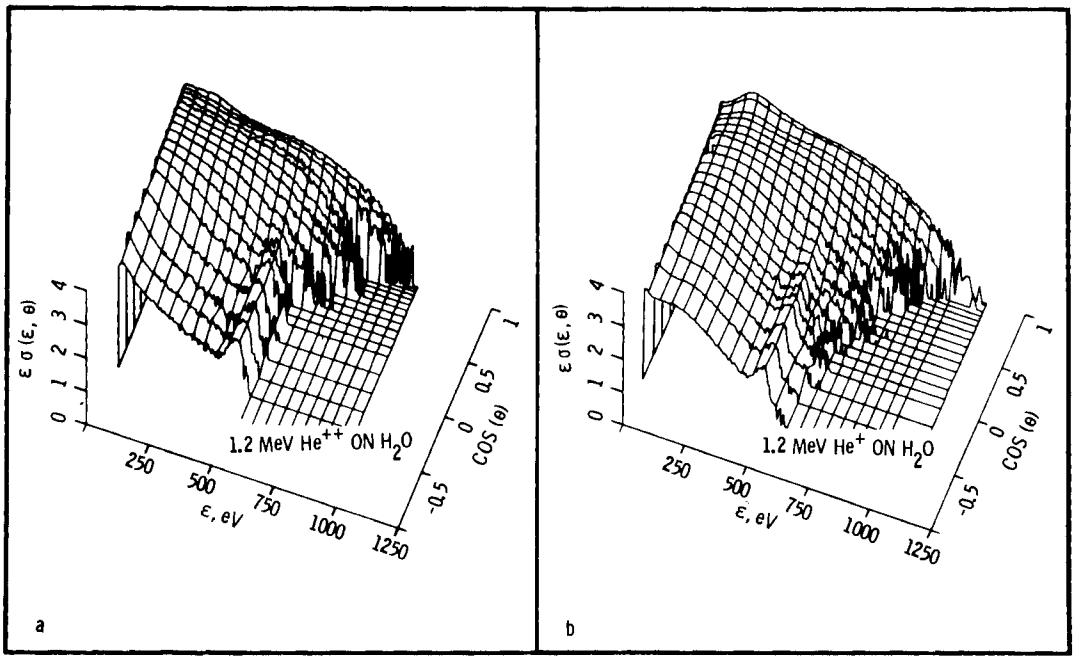

FIGURE 2.1. Cross Section Surfaces Generated by Differential Cross Sections for Ionization of Water Vapor by 1.2 MeV He^+ and He^{++} Ions. The $\epsilon\sigma(\epsilon, \theta)$ axis is scaled as the $\log_{10}$ of the product of cross section and corresponding ejected electron energy in units of 10^{-20} cm^2/sr.

the ejected electron energy, ε, and the cosine of the ejection angle, θ. The data shown in Figure 2.1 emphasize the common He^+ and He^{++} spectral features observed for He^+ and He^{++} impact. The cross sections maximize for emission of low energy electrons and, for a given electron energy, the cross sections increase with decreasing emission angle. Evidence of a broad Bethe Ridge is observed for emission angles less than 90^0, and Auger electron emission is apparent as a ridge centered at electron energies near 500 eV. The basic differences between the surfaces generated by He^+ and He^{++} are the magnitude and shape of the low energy portion of the spectra and the contribution to the He^+ spectra from electrons stripped from the ion. These stripped electrons are released with nearly zero velocity in the rest frame of the moving ion and are observed as a broad ridge in the cross-section surface centered at electron energies corresponding to electrons with velocity comparable to the incident ion. This ridge is centered near 160 eV in Figure 2.1b.

The differences between cross sections for electron ejection for He^+ and He^{++} are more clearly illustrated in Figure 2.2 where a direct comparison of data at selected angles is shown. The effect of screening the He^+ nuclear charge by the bound electron is particularly important in the cross sections for production of low energy ionization electrons (below 100 eV). For the large impact parameter collisions associated with these small energy transfers, the He^+ ion is effectively screened, and the emission cross sections are much smaller than they are for the bare He^{++} ion. For the larger energy transfer, small impact parameters dominate, and the collision occurs within the screening radius of the He^+ electron. Thus, the cross sections for ejection of high energy electrons are equal for He^+ and He^{++}. From these results, it is clear that a single constant value for the effective nuclear charge is not appropriate to describe the interaction of He^+ ions with a molecular target.

Figure 2.2 data also show the significance of the He^+ electron as a contributor to the ionized electron spectra. For fast projectiles, the probability of stripping the electron from the incident ion is high, and these electrons are observed as a prominent peak in the electron spectrum. This contribution is the dominant structure in the 0.5 MeV/amu He^+ spectrum in Figure 2.2, where the 0.2 MeV

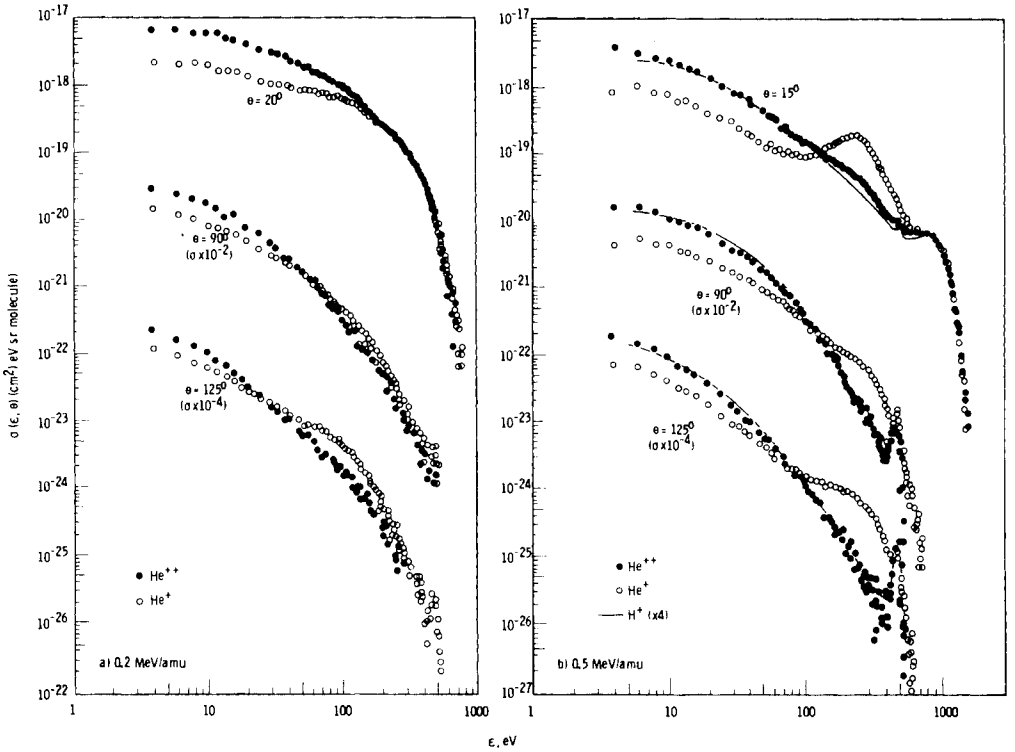

FIGURE 2.2. Electron Energy Distributions for Selected Ejection Angles and Incident He^+, He^{++} and H^+ Ions. The proton data from our earlier work are described in Ref. 3 and multiplied by 4 in accord with Z^2 scaling for comparison to the helium ion data.

results show only a small indication of projectile stripping. Because these electrons are stripped from the He^+ ion with essentially zero energy in the rest frame of the ion, the major contribution expected for electron energies in the laboratory frame is given by the equation:

$$\epsilon = 1/2 m_e v_i^2 \qquad (1)$$

where

m_e is the electron mass and v_i is the ion velocity. The distribution width is a function of the initial distribution of the bound electron velocities in the He^+ ion after translation to the laboratory reference frame.

Evidence of a departure from Z^2 scaling between protons and equal velocity alpha particles is illustrated in Figure 2.2b. The proton results from our previous work (Toburen and Wilson 1977) have been multiplied by 4 for comparison to the alpha particle results that are in accord with Z^2 predictions of the Born approximation. Although excellent agreement is observed between scaled proton cross sections and alpha particle cross sections throughout the energy spectra for large emission angles, differences on the order of 20% are noted at ejected electron energies from 100 eV to about 600 eV in the energy spectra for small emission angles. This difference occurs in the energy and angular region where ionization of the target through the process of charge-transfer-to-the-continuum is important (Rudd and Macek 1972, and Manson et al. 1975).

An understanding of He^+ interactions is particularly important in the study of track structure of alpha particles as the particles slow to energies below about 2 MeV. Charge-changing collisions in the media result in an equilibrium of charge states. About 10% of the ions are He^+ at 2 MeV and about 65% at 0.5 MeV (Allison 1958). Accurate calculations of track structure must take into account the difference in emission cross sections as the charge fluctuates.

The radiobiological implications of the helium ion measurements are best illustrated by the results shown in Figure 2.3. The

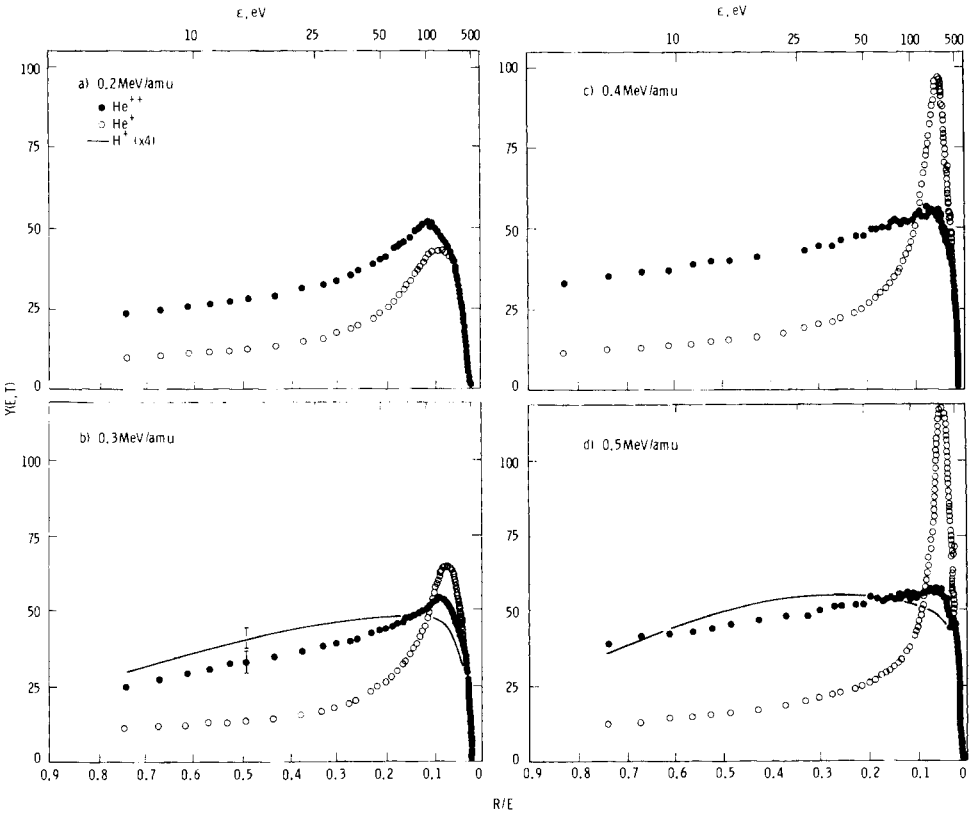

FIGURE 2.3. Ratios of Measured Electron Emission Cross Sections to the Corresponding Rutherford Cross Sections for Ionization of Water Vapor by He^+, He^{++} and H^+ Ions of Several Energies. The proton cross sections are from our previous measurements described in Ref. 3.

quantity Y(E,T) in Figure 2.3 is the ratio of the measured electron emission cross section, which is integrated over all emission angles, to the corresponding Rutherford cross section; E is the energy loss, given as the sum of ejected electron energy and binding energy (E = ε + 12.6 for ionization of water vapor); and T is the kinetic energy of the projectile in units of the equivalent velocity electron energy (Toburen, Manson and Kim 1978). The area under the curve in Figure 2.3 is proportional to the total ionization cross section; equal areas contribute equally to the ionization process. We have recently published a detailed description of the analysis of differential ionization cross sections for proton impact using the ratio Y(E,T). This work, in collaboration with Y.-K. Kim of Argonne National Laboratory and S. T. Manson of Georgia State University, provides the theoretical framework for analysis of cross sections for heavy charged particles (Toburen, Manson and Kim 1978).

The principal features illustrated in Figure 2.3 are the reduction in the value of Y(E,T) for low energy He^+ impact relative to the He^{++} results from screening, and the enhancement of the cross sections for He^+ caused by stripping the bound electron from the electron incident ion. The importance of the stripping increases with increasing particle energy. Therefore, ionization by He^+ results in a proportionately higher number of fast electrons than ionization by He^{++} or H^+ impact. Although the total cross section for ionization is smaller for He^+ than for He^{++} impact, the mean energy of electrons released to the media is considerably higher. This is particularly significant to radiobiological or radiochemical reactions, which depend on the concentration of energy along the particle track.

A summary of the total ionization cross section σ_T, mean energy of ejected electrons $\bar{\varepsilon}$, and partial stopping power contributed as kinetic energy of electrons $\bar{\varepsilon}\sigma_T$ is given in Table 2.1 for ionization of water vapor by He^+, He^{++} and H^+ ions. The total ionization cross section for He^{++} is about twice that for He^+, and the He^{++} cross sections are about a factor of 4 greater than equal velocity H^+ results, which is in agreement with Z^2 scaling predictions. The mean energy of electrons is about the same for H^+ and He^{++} impact but the He^+ results are considerably larger. The partial stopping power $\bar{\varepsilon}\sigma_T$ for He^+ and He^{++} are equal at 0.5 MeV/amu even though the mean energy of ejected electrons differs by a factor of 2.

Ionization by Fast Protons

L. H. Toburen and S. T. Manson*

A thorough understanding of the process of energy deposition by fast charged particles depends on knowledge of the basic interaction mechanisms. Interaction mechanisms are studied by comparing measured differential cross sections with those obtained from calculations that use reliable wave functions for the collision system. Our first comprehensive comparison of experimental and theoretical cross sections (Manson et al. 1975) provided quantitative information on the range of validity of the Born approximation and the importance of continuum-charge-transfer in the ionization of helium by protons.

We have now extended this study to the ionization of neon by protons. This investigation provides information about the effects of inner electronic shells on the ionization process. The comparison of experimental and theoretical cross sections shown in Figure 2.4 for ejection of 60 eV electrons from neon by 1.0 and 1.5 MeV protons illustrates the results of this work.

The theoretical cross sections are the results of a Born approximation calculation using Hartree-Slater initial discrete and

*Consultant, Dept. of Physics, Georgia State University, Atlanta, GA.

TABLE 2.1. Summary Table, Ionization of Water Vapor by He^+, He^{++}, and H^+ Ions.

Ion Energy, MeV/amu	He^+			He^{++}			H^+		
	σ_T, cm^2[a]	$\bar{\varepsilon}$, eV[b]	$\bar{\varepsilon}\sigma_T$, $eVcm^2$[c]	σ_T, cm^2[a]	$\bar{\varepsilon}$, eV[b]	$\bar{\varepsilon}\sigma_T$, $eVcm^2$[c]	σ_T, cm^2[a]	$\bar{\varepsilon}$, eV[b]	$\bar{\varepsilon}\sigma_T$, $eVcm^2$[c]
0.075	8.38×10^{-16}	39	3.30×10^{-14}						
0.20	6.61×10^{-16}	63	4.16×10^{-14}	1.23×10^{-15}	45	5.56×10^{-14}			
0.30	5.57×10^{-16}	78	4.33×10^{-14}	9.0×10^{-16}	52	4.7×10^{-14}	2.57×10^{-16}	45	1.16×10^{-14}
0.40	4.76×10^{-16}	92	4.41×10^{-14}	9.5×10^{-16}	49	4.67×10^{-14}			
0.50	3.62×10^{-16}	112	4.05×10^{-14}	7.7×10^{-16}	51	3.95×10^{-14}	1.70×10^{-16}	56	0.96×10^{-14}

[a] Total ionization
[b] Mean energy of ejected electrons
[c] Kinetic energy of electrons

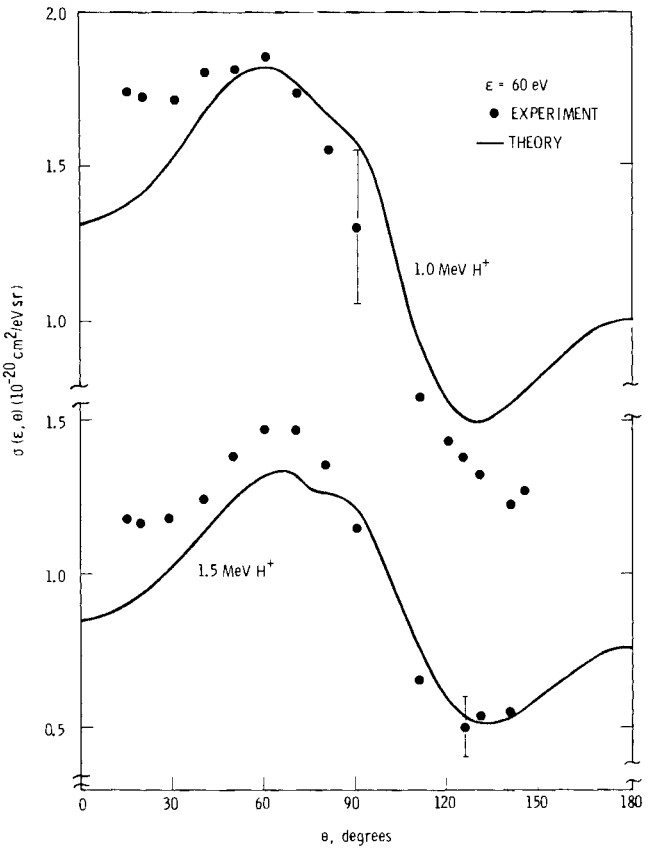

FIGURE 2.4. Angular Distribution of 60 eV Electrons Ejected from Neon by 1 and 1.5 MeV Protons. The solid line represents the Born calculation using Hartree-Slater wave functions for initial discrete and final continuum states.

final continuum wave functions for the collision system. The apparent two-component binary encounter peak centered near 70^{0} in the theoretical curve is attributed to electrons that originate from the 2s and 2p subshells of neon. Because the binding energy differs for these subshells, the maximum contribution to the respective binary encounter peaks appears at slightly different angles. Because this structure does not appear to be confirmed by the experimental data, we are now looking closely at the interaction channels predicted by theory to determine what implications these differences may have.

The differences betweeen experimental and theoretical cross sections for electron emission into small angles observed in Figure 2.4 are explained by the continuum-charge-transfer mechanisms, which enhance the measured cross sections but are not included in the theoretical formulation. The differences between calculated and measured cross sections at large angles disappear as the proton energy is increased. We are now planning to extend our measurements to higher proton energy to determine if the agreement at 1.5 MeV is coincidental or if we have reached sufficiently high energy for theory to be reliable for ejection of electrons in this electron energy and angular range.

Ionization by Heavy Ions

L. H. Toburen

A complete description of charged particle track structure that is relevant to the dosimetry of fission and fusion neutrons requires knowledge of the interaction cross sections of all recoil ions arising from interactions of these neutrons with biological material. Information about the systematics of ionization electron yields, including ejected electron energies and emission angles for heavy ion recoils such as carbon, oxygen, and nitrogen ions, are needed in addition to extensive data for protons.

Our recent cross-section measurements for He^{+} ions demonstrate how difficult it is to predict ionization properties for even the simplest structured projectiles. Projectile electrons screen the nuclear charge of the

incident ion and contribute to the spectra of electrons released to the media. For ion energies less than a few hundred keV/amu, the collision can no longer be classified as fast, and an analysis of the interaction must consider the combined system of the incident particle plus the target.

Fast collisions can be separated into two distinct factors, one dealing with only the incident particle and one dealing with only the target (Inokuti 1971). This characteristic of fast collisions has led to success in the development of theory, such as the Born approximation. Theoretical investigation of slow and intermediate energy collsions are primarily limited to the study of inner shell excitation and ionization (Madison and Merzbacher 1973). Therefore, interaction probabilities and ejected electron distributions for outer shell ionization by heavy ions of radiological interest ($E \lesssim 1$ MeV/amu) must be obtained by experimental means.

During the past year, we initiated a study of electron emission resulting from carbon ion impact. This work uses our 2 MV tandem accelerator coupled with a sputter ion source that provides the required negative carbon ions for injection into the tandem. Vacuum in the beam transport system is maintained at better than 5×10^{-7} torr to insure charge state purity. Our initial investigation of systematics of interaction cross sections for heavy ions as a function of the ion charge state is illustrated in Figure 2.5. The Born approximation predicts that the interaction should depend on the square of the incident particle charge (Inokuti 1971). However Z^2 scaling of differential ionization cross sections for structured projectiles, such as those for He^+ impact, depends on the quantity of energy transferred during the collision caused by the bound electron screening of the helium nucleus. For large energy transfer (high energy ejected electrons), the He^+ ion interacted as

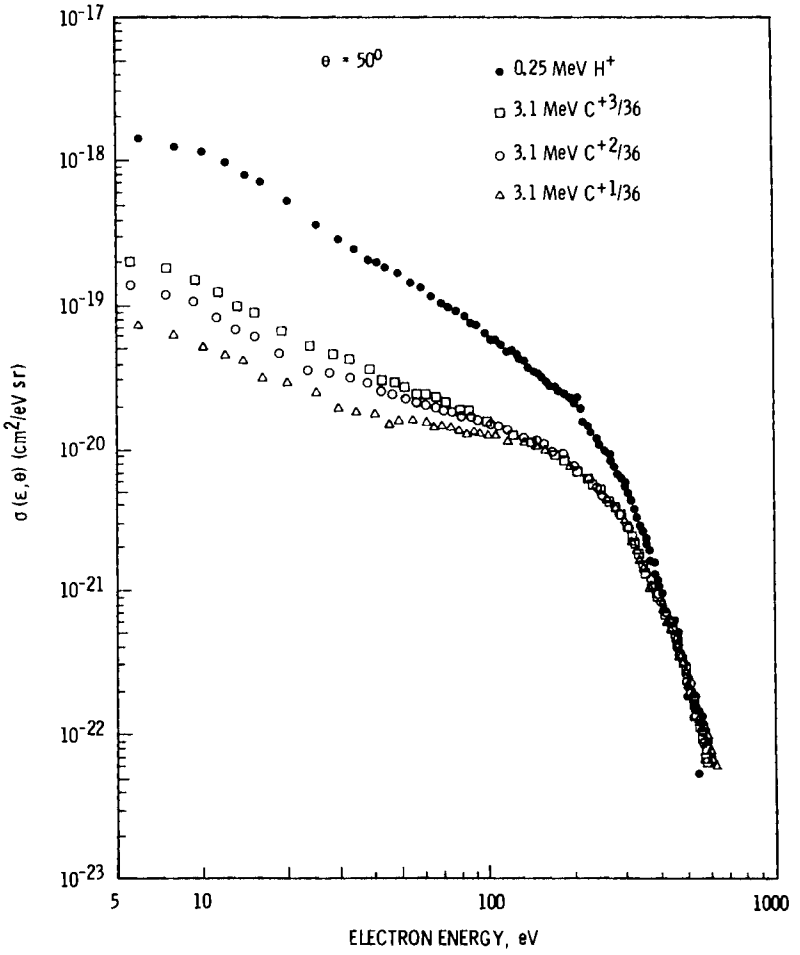

FIGURE 2.5. Double-Differential Cross Sections for Ejection of Electrons from Argon by C^{+1}, C^{+2} and C^{+3}. The carbon impact cross sections have been scaled by Z^2, Z equal to the nuclear charge, for comparison to previous measurements for incident protons. The proton results are unpublished data from our laboratory.

an unscreened bare charge. The cross sections for carbon ion impact shown in Figure 2.5 were divided by 36 to determine if the cross sections for large energy transfer would also asymptomatically approach a value characteristic of a bare charge. The results, also shown in Figure 2.5, are similar to what we have observed for He^+ impact, i.e., for sufficiently large energy transfer (high energy ejected electrons), the nuclear charge (Z) is essentially unscreened and the cross sections scale as Z^2 of the projectile. For small energy transfer, screening is important and the cross sections scaled using the bare nuclear charge differ by more than an order of magnitude from proton results. If the low energy cross sections are scaled by the projectile charge rather than nuclear charge, the difference between low energy emission cross sections is reduced to about a factor of 4.

We plan to continue this study and incorporate a broad range of projectile energies and charge states into the study of interaction systematics for carbon ions.

Molecular Fragmentation by Fast Charged Particles

L. H. Toburen

The interaction of a fast charged particle with a molecular target will leave the target molecule in one of many states of ionization and excitation. Subsequent deexcitation, which may include dissociation of the target molecule into charged fragments, is expected to have a direct effect on the induced radiation damage. Identification of the generated charged fragments, their energies, and the variation of these parameters with incident beam energy and particle type will provide insight into the production of active chemical species along a charged particle track.

To identify the molecular fragments resulting from collisions with fast charged particles, we have been using a quadrupole mass spectrometer to measure the spectra of charged molecular fragments. The mass spectrometer was positioned to view the target gas cell at 90^o with respect to a proton beam for preliminary measurements that were designed to investigate experimental parameters such as the solid angle and required target density. The target cell, which was previously employed for electron ejection measurements, was used with gas pressures of about 5×10^{-3} torr. The spectra obtained for a mixture of argon and methane gases (90% Ar - 10% CH_4) are shown in Figure 2.6. Argon gas provides accurate mass calibration at mass 40 (Ar^+) and 20 (Ar^{++}) to assure proper identification of the observed hydrocarbon fragments.

This measurement demonstrated experimental feasibility. We are now fabricating an apparatus that assures proper alignment of the spectrometer with the target cell and proton beam. The alignment apparatus will allow measurement of angular distributions of molecular fragments. It has an angular

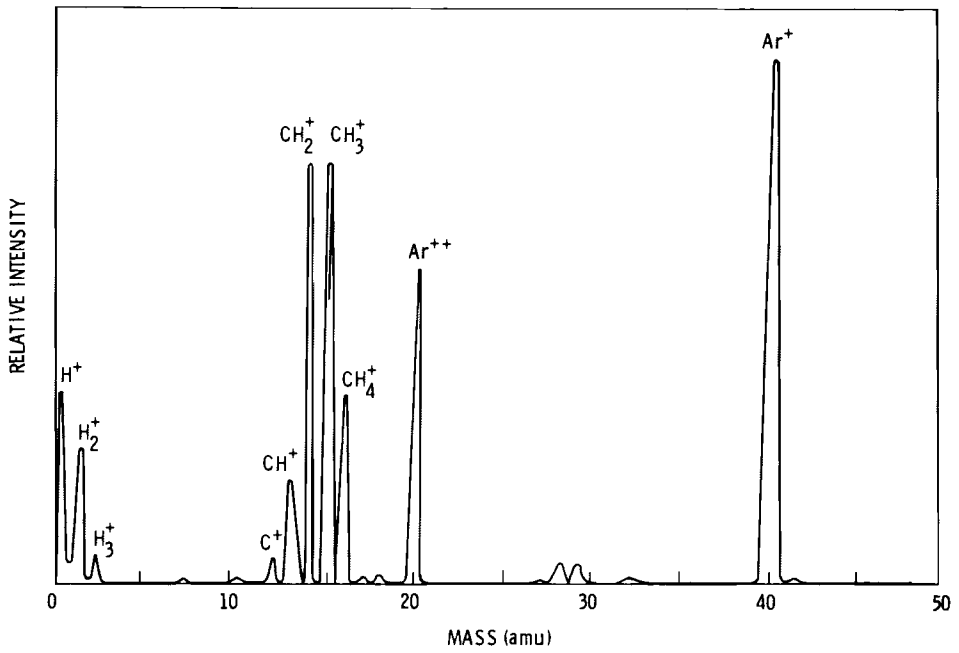

FIGURE 2.6. Mass Spectrum of Charged Fragments Produced by Ionization of a Mixture of 90% A - 10% Ch_4 by 1.7 MeV Protons.

range of approximately $\pm 40^{0}$ of the normal to the ion beam. Initial measurements will concentrate on the effect of varying the incident ion energy on the fragment pattern.

This study will provide indirect evidence of the importance of inner shell ionization to molecular dissociation.

• Track Structure

Ionization Distributions in Condensed Phase

W. E. Wilson, L. H. Toburen and
H. G. Paretzke*

Major shortcomings in experimental methods for determining energy deposition spectra make it attractive to consider calculating the statistical distributions of interactions (ionizations) for very small volumes. At the present time, the most promising method that retains the inherent stochastics for handling particle transport in calculations of charged particle track structure is the Monte Carlo method. The Monte Carlo method requires accurate secondary electron data to be truly useful in a quantitative sense. By far the largest number and most accurate data for source terms come from experimental measurements in gaseous phase. Therefore, the validity of calculations for condensed phase based on such source terms must be carefully established.

We have developed a new Monte Carlo code (MOCA13) that makes extensive use of experimental ionization cross sections and recent improvements in electron transport based on the critical evaluation of data on electron interactions. Details of this code and its application to the study of energy loss in both gas and condensed phase were presented at the Radiation Research Society Meeting in Toronto (Wilson, Toburen, and Paretzke 1978a) and at the Microdosimetry Conference in Brussels (Wilson, Toburen and Paretzke 1978b).

Fast positive ion tracks are simulated by randomly selecting events from tables of various interaction probabilities. The probability tables for direct primary ionization of the target by fast ions are obtained from a phenomenological model based on measured cross sections for proton ejection of electrons from water vapor (Wilson and Toburen 1978). The model provides a detailed description of the angular emission as well as the energy of the secondary electrons. Subsequent energy transport by secondary electrons is calculated in detail by including elastic scattering, eleven discrete excitation cross sections, and inner and outer shell ionization. Outer shell ionization is further specified according to glancing and Mott collisions (Paretzke and Berger 1978). Interaction variables such as coordinates, inelastic energy loss, and secondary electron energy can be used to obtain distributions of ionization and energy deposition within an absorber as well as energy and angle of emission of secondary electrons at the boundary of the absorber.

Because real problems of radiological interest generally relate to energy loss in condensed phase, we are investigating ways to apply calculations based on gaseous phase data to the condensed phase. Unfortunately, direct measurements of ionization or energy deposition distributions in condensed phase are not available nor are they technically feasible. We have, therefore, devised an alternative test in which the ionization is created in condensed phase and detected in gas phase (vacuum)(Toburen, Paretzke, and Wilson 1976). Delta-ray energy spectra resulting from 1 MeV proton bombardment of thin carbon foils were obtained by using the electron energy analysis system employed in previous studies of single collision interactions (Toburen 1971). For the present problem, the differentially pumped gas target was replaced with a foil holder that supported a solid carbon foil oriented at 90° with respect to the proton beam. Foil thickness was "thin" to the proton but "thick" for the ionization electrons, i.e., the secondary electrons multiply scatter before exiting from the foil. Electron energy spectra were recorded from 10 eV to 3 keV for electrons leaving the foil at angles from 50° to 125°. The supplier's specification of the foil thickness was 3 $\mu g/cm^2$ and was not otherwise verified.

Secondary electron emission spectra from a simulated 3 $\mu g/cm^2$ foil were calculated using the MOCA13 code with source terms and interaction cross sections derived from gaseous phase water vapor data. Calculations were restricted to electrons above 50 eV to obtain, within a reasonable computation time, an acceptable statistical accuracy where the experimental spectra are most reliable. A comparison between calculated and measured electron spectra is shown in Figure 2.7. The curves shown are for electrons with energy greater than 50 eV ejected from the foil at forward angles 50°, 60° and 70°, and backscattered at angles 110° and 125°. The curves

*Address: Institut für Strahlenschutz,
D 8042 Neuherberg, Germany

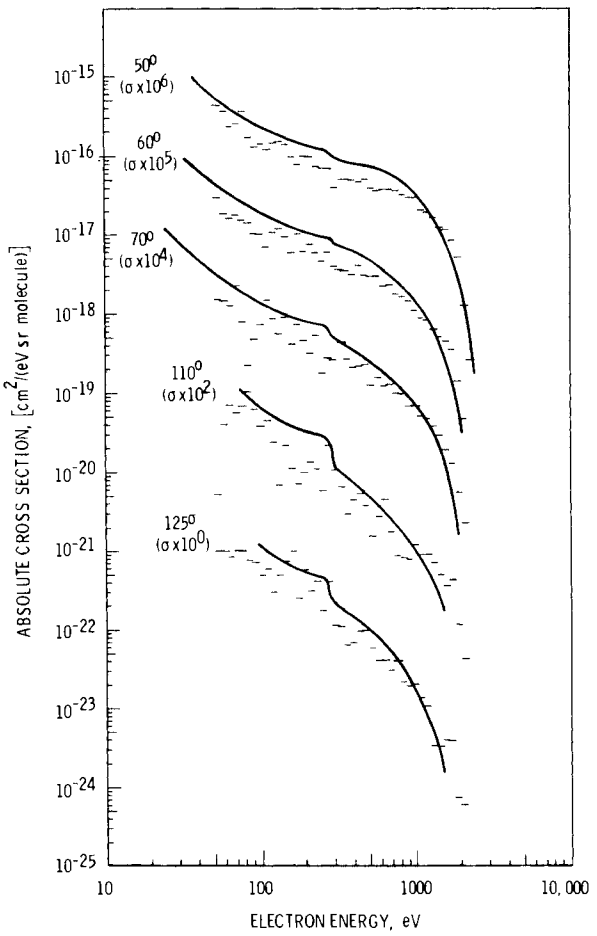

FIGURE 2.7. Secondary Electron Emission for 1.0 MeV Protons Passing Through a 3 $\mu g/cm^2$ Foil. Smooth curve is experiment; histogram is calculation with MOCA13. Curves are successively offset by factors of 10 for clarity. Calculation is absolute, i.e., there are no arbitrary normalizations.

are progressively offset by decade(s) for clarity. Overall, the agreement between the Monte Carlo calculation and measured cross sections is excellent.

The energy distribution shown in Figure 2.7 varies by over three orders of magnitude from 50 eV to 2 keV, and the angular distributions by more than an order of magnitude from 50° to 125°. Over this considerable range of variation in the absolute yields, experimental and Monte Carlo calculations agree very well. Insufficient statistical accuracy in the calculated spectra precludes any conclusion about the carbon-Auger structure that is evident in the experimental spectra near 250 eV. The experimental data should be extended to angles of emission less than 50° and the calculations extended to energies less than 50 eV to complete the comparison. We can conclude that the Monte Carlo method with moderately sophisticated source terms derived from gas phase data can be used to simulate the emission of 50 eV or greater electrons around proton tracks and the subsequent transport of those delta rays in condensed phase.

Positive Ion Track Structure

W. E. Wilson and H. G. Paretzke

The importance of the microscopic pattern of primary molecular changes in determining the type and extent of final macroscopic radiation effects has been recognized for decades. However, until recently, progress was hampered by lack of adequate experimental equipment and computational tools. Also, the microtopography of primary events could be neither measured nor calculated with reliable accuracy. The advent of channeltrons, capacitance monometers, and fast electronic counting equipment, as well as large digital computers, has made experiments possible that can obtain the quantitative information on the details of radiation and matter interactions. This information is the source data for computer programs that simulate the production of molecular changes along the tracks of charged particles with high spatial resolution. For several years we have devoted much effort to the development of Monte Carlo programs that allow us to calculate, with reasonable accuracy, spatially dependent probability distributions of localized events about tracks of charged particles. The reliability of such calculations has been checked in part by comparison with experimental results. See, for example, the previous section of this report and Wilson, Toburen and Paretzke (1978a and 1978b).

We have calculated the spatial dependence of ionization and energy dependence of ionization and energy deposition in regions as small as 1 nm and as large as 200 nm diameter for 0.25 to 3.0 MeV protons (see Wilson and Paretzke, "Calculation of Energy Deposition and Ionization in Very Samll Volumes," reported in the Radiation Dosimetry section of this report). Calculations for the smallest of these volumes approach the scale of atomic dimensions. Two interesting physical observations are apparent from initial calculations. For protons passing diametrically through a site, the mean event size (imparted energy divided by site diameter) varies from L_∞ for large sites (about 1000 nm) to about 0.4 x L_∞ for very small sites ($\sim$1 nm). This latter value can be understood in terms of the cross sections for electron ejection and the ejected electrons' energy spectrum. Stopping power, S, can be partitioned into

$$S = S_E + S_I + S_{KE} \qquad (2.1)$$

where

$$S_E = \sum_n E_n \sigma_n \qquad (2.2)$$

$$S_I = \int_0^\infty \sigma(\varepsilon)\ I_p\ d\varepsilon = I_p \cdot \sigma_{ion} \qquad (2.3)$$

and

$$S_{KE} = \int_0^\infty \sigma(\varepsilon)\ \varepsilon d\varepsilon \qquad (2.4)$$

where S_{KE} is that part of S that is transferred to kinetic energy ε of secondary electrons and is, therefore, transportable. S_E and S_I are localized energy depositions that represent the portions of S that go into excitation and overcome binding energy during ionization, respectively (Wilson 1972). Using real cross-section data for $\sigma(\varepsilon)$, we have shown that S_{KE} for protons in hydrogen gas is about 60% of S (Wilson 1972). None of our cross-section measurements for low-Z polyatomic molecules indicates that this fraction will be significantly different for tissue-like materials. Therefore, approximately 40% of the combined stopping power is for S_I and S_E. The Monte Carlo calculations indicate that the mean event size reaches this magnitude for site sizes $\simeq$ 1 nm. This implies that energy transport via secondary electron escape is essentially 100% for sites of 1 nm.

The track structure studies also revealed an interesting item about imparted energy to produced ionization. For most situations in traditional dosimetry, this ratio is fairly constant and independent of radiation type. Indeed, much quantitative dosimetry is based on the assumption that there is a unique proportionality factor relating energy deposited in a volume to the number of relevant atomic or molecular changes in the same volume. Our track structure calculations indicate that the factor is not unique when the involved atomic or molecular changes are ionizations. For proton tracks passing through a 100 nm site, the ratio of imparted energy to produced ionizations is 32 eV/ion pair. For tracks passing just outside the site, values as high as 36 eV for the ratio have been observed. This illustrates that on a microscopic track structure basis, one cannot a priori expect a unique proportionality between deposited energy and atomic or molecular change.

• Energy Transport

Track Structure in Radiation Chemistry

J. H. Miller and M. L. West

The measurement of primary interaction cross sections and the incorporation of these data into track structure calculations provide detailed information about the initial spatial distribution of absorbed energy. The primary products from this energy deposition undergo simultaneous diffusion and chemical reactions; consequently, the initial distribution influences the chemical yield at later times. A new model of diffusion kinetics has recently been developed that incorporates detailed track structure information in chemical yield calculations. A brief description of this model was presented at the Radiation Research Society Meeting in Toronto (J. H. Miller 1978) and published in the Biophysical Journal (Miller in press). Most previous calculations have assumed either a spherical geometry for radiation with small linear energy transfer (LET) or a cylindrical geometry for high LET radiation (Kupperman 1974). Mozumder and Magee (1966) partitioned the initial distribution of reactive species into spurs, blobs, and short tracks on the basis of absorbed energy but did not allow for interaction between these track entities. In the present model, we treat each inelastic collision that slows down the primary ion and secondary electrons as a source of chemical species. The reactant yields from each event are proportional to the deposited energy, and their spatial distribution relative to the position of the event is assumed to be a spherical Gaussian. The distribution variance increases linearly with time because of diffusion.

The position of events and the deposited energy are stochastic variables determined by the Monte Carlo method (Paretzke 1973). The yield of reactants and the initial width of their distribution are parameters that must be determined by best fit to experimental data. In this report, we will discuss application of the model to the fluorescence decay of dilute solutions of benzene in cyclohexane. With these solutions, it has been observed that the amount of quenching depends upon the initial distribution of reactive species (West 1976 and Miller and West 1977). In this nonpolar solvent, a large fraction of the deposited energy results in the formation of geminate ion pairs. Consequently, the thermalization distance of low energy electrons is expected to be the predominate factor that determines the initial width of the distribution of chemical species relative to the site of the energy deposition. Dodelet and Freeman (1972) have estimated this distance to be about 50Å. This estimate is based on the dependence of the free ion yield on external electric fields.

Excited states of benzene are quenched by interaction with the solvent as well as with chemical species produced by the radiation. The solvent interaction quenching is characterized by a time independent rate, k_{uv}, which may be determined by exciting the liquid with ultraviolet (UV) photons. The rate of radiation-induced quenching can be time dependent from both diffusion and decay of the species involved (probably free radicals); however, in this model, we consider only the time dependence caused by diffusion. Under the assumptions we have made, the fraction of excited states decaying in the interval dt at time t is

$$\frac{-dN_*}{N_* dt} = k_{uv} + k_{R*} \left\langle \sum_j \frac{\gamma_R \varepsilon_j}{(2\pi^{1/2}\sigma)^3} \exp\left[\frac{-(\vec{r}_j - \vec{r})^2}{4\sigma^2}\right] \middle| \vec{r} \right\rangle \tag{2.5}$$

where k_{R*} is the quenching rate constant, γ_R is the yield of quenchers per unit energy absorbed, ε_j is the energy deposited in the inelastic collision at position $\vec{r}_j$, and $\sigma^2 = \sigma_0^2 + 2Dt$ is the variance of the distribution of quenchers about $\vec{r}_j$. The angular bracket denotes an average with respect to the position $\vec{r}$ of the excited state.

The factor $(\gamma_R \varepsilon_j)/(8\pi^{3/2}\sigma^3)$ may be interpreted as the concentration of quencher from the j^{th} inelastic event, or spur. The exponential factor in Eq. (2.5) is the probability that quenchers from the j^{th} event will react with the excited state. As the spur radius, σ, increases because of diffusion, the number of spurs that must be included in the sum increases, and the significance of

the details of the track structure near r is reduced. When the spur radius becomes larger than the range of secondary electrons, the difference in radial coordinates of two events has a negligible effect on the probability of reaction. In this limit, which we call the LET approximation, we may treat the track segment containing the excited state as a continuum of energy deposition with stopping power S and approximate the sum in Eq. (2.5) by an integral to obtain:

(2.6)

$$\frac{-dN_*}{N_* dt} = k_{uv} + \frac{k_{R*}\gamma_R}{(2\pi^{\frac{1}{2}}\sigma)} \left(<\varepsilon> + 2\pi^{\frac{1}{2}}\sigma S\right)$$

The first term in the parentheses is the mean energy deposited in single events and results from the contribution to the sum in Eq. (2.5) from quenchers and excited states produced in the same spur. By integrating Eq. (2.5), we obtain the predicted fluorescence decay in the LET approximation:

(2.7)

$$\ln\left(\frac{I}{I_{uv}}\right) = -\frac{k_{R*}\gamma_R S}{8\pi D} \ln\left(1 + \frac{2Dt}{\sigma_o^2}\right) - \frac{k_{R*}\gamma_R <\varepsilon>}{8\pi^{3/2}\sigma_o D}\left(1 - \left(1 + \frac{2Dt}{\sigma_o^2}\right)^{-\frac{1}{2}}\right)$$

As time increases, the quenching from isolated spurs becomes negligible, and the ratio of radioluminescence to UV luminescence becomes linear on a log-log plot. The slope of the asymptotic time dependence should be proportional to the LET of the incident particle. This behavior is illustrated in Figure 2.8 for proton radioluminescence. The insert in Figure 2.8 shows the slope of the asymptotic time dependence of the ratio I_{H+}/I_{uv}

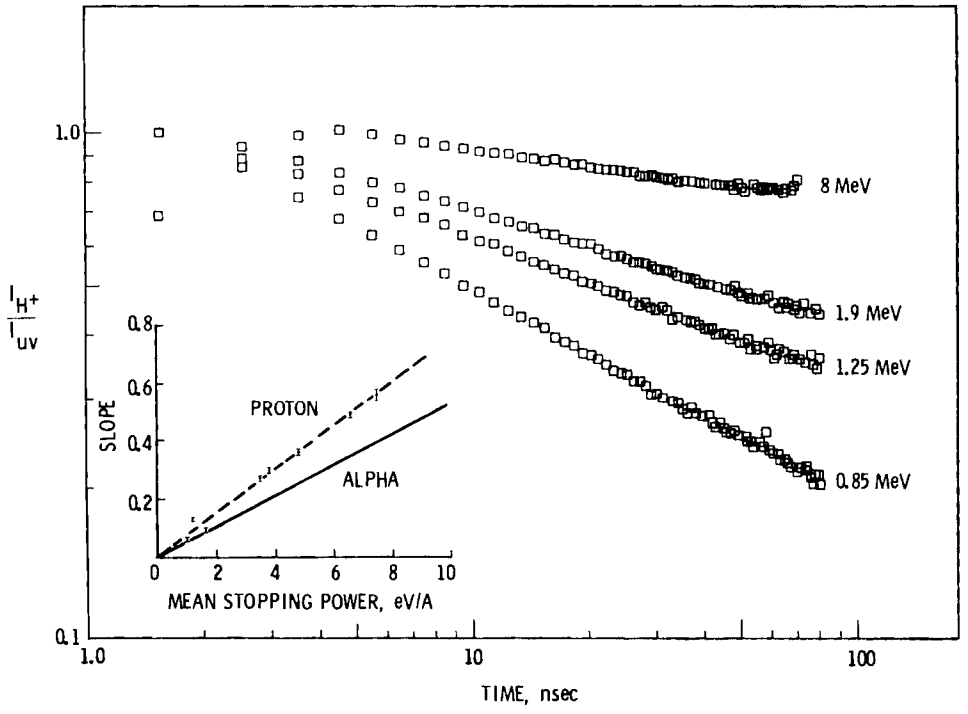

FIGURE 2.8. Time Dependence of the Ratio of Proton and UV-Induced Benzene Fluorescence at Several Proton Energies. Insert shows the proportionality between the slope of the asymptote and the mean stopping power as predicted by Eq. 7. Solid line is the expected result for alpha-induced fluorescence.

as a function of LET. The points are derived from the experimental data for protons and the dashed line is predicted from our kinetic diffusion model. The full line represents the expected behavior for alpha particles; a description of this calculation follows.

In the LET approximation, all types of radiation with the same stopping power should have identical fluorescence decay. This is not true of predictions based on Eq. (2.5). If two ions of equal stopping power have different velocity, the ion with the higher velocity will have a larger inelastic mean free path and a more energetic secondary electron spectrum. Hence, the radial distribution of absorbed energy is more diffuse for the ion with the higher velocity. In Figure 2.9, we plot the ratio of the radiation-induced quenching rate predicted by Eq. (2.5) to that obtained using Eq. (2.6) for protons and alpha particles of various energies. The stopping power for each case is also shown. The ratio is plotted as a function of spur radius. The corresponding time following energy deposition, which assumes an initial spur radius of 50 Å and a diffusion coefficient of 1.5×10^{-5} cm^2/sec, is shown at the top of the figure. Deviation from LET approximation is seen in all cases when the spur radius is small. For protons, these deviations become negligible when the spur radius exceeds about 100 Å; however, for alpha particles, the quenching rate continues to be about 75% of the predicted rate based on the stopping power at the largest times investigated. The deviation from the LET approximation calculated for alpha particles does not have a very significant time dependence. Consequently, we expect the time dependence of the alpha radioluminescence to conform to Eq. (2.7) but with an LET that is about 75% of the total

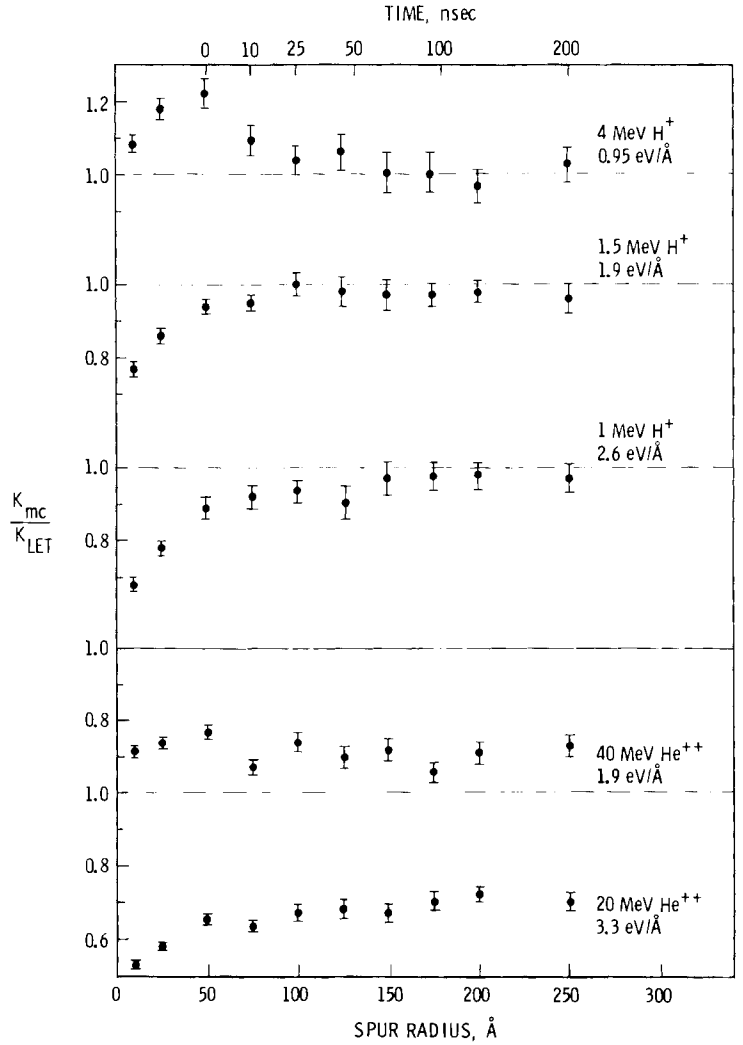

FIGURE 2.9. Ratio of the Radiation-Induced Quenching Rate Calculated by the Stochastic Model (Eq. 2.5) to that Obtained in the LET approximation (Eq. 2.6).

stopping power. This prediction is illustrated by the solid line in Figure 2.8.

Experimental Studies of Fluorescence Quenching in Pulsed Proton Irradiation

M. L. West and J. H. Miller

Energy Dependence

The diffusion kinetics model developed in the previous section uses the concept of overlapping spurs in estimating the spatial distribution effects of energy deposition on the decay of radiation-induced fluorescence. Such a model makes several important predictions that can be explored experimentally. First, differences should be observed in the induced fluorescence for protons and alpha particles of the same stopping power. Second, a quenching contribution is predicted from isolated spurs for high energy protons. Third, where contributions from isolated spurs become negligible, the ratio of radioluminescence to the UV luminescence should approach a straight line in a log-log plot in the limit of high LET. The slope of this line then gives the quenching parameter, which also has a predicted variation with incident energy.

An analysis of the energy dependence of fluorescence decay for the limiting case of no contribution from isolated spurs has been made previously for the range of projectile energies available from the 2 MV accelerator (Miller and West 1977). Parameters of the quenching model were shown to have the predicted energy dependence. However, to provide more critical tests of the model, a wider range of projectile energies is needed, as are projectiles of different velocities but with same LET.

We initiated an experimental investigation of the time-resolved emission induced by high energy protons and alpha particles with the 20 MV tandem accelerator facility at the University of Washington Nuclear Physics Laboratory.* Pulsed particle beams are available from a three gap klystron buncher, and pulses as short as 0.75 nsec full width-half maximum (FWHM) have been reported (Weitkamp and Schmidt 1974). Initial studies of the bunched beam profile provided a time resolution of approximately 3 nsec FWHM, which is adequate for our study of quenching by high energy protons.

Samples of 0.04 M benzene in cyclohexane were irradiated with protons of energies 6, 8, and 13 MeV at a sample temperature of 20°C.

*Our experimental apparatus for single photon counting has been moved to the Nuclear Physics Laboratory.

The 8 MeV data, together with low energy measurements from the 2 MV accelerator, are shown in Figure 2.8. Neglecting contributions from isolated spurs, the model predicts from Eq. (2.7):

$$\ln\left(\frac{I_{H^+}}{I_{uv}}\right) = -\frac{k_{R^*}\gamma_{RS}}{8\pi D}\ln\left(1+\frac{2Dt}{\sigma_o^2}\right) \qquad (2.8)$$

which becomes a straight line on a log-log plot when $t \gg \sigma_o^2/2D$. This prediction has been verified at energies from 0.85 to 13 MeV. Slopes of the asymptotic time dependence for the high energy data are shown in the insert in Figure 2.8 as the points with mean stopping power less than 2 eV/Å. The points are in good agreement with the predictions of the quenching model.

The solid line in the insert of Figure 2.8 shows the expected change in asymptotic slope with mean stopping power for alpha-induced fluorescence. Experimental tests of this prediction are planned using the University of Washington tandem accelerator. Alpha particles with energies up to 24 MeV are available from this facility, which will permit comparison with proton data with mean stopping powers greater than about 5 eV/Å. If subnanosecond time resolution can be achieved with this accelerator, an attempt will be made to look for quenching in isolated spurs with high energy protons.

Concentration Dependence

Our investigation of the temperature dependence of proton-induced fluorescence, which was recently presented at the Radiation Research Society Meeting in Toronto (West and Miller 1978), and previous measurements of the proton energy dependence (Miller and West 1977) support our model of intratrack quenching by radiation products. We do not know the exact nature of these quenching molecules, but they are created initially in high density along individual proton tracks. We have also tentatively assumed that these quenchers are products of solvent radiolysis. To gain further insight into the postulated quenching mechanisms, we have undertaken a systematic study of the concentration dependence of proton-induced fluorescence.

Solutions of benzene in cyclohexane were irradiated with subnanosecond pulses of protons. Changes in the time resolved emission were studied as a function of benzene concentration. Figure 2.10 shows results for 0.4, 0.1, 0.05, 0.025 and 0.0125M concentrations of benzene in cyclohexane for 1.7 MeV incident protons energy. The data plotted in this manner should approach a straight line

with a slope α given by

$$\alpha = \frac{k_{R*} Y_R S}{8\pi D} \qquad (2.9)$$

The straight line dependence of the ratio I_{H+}/I_{UV} shown in Figure 2.10 indicates that these data are consistent with our model over the range of investigated concentrations. The change in slope shown in the insert of Figure 2.10 demonstrates that α is concentration dependent. This relationship suggests that the number of quenching molecules per unit track length depends on the number of benzene molecules present in solution. Such a dependence is possible if benzene alters the radiolysis products of cyclohexane or if radiolysis products of benzene itself are responsible for the observed quenching.

We can determine the yield of quenchers from Eq. 2.9 if the quenching rate constant k_{R*}, diffusion coefficient D, and stopping power S are known. Even for a diffusion limited quenching rate constant of 10^{10} ℓ/mole-sec, the concentration of quenching molecules is larger than the concentration of benzene. Consequently, at least a part of the quenching must be derived from radiolysis of cyclohexane. We are currently investigating whether the concentration dependence of α is related to the radiation protection aspect of benzene in cyclohexane (Spinks and Wood 1964).

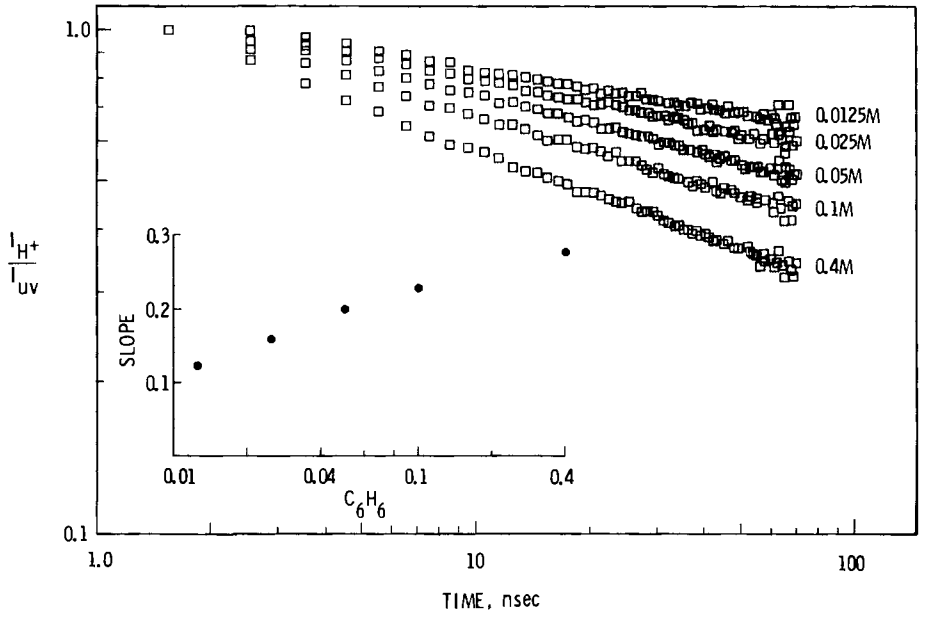

FIGURE 2.10. Time Dependence of the Ratio of Proton and UV-Induced Benzene Fluorescence at Several Concentrations of Benzene in Cyclohexane. Insert shows the asymptotic slope as a function of benzene concentration.

• Radiation Dosimetry and Radiation Biophysics

Radiation dosimetry and radiation biophysics are two closely integrated programs whose joint purpose is to explore the connections between the primary physical events produced by radiation and their biological consequences in cellular systems. The radiation dosimetry program includes the theoretical description of primary events and their connection with the observable biological effects. This program also is concerned with design and measurement of those physical parameters used in the theory or to support biological experiments. The radiation biophysics program tests and makes use of the theoretical developments for experimental design. Also, this program provides information for further theoretical development through experiments on cellular systems.

Dose-Rate and Fractionation Theory

W. C. Roesch

Radiobiological experiments at the low doses and dose rates applicable to radiation protection are seldom possible because of the large number of subjects that are required. Thus, the theory of radiobiological phenomena at conventional laboratory doses and dose rates is important because it can enable confident extrapolation to the low doses and rates. We have been studying how changes in dose rate and fractionation of the low-LET radiations affect this extrapolation. This is important for the protection of workers and the public during energy generation by fission or fusion. Last year we reported studies of the effects of multiple biological repair processes that may strongly influence how radiation hazards are estimated. Much of the theoretical work this year was aimed at enlarging our understanding of the multiple processes.

When repair processes occur simultaneously, they can interact in different ways depending on what is being repaired and in what sequence the repair takes place. Last year's initial study (Roesch 1978a and 1978b) treated each possibility separately. This year, a general formulation of the theory was worked out that carries out as much of the event-time averaging as possible before introducing the characteristics of specific processes. This makes the theory much more compact and makes it easier to understand how the processes manifest themselves.

The general formulation also makes the study of new combinations of processes easier. One combination that was studied before, the two-step kinetic process, was extended this way to multiple-step kinetics. Investigation of these processes is important because for very high dose rates, the two-step model gives survival curves in which the logarithm of the surviving fraction is the sum of a quantity proportional to the first power of the dose and one proportional to the dose cubed. This is the only model known to do this. N-step models give a first power term plus an (N + 1)-th power term. These models may be helpful in understanding very radio-resistant organisms where such curves are typical. Figure 2.11 shows survival curves of such an organism, three of the strains of the slime mold Dicytostelium discoideum studied by Deering et al. (1970). The curve functions are square, cubic, and quartic, respectively.

Another combination of processes was suggested by our studies with Chlamydomonas reinhardi (Nelson, Braby and Roesch 1978). In split-dose (two fractions) experiments, $\ln(S_m/S)$ for the shortest interfraction time is consistently lower than for those times greater than 15 s. According to the models, it should not be lower. So far, we have not found any experimental factor that makes it lower; therefore, we have explored the possibility that it is due to a third fast repair process. The lower point implies a two-step kinetic, or similar, model. Figure 2.12 shows split-dose results calculated for C. reinhardi on the assumptions that either one of the recognized repair processes is two-step kinetic. Three possible values for the third mean repair time were used. The range of possible values is limited if the points <15 s are to be lower than the value expected for the simultaneous 2-min plus 25-min repair processes but higher

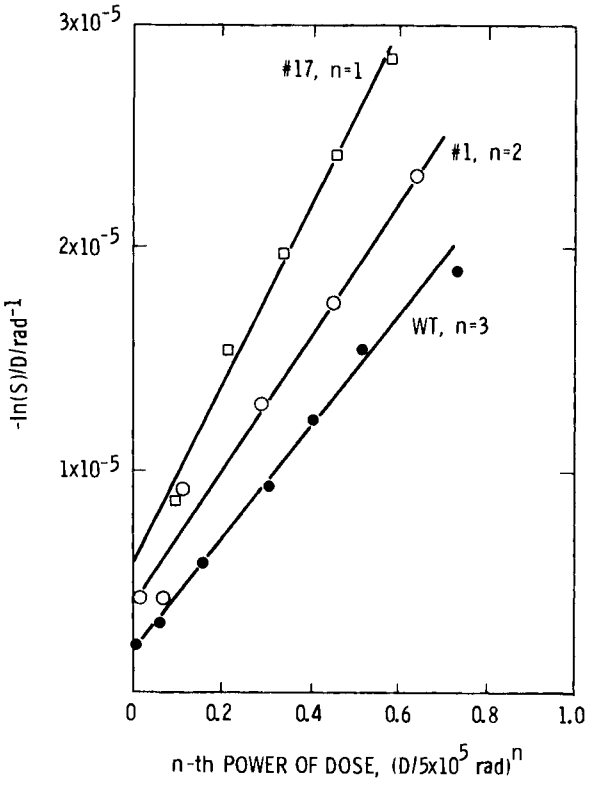

FIGURE 2.11. Survival Data for Three Strains of *Dicyostelium discoidem*, Presumed One-, Two-, and Three-Step Model Systems.

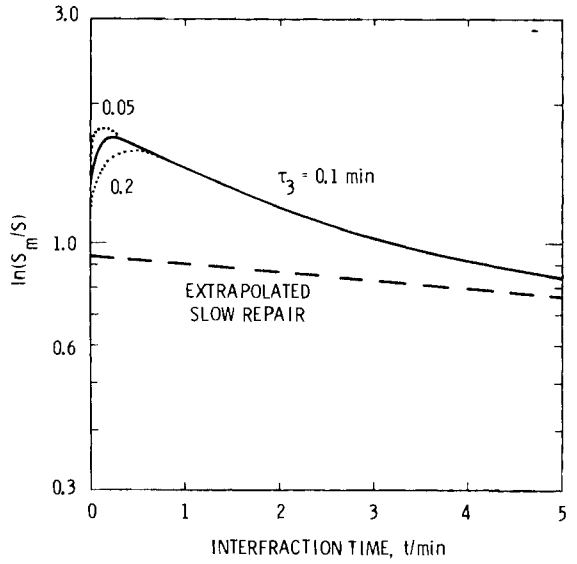

FIGURE 2.12. A Hypothetical, Third, Very Fast Repair Phenomenon in *Chlamydomonas reinhardi*.

than for a 25-min process alone; the range is about 5 to 30 s. These calculations indicate the feasibility of an experiment to demonstrate and measure a third repair process; we are modifying the electron accelerator to provide interfraction times in the required range of 1 to 30 s. Calculations of the survival at a given dose as a function of dose rate show the third process, after reaching a minimum, increases the survival with increasing dose rate, the reverse dose-rate effect. Detection of the increase would be another way to demonstrate the third process, but we believe the split-dose experiment would be easier and would provide a better determination of the third repair time.

The theory was also extended to split-dose experiments in which the dose is split into n fractions (where n is any integer) rather than just two fractions. This extension has application when interpreting very high dose-rate experiments in which many of the radiation machines operate with short radiation pulses. Trains of these pulses are used to give adequate total doses. The interval between pulses is much longer than the pulse length. Some radiation phenomena are so short lived that they disappear completely in the intervals between pulses. However, these phenomena are expected to give survival curves that are simple-exponential functions of the dose when analyzed with the theory extension. Most measured curves are not simple exponentials and, therefore, indicate the presence of longer-lived phenomena. Equations were derived for processes or combinations of processes of any repair rate.

The pulse-train theory gave an explanation for some previously puzzling data. Purdie et al. (1974) measured survival of Bacillus megaterium spores as a function of dose rate and pulse length. The inactivation constants (k) which they measured, shown in Figure 2.13a as a function of dose rate, were difficult to interpret. The theory predicts k should be a linear function of the dose (D_1) per pulse. Figure 2.13b shows this is indeed the case for all but one point. Other evidence suggests this point, at the highest dose per pulse, may be low because of the influence of radiolysis products.

A portion of our work was unrelated to multiple processes and dealt with the Laurie-Orr-Foster (LOF) model (Laurie, Orr, and Foster 1974). We were interested in the model for two reasons. First, it prompted us to measure the mean repair time for C. reinhardi by both split-dose and dose-rate methods (Nelson, Braby, and Roesch 1977) to seek evidence against the LOF pool model. We showed that the two methods give the same repair time, but we could not use this as

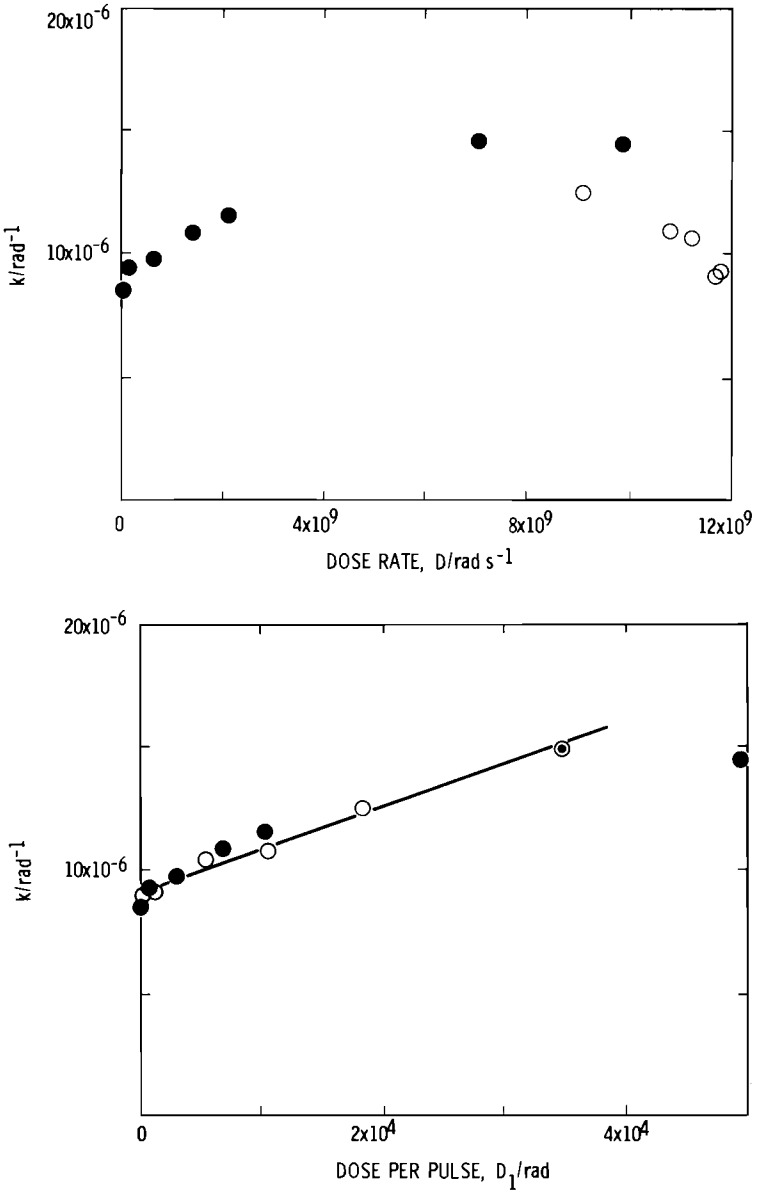

FIGURE 2.13. Theory of Pulse-Train Irradiation applied to *Bacillus megaterium* Spores. (a) unanalyzed data; (b) theoretically analyzed data.

evidence either for or against the LOF model. Consequently, we began a search for other conclusions of the model better suited to experimental test. We found that LOF survival curves show peculiar shapes at low doses but limited accuracy in survival measurements and interference by other repair modes make use of this fact difficult. However, we finally found a way to use the LOF survival curves that may work. According to the accumulation model, in a split-dose experiment, the quantity $(\ln(S_m S))/(D^2 e^{-bt})$ is a constant for a single repair process, which is about 2.6×10^{-8} rad^{-2} for the slow repair process in C. reinhardi. The solid line in Figure 2.14 shows this quantity calculated from the LOF model. At low survival, it is nearly constant and the right value; at high survival, however, it decreases. We think that improvements in our cell scanning and counting system will permit measurements of sufficient accuracy to show if the decrease actually takes place. The slow repair component can be isolated for this study by using interfraction times of about 5 min or more. The dotted lines are extreme estimates of the uncertainty in the calculation because of uncertainties in the choice of model

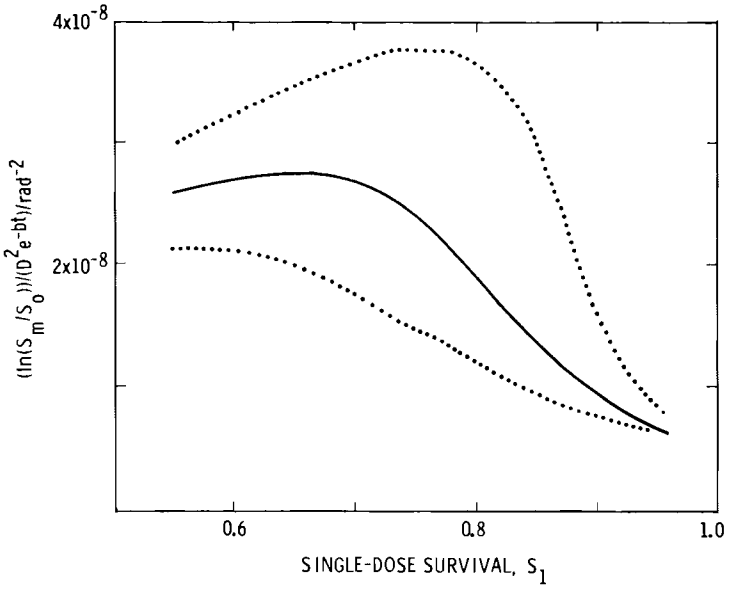

FIGURE 2.14. Prediction of the Laurie-Orr-Foster Model for Split-Dose Experiments with *Chlamydomonas reinhardi*.

parameters. These estimates do not change the conclusion of feasibility.

We were also interested in the LOF model because we used it in our dose-rate study (Brady and Roesch, in press). We showed in this study that data for C. reinhardi fall on a single curve for all dose rates as suggested by the accumulation model but not by other models. The LOF model reduces to coupled nonlinear differential equations that have not been solved numerically; thus, we had to use estimates of the model's behavior under limiting conditions to conclude that it did not produce a single curve. Further study convinced us that we could make better estimates for the model; the results are shown in Figure 2.15. The solid

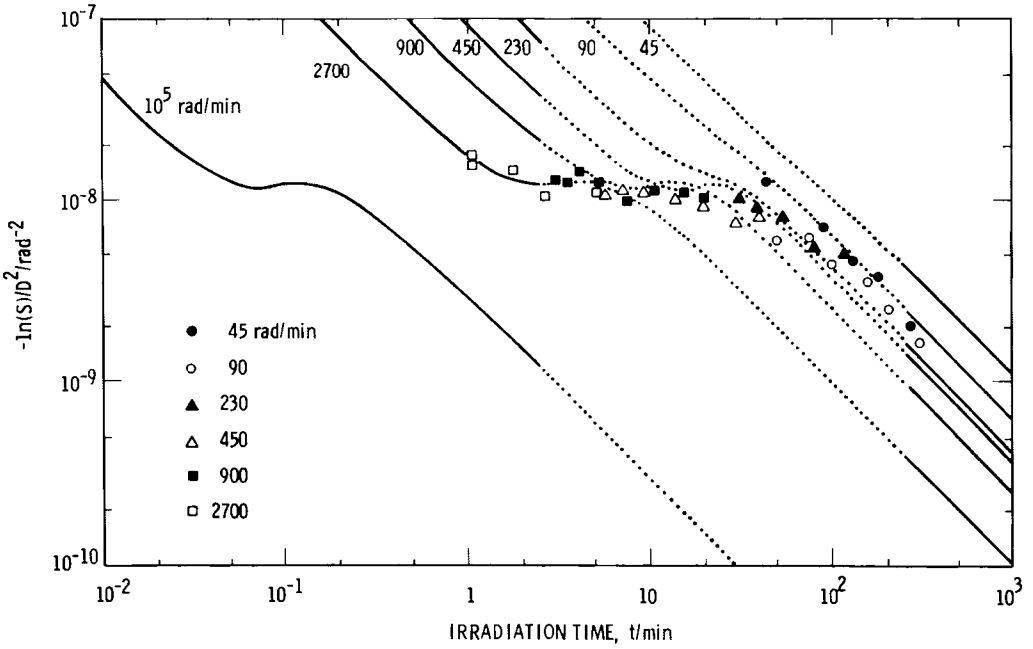

FIGURE 2.15. Prediction of the Laurie-Orr-Foster Model for a Dose-Rate Experiment with *Chlamydomonas reinhardi*.

lines are reliable estimates for very long and very short irradiation times. The dotted lines connect them in what we think is a reasonable way. At low dose rates, the estimates are so close, little uncertainty exists in the dotted lines. At high dose rates, the curves are more complex, but the shape must be like that shown for very high dose rates (the 10^{-5}rad/min curve). The figure shows that theoretically no single curve suffices for all dose rates, but that the practical choice of irradiation times and survival values has led to data points where the different curves are indistinguishable. Therefore, our argument for rejection of the LOF model is weakened. We still feel that detailed comparison of the model and the data will be unsatisfactory. We intend to calculate the actual curve of dotted lines so that we can make the comparison.

Cell-Cycle Modeling

W. C. Roesch

In 1976, we reported an n-step cyclic model of the cell cycle that proved useful for modeling the mitotic selection technique and the radiosensitivity changes during the cell cycle, as well as for investigating mathematical approximations for cell-cycle calculations. However, the model was based on a sequence of biochemical reaction steps to which all other occurrences in the cell cycle are related. While this is a reasonable foundation for a model, radiation or drug-induced changes in the cell-cycle may not be related to these fundamental steps.

The whole model, therefore, was revamped along the line suggested by von Foerster (Manson et al. 1975). The revision permits us to divide the cycle into any number of parts according to distinguishable features of the cells and to derive the density in age for each part from the distribution in transit times through that part of the cycle. Figure 2.16 shows an example calculated with the model: the densities in age for cells in G_1, S, G_2, and M for exponentially growing cells (age and time measured in units that make the mean cycle time unity). The dotted lines show the common "water-in-a-pipe" approximation. The disappearance of the discontinuities in the present model is due to the distribution in transit times. These distributions introduce the desynchronization lacking in the "water-in-a-pipe" model.

This model can be applied to theories explaining departure from the normal cell cycle. The only application of the model so far has been to our division delay experiments, where it is proving quite fruitful (Schneiderman, Braby, and Roesch 1977).

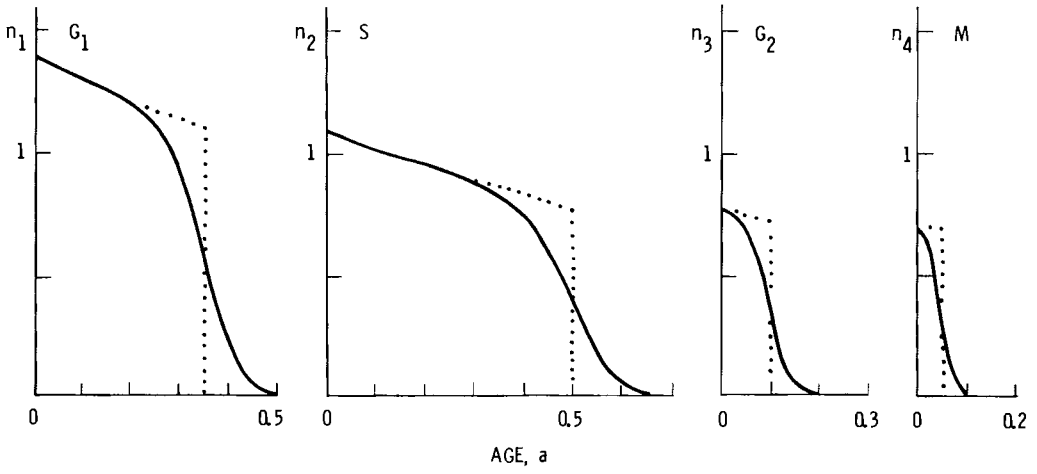

FIGURE 2.16. Example of the Densities in Age for Cells in the G_1, S, G_2 and M Phases of the Cell Cycle.

Rapid Repair Processes in Irradiated Chlamydomonas reinhardi

J. M. Nelson, L. A. Braby, and W. C. Roesch

The modeling of various combinations of two or more different repair processes and an extensive dose-rate and LET effects analysis of other models have been used to evaluate the effects of combined repair processes on the interpretation of split-dose and dose-rate experiments. The LET phenomena may, in fact, represent dose-rate effects where repair is very fast relative to the dose rates and radiation times typically employed for these kinds of studies.

A modeling prediction was that if the irradiation time for each dose in a split-dose experiment were comparable to the mean repair time, the survival after a single dose would be significantly less than that indicated by extrapolation from split-dose data. Such behavior was frequently observed in our experiments with Chlamydomonas reinhardi. This is shown in the upper part of Figure 2.17. Survival in terms of the

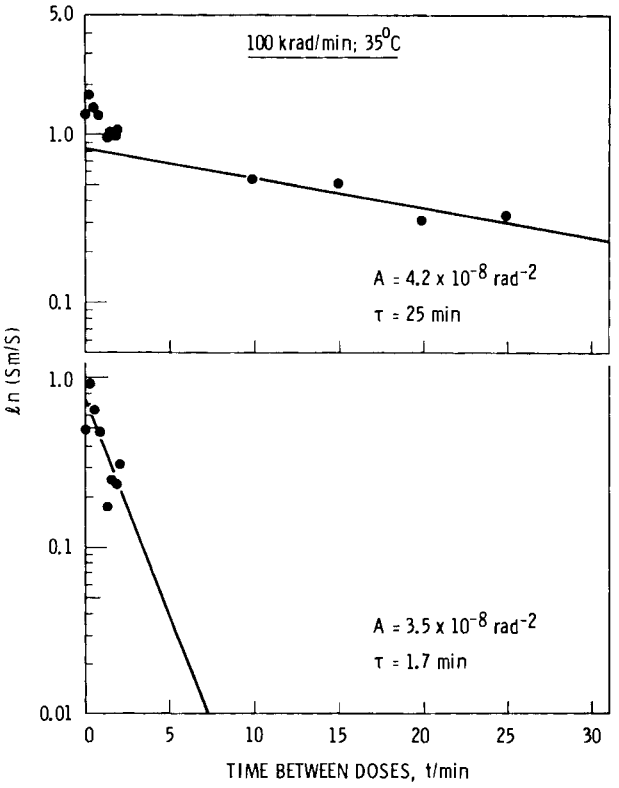

FIGURE 2.17. Results of a Typical Split-Dose Experiment Analyzed in Terms of the Accumulation of Damage Model and Plotted with the Logarithm of ln(Sm/S) as a Function of Time Between Doses. Sm is the square of the survival after a single fraction and represents the hypothetical maximum after two doses separated by an infinitely long interval. The two-event factor, A, and the mean repair time, τ, are parameters used in the accumulation model; see text.

The upper curve is fitted to those data points for intervals of 10 minutes or greater and corresponds to the conventional Elkind-Sutton repair process. The lower curve is fitted to points representing the net differences between the short interval data and the corresponding values extrapolated from the upper curve, and represents the rapid repair component.

logarithm of ln(Sm/S) has been plotted as a function of the time between doses, where Sm is the product of the survival after each of the single exposures in a split-dose experiment, which represents the hypothetical maximum survival after two doses that are separated by an infinitely long interval.

The suggestion of a second and more rapid repair process was investigated by conventional split-dose irradiation techniques using two equal doses, given at 100 Krad/min, separated by intervals as short as 15 s (see also Nelson, Braby, and Roesch 1978a). Surviving fractions of irradiated organisms were determined by a clonogenic cell assay method. The nonsurvivors were enumerated along with those cells that had retained their capacity for unlimited proliferation. Survival data were then analyzed with an accumulation of damage model (Roesch 1978b). With this model, the two-event factor, A (a measure of the probability of producing and expressing sublethal damage), and the mean repair time, τ (a measure of the average time required for repair of a sublethal lesion), may be estimated and analyzed independently. The model also makes it easier to separate the information corresponding to each process. Figure 2.17 illustrates the two concurrent repair processes, which have been separated.

Our experiments have demonstrated the existence of at least two independent repair components in exponentially growing cultures of this eukaryote. Futhermore, our experiments suggest that each process probably represents repair of a distinctly different kind of damage. As shown in Figure 2.18, the rapid process is characterized by a 2 to 4 min mean repair time, contrasted to 30 to 40 min for the slower Elkind-Sutton type repair at the same temperatures.

The existence of multiple processes that are associated with repair of sublethal damage and directly associated with reproductive integrity has been suggested by other workers. These studies have been thoroughly summarized by Nelson, Braby, and Roesch (1978b). Repair rates, however, had not previously been measured. Furthermore, a rapid component had been suggested only for noncycling plateau phase cultures of mammalian cells and had never been indicated before in a proliferating eukaryotic cell system.

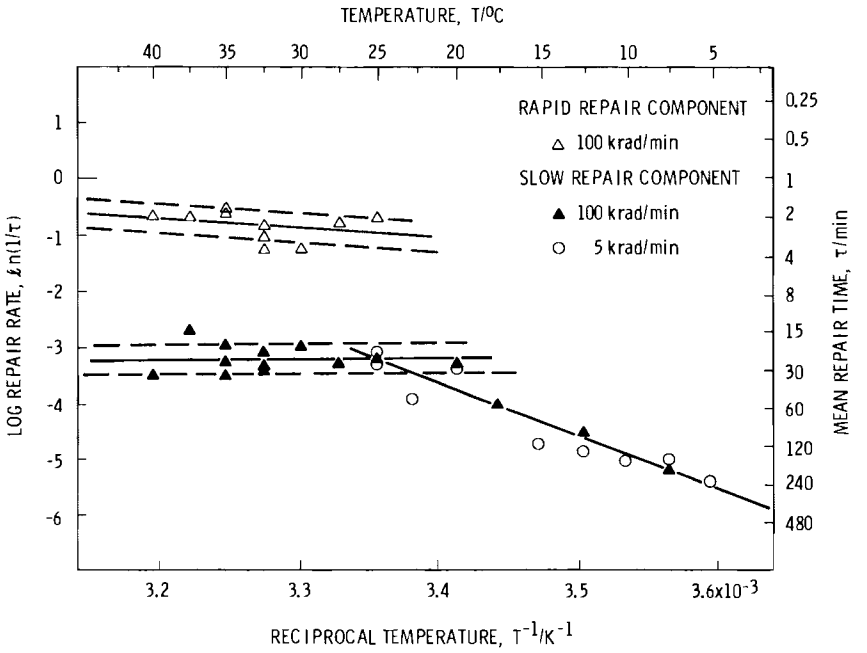

FIGURE 2.18. Arrhenius Plot of the Mean Repair Time (τ) for Both the Fast and Slow Components Where the Logarithm of the Repair Rate has been Plotted as a Function of Reciprocal Absolute Temperatures Above 25°C and Surrounded by the Standard Error of Estimation (dashed lines), a Regression Statistic Analogous to the Standard Deviation. Evidence for rapid repair has not been observed at temperatures below about 25°C.

Inactivation and Repair of Chlamydomonas reinhardi as a Function of Temperature

L. A. Braby, J. M. Nelson, and W. C. Roesch

As reported last year (Braby, Nelson, and Roesch 1978), we are measuring the radiosensitivity and repair rate of damage in C. reinhardi as a function of temperature. These measurements are necessary for comparing our results with those of other experiments that have been performed at different temperatures. These experiments also provide valuable information about the nature of the cellular response to radiation. Some of this work has been reported by Braby, Roesch, and Nelson (1977).

Last year's work provided good values for the parameters A and τ (the two-event factor and mean repair time, respectively) from 5^{o} to 25^{o}C; however above 25^{o}, substantial differences between results were obtained with dose rates of 5 and 100 Krad/min. These measurements have now been extended and we find that there is no reproducible difference in the value of τ for the normal repair process when measured using these two dose rates. Figure 2.18 shows the temperature dependence of A and τ for two repair processes over the range of 5^{o} to 40^{o}C. Above 25^{o}, values of τ become nearly temperature independent. The fast repair process has not been detected below 25^{o}C. The values of A, which essentially indicate radiation sensitivity, show more scatter than those of τ, suggesting a strong dependence of A on the cell's physiological condition. However, the radiation sensitivity of the cells appears to become less temperature dependent above 25^{o}.

Survival of Mitotic Mammalian Cells

J. M. Nelson and L. A. Braby

Roesch reported in a previous article in this report, "Cell-Cycle Modeling," that one aspect of the cell-cycle modeling has been directed toward the changes in radiosensitivity of mammalian cells during their cycle, and the study is intended to explore specific applications to

- synchronized populations
- exponentially growing populations
- noncycling plateau phase populations of mammalian cells.

Our experiments with fast repair processes in eukaryotes are intended to determine if there are processes in Chinese hamster ovary (CHO) cells similar to those found in Chlamydomonas reinhardi. Also, we are measuring survival of CHO cells irradiated during mitosis in order to test parts of the cell cycle model.

We have designed and assembled the necessary apparatus to aseptically select mitotic mammalian cells and establish synchronized populations of Chinese hamster ovary (CHO) cells that have been irradiated while in mitosis. We have also developed a computer-controlled video-microscope scanning apparatus that is needed to assess the viability and reproductive integrity of these treated cells. We can now select large numbers of mammalian cells at a very specific age within their cycle, irradiate them, and evaluate survival.

We are concerned only with cells that are of the same age at the time of treatment. Therefore, only those cells that have been irradiated in early mitosis are mechanically selected and transferred to a clean culture vessel. Although this selection process is relatively effective, it is not 100% efficient, and the small contamination by nonmitotic cells is not tolerable because it effectively invalidates the data. Consequently, a further selection process is performed with the scanning video-microscope. Cells passing through mitosis produce two daughter cells (doublets or twins) within a few minutes. This characteristic makes them morphologically identifiable from all other cells that have been transferred. By scanning the culture dish shortly after the mitotic cells have been plated, each doublet or twin can be clearly identified and the images of selected cells meeting this criterion are recorded on video tape. These recorded images are used as a reference when the cells' progeny are viewed later on. Only cells that have retained their capacity for unlimited proliferation and have demonstrated this fact by growing into clones of 50 or more viable cells within a period of five days are considered to be survivors.

Preliminary experiments using x-ray doses ranging from 37 rad to 250 rad indicate that mitotic CHO cells are a relatively sensitive population yielding survival parameters consistent with published values. These results are illustrated in Figure 2.19. They are plotted as survival in the conventional manner on the left and as negative ln(S)/D according to the accumulation of damage model on the right. Further mammalian cell experiments are currently underway to determine the existence of a rapid repair component of sublethal damage that would be analogous to that found in Chlamydomonas reinhardi.

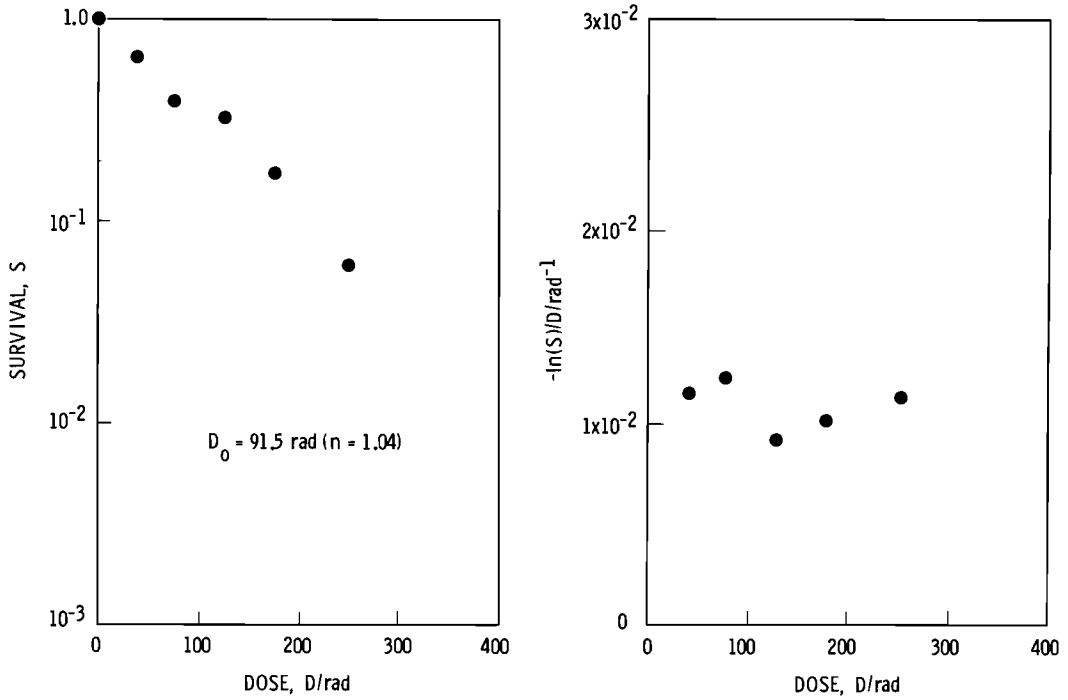

FIGURE 2.19. X-Ray Dose Survival Curves for Mitotic Chinese Hamster Ovary (CHO) Cells Selected Immediately After Irradiation and Identified as a Pure Population of Cells of Known Age. These results of a preliminary experiment have been illustrated both in the conventional manner (left) where survival is plotted (on a logarithmic scale) as a function of dose and as indicated by the accumulation of damage model (right) where -ln(S)/D is plotted as a function of dose.

Noncycling Plateau Phase Mammalian Cells

J. M. Nelson

As reported last year (Nelson 1978a) the algal eukaryote Chlamydomonas reinhardi has been used as a test organism in experiments performed to test models or to obtain modeling information. These cells are used because their radiation sensitivity does not change significantly as a function of time over an extended period. This feature permits the long exposures and interfraction intervals necessary in dose-rate or split-dose experiments. Also, the study of sublethal damage repair is possible.

In contrast, the radiosensitivity of proliferating mammalian cells changes rapidly. This prohibits their satisfactory application to these kinds of experiments. However, normal passage of mammalian cells through the phases of their cycle may be prevented and the cells can be arrested or synchronized in various ways. We believe we can use noncycling stationary populations of Chinese hamster ovary (CHO) cells in the same way as we have used C. reinhardi to study repair of sublethal damage. Although cells may be arrested at various positions in the cycle, we intend to use noncycling plateau phase cells. These cells are preferable to cells blocked in other ways that may cause extraneous or deleterious side effects from the blocking agents.

Techniques to stop logarithmic growth and establish a parasynchronous nonproliferating population of otherwise normal mammalian cells have been developed (see also Nelson 1978). These noncycling plateau-phase culture conditions may be induced either by nutritional deficiencies or by density and/or contact inhibition and, in fact, may represent a natural environmental state common to the normal physiology. Unfortunately, the existence of such a population density plateau is not in itself evidence of the noncycling or resting status or even of greatly attenuated growth. Some cell systems can maintain an equilibrium density in the presence of relatively high cellular turnover and a near normal renewal rate (Nelson 1978b). Therefore, much of our effort has been directed at determining growth parameters of plateau-phase CHO cells so that we can be sure we have induced a truly noncycling population.

Earlier experiments had shown that both density or contact-inhibition culture techniques as well as nutritional-inhibition culture techniques could result in true

noncycling stationary populations. These populations represented kinetically inactive equilibrium plateau states, their status having been determined by iodinated uridine (^{125}I-UdR) uptakes following appropriate labeling periods. These procedures give us a direct measure of DNA synthetic activity, a cellular function required for proliferation. Both culture techniques were found to yield a significantly depressed uptake of the uridine analog in the presence of large numbers of viable, metabolizing cells.

When comparing the two inhibition methods, however, one feature became apparent. Although DNA synthetic activity is equally suppressed in each case, the numbers of viable cells are considerably greater in density-inhibition cultures than they are in nutrition-inhibition cultures. In both case, the populations had been labeled for a 24-hr period. This gave us an index of participation in the DNA synthesis and an estimate of the fraction of cells that had incorporated the analog within the 24-hr period. This cell fraction is the cycling cells, and the relative values of these indices may be used to estimate the growth fraction of cycling cells in the population. We are aware of the complications associated with attempting to label noncycling populations, but we feel that a 24-hr uptake can be used to advantage to monitor this growth fraction.

Nutritional inhibition has some serious complications. In addition to lower cell numbers in this case, large variations were found in the ^{125}I-UdR uptakes, which makes prediction of kinetic status extremely risky. Furthermore, although these cells remained viable (as determined by dye-exclusion techniques), their ability to resume exponential growth behavior when replated after an extended period was greatly impaired. In contrast, density-inhibited cultures not only gave more definitive indications of cycling activity, but these cells readily entered exponential growth when replated at even lower densities. Unfortunately, data from these experiments were not sufficient to indicate the true extent of kinetic suppression nor the length of time that the population could persist under these conditions.

Further experiments that dealt only with density-inhibited plateau phase cells were performed to clarify these points. The medium was exchanged every other day, which is a realistic approach, but one that led to the sawtooth characteristics of the 24-hr label curve seen in the upper panel of Figure 2.20. Each point in this experiment represents a mean plus or minus one standard deviation with several replicate plates. The upper panel of Figure 2.20 shows that the relative 24-hr ^{125}I-UdR uptake had fallen to less than 0.1 to 0.2 percent of that measured during exponential growth. This implies that only 0.1 to 0.2 percent of the population had been labeled during a 24-hr period or that the uptake per cell had been reduced to 1 or 2 thousandths of that found in a normal cycling cell. The latter implication, of course, is not consistent with our current understanding of DNA replication. Similarly, 2-hr pulse labeling experiments, illustrated in the lower panel of Figure 2.20, indicate that DNA synthetic activity had been supressed to less than 1/2 of 1 percent. This would imply that either 0.5 percent of the population was going through S-phase or that the uptake per cell during DNA synthesis had been reduced to less than 0.5 percent of its normal value; again, the latter implication is not consistent with current understanding. Near the end of these experiments, the ^{125}I-UdR uptake in each case began to rise and became extremely variable. This can be seen in both the 2-hr and 24-hr labeled data curves in Figure 2.20. One explanation for this phenomenon is that the cell density is falling because of decreasing viability; such a cell loss situation would permit other cells to be recruited back into the proliferative cycle. Even at 32 days, most of the cells remain viable and actively metabolizing, determined by erythrocin-B dye-exclusion viability techniques. These cells rapidly resume logarithmic growth when replated.

Our experiments have conclusively shown that this population density plateau corresponds to a noncycling cell population, and these characteristics persist under conditions of high density contact inhibition for extended periods. The noncycling state is induced around the 14th day and persists for another two weeks. At the end of this interval, cells either die or lose their noncycling status and again synthesize DNA. It is during this two-week noncycling period that we will perform experiments to investigate phenomena associated with radiation repair processes.

The Oxygen Effect as a Tool for the Study of Repair Processes

L. A. Braby, J. M. Nelson, and W. C. Roesch

Two articles in this report "Dose-Rate and Fractionation Theory," and "Rapid Repair Processes In Irradiated Chlamydomonas reinhardi," have already discussed the relative values of the two-event factor, A, which is associated with the repair processes. These values provide information about the types of damage being repaired. However, the difference in the values of A are small under normal conditions for the two repair processes in Chlamydomonas reinhardi. Therefore, it is difficult to be certain that there is a difference in the values, and to determine the magnitude of the difference we have shown

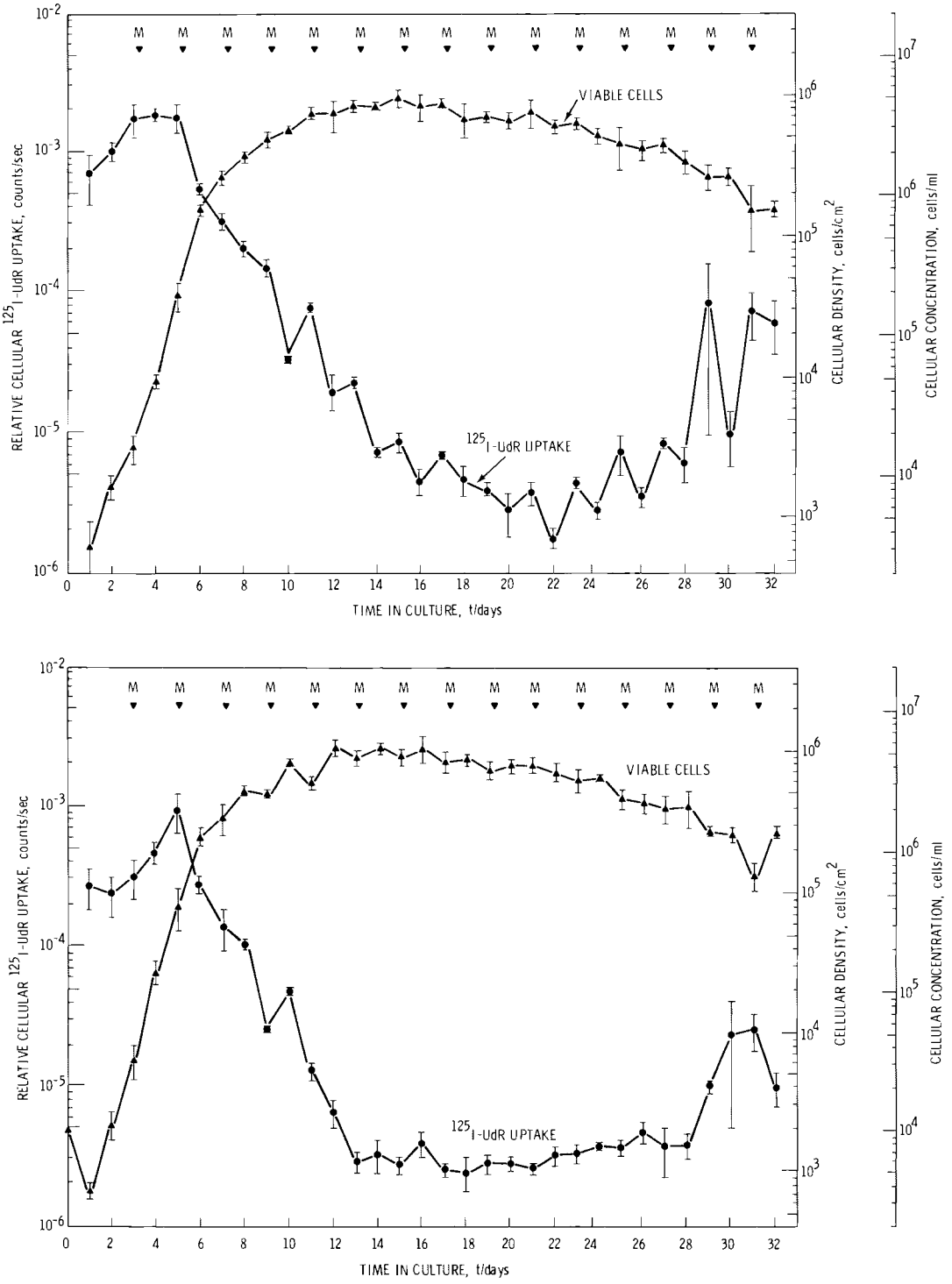

FIGURE 2.20. Relative Continuous Labeled (24 hours) ^{125}I-UdR Uptakes and Viable CHO Cell Densities (upper panel) and 2-Hour Pulse Labeled ^{125}I-UdR Uptakes and Viable CHO Cell Densities (lower panel) Plotted as a Function of Time After Plating. The radically reduced proliferative activity seen in both cases persists from abut the 14th day to the 21st day.

that the values of A measured in split-dose experiments seem to depend strongly on the physiological condition of the cells at the time of irradiation (see the article, "Inactivation and Repair of Chlamydomonas reinhardi as a Function of Temperature.") This observation suggests a possible method for determining the relative values of A for two or more types of damage. Oxygen concentration alters radiation sensitivity, hence values of A, but it does not affect the repair rate (Bryant 1970). Therefore, altering the oxygen concentration during irradiation may heighten the effect of one type of damage so that it can be studied with less interference from another.

Split-dose experiments are probably the most efficient and accurate way to determine values of A for two simultaneous processes; however, in anoxic irradiation, this method presents some complications. One problem is that a large number of dishes must be irradiated individually while all of the dishes are held at controlled oxygen concentration and temperature throughout the experiment. We have been able to do this by using a group of double-windowed nylon chambers each holding one 35 mm petri dish. These chambers are fitted with self-sealing serum bottle caps so that nitrogen inlet and outlet connections can be made with hypodermic needles without introducing significant air into the chamber. Oxygen in the exhaust is monitored using a fuel cell detector with 0.05 ppm oxygen sensitivity. Oxygen concentration in the exhaust gas was kept below 50 ppm during an electron beam irradiation of Chlamydomonas reinhardi in prototype chambers. This trial experiment resulted in an oxygen enhancement ratio of approximately 2.5 at 8 rad, which is about what would be expected based on data in the literature.

A Noise-free Determination of $\bar{z}_1$

L. A. Braby and W. C. Roesch

Currently evolving theories about the dependence of cellular radiation sensitivity on the energy transfer characteristics of charged particles generally employ microdosimetric concepts. A reasonable expectation is that some aspect of the energy absorbed in sites roughly the size and shape of the nucleus of a cell will be related to biological effectiveness. One such quantity is the mean energy deposited in single events, ($\bar{z}_1$) (Roesch 1978b, Booz 1978, and Kellerer and Rossi 1972). Unfortunately, $\bar{z}_1$ is difficult to measure for low stopping power radiation because the individual events may be as small as a single ionization and thus cannot be distinguished from the detector system noise. This leads to an unrealistic number of small events in measured single event distributions. We have developed a way to determine $\bar{z}_1$ that is essentially free of this noise. Related work has also been recently reported (Braby and Roesch 1978a and Braby and Roesch 1978b).

A common way of removing the noise in the $f_1(z)$ distribution when calculating $\bar{z}_1$ is to extrapolate the function linearly when plotted as $\ln z f_1(z)$ versus $\ln z$ (Booz 1978). Details of this extrapolation have little effect on the value of the dose mean, $\bar{z}_D$, because the events that are involved contribute little energy. However, because there may be many small events in the observed frequency distribution, the frequency mean, $\bar{z}_1$, can be affected significantly.

The function $f(z)$ may be measured directly by using the pulsing capability of the electron accelerator. Independent determination of the mean number of events, m, can be made so that the value of $\bar{z}_1$ results from the relationship $\bar{z}_1 = \frac{\bar{z}}{m}$. The function $f(z)$ is measured directly by making the accelerator pulse shorter than the resolving time of the wall-less proportional counter system. All of the ionizations in the detector that are produced by an accelerator pulse then contribute to a single detector pulse. If all of the accelerator pulses are of the same charge (Q), the $f(z)$ for the corresponding m is measured the same way that the distribution for single events is normally measured. Because m is the mean of a Poisson distribution, the mean number of events in the site, m, for a given size accelerator pulse can be determined by making the reasonable assumption that m is proportional to Q.

One way of testing for data consistency and for adequacy of the convolution technique is to measure $f(z)$ and Q at different values of Q and then perform the non-integral convolution of the distribution for the lower Q by the ratio of the Qs. Figure 2.21 illustrates the results of this for two spectra where z values were larger; that is, excessively small events were not encountered. The calculated spectrum was derived from one with $m = 4.9$ and calculated for $m = 30$ using a technique developed by Roesch (1971). The other spectrum was measured directly for $m = 30$. Small errors in the measurement of Q and limited statistics for the rare large events in individual spectra would be expected to result in increasing discrepancies between directly measured and folded spectra as the ratio of the involved Qs becomes larger.

The single event distribution can be calculated from the multiple event distribution using a Fourier transform deconvolution technique. This is practical only if a spectrum for $m \simeq 1$ is used as a starting point because

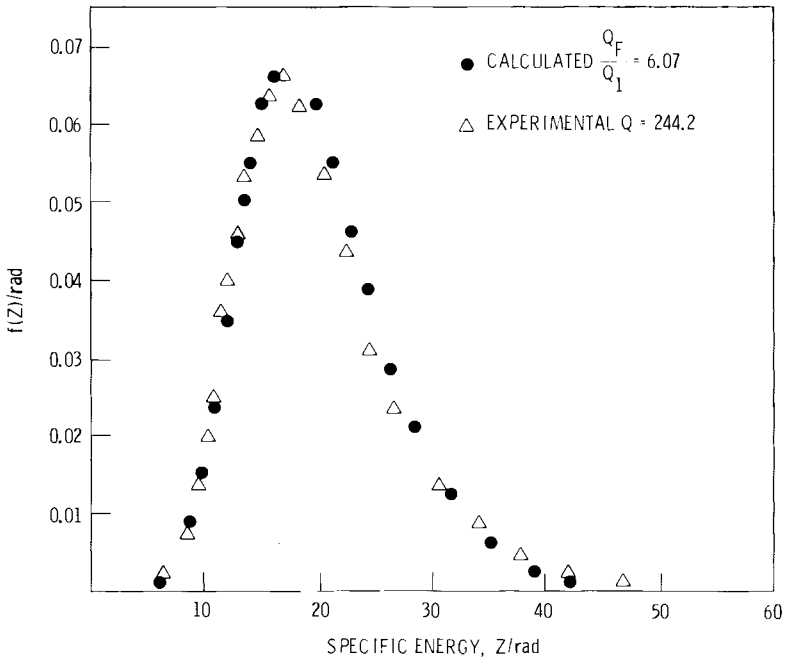

FIGURE 2.21. The Distribution, f(z), for Approximately 30 Events Measured Directly and Measured for m = 4.9 and Folded to m = 30; 1.0 MeV Electrons and a 1.89 $\mu g/mm^2$ Diameter Site.

of the decrease in information in f(z) as m increases. Figure 2.22 shows a comparison of the results of a single event calculation. The approximation to $f_1(z)$ was obtained by renormalizing f(z) for m = 0.12. Even for this small value of m, the effects of multiple

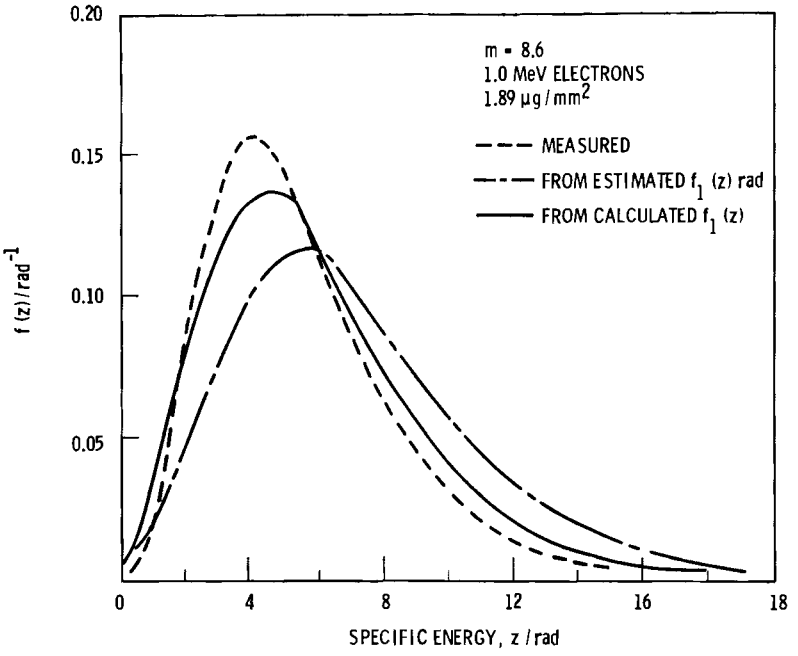

FIGURE 2.22. The Distribution, f(z), for m = 8.6 Measured Directly, Calculated from $f_1(z)$ Obtained by Deconvolution of f(z) for $m \simeq 1$, and Calculated by Renormalizing f(z) for m = 0.12.

events can be seen in the f(z) calculated for m = 8.6.

The best estimate for $\bar{z}_1$ is the quotient of the average of several values of $\bar{z}$ for large values of Q. The value of m is determined from a plot of α versus Q ($\alpha = e^{-KQ}$) for α in the range of 0.9 to 0.1. Table 2.2 presents values of $\bar{z}_1$ for the site sizes and energies that were measured.

TABLE 2.2.

Initial Electron Energy, MeV	Site Diameter, $\mu g/mm^2$ 1.2	1.9	2.8
	$z_1/20.4\ d^{-2}$		keV/μm
1		0.174	
1.5	0.121	0.151	0.171
1.8		0.191	
^{60}Co γ-Ray Energy 1.253	0.312[a]	0.332[b]	0.296[b]

[a]Goppola, et al., 1976
[b]Braby, et al., 1971

The values of $\bar{z}_1$ that we obtained for electrons are substantially lower than have been obtained in the past for ^{60}Co γ-rays (Braby and Ellott 1971). This should be expected because the electrons reaching the detector are essentially monoenergetic while the electrons from ^{60}Co irradiation have a broad spectrum with a mean initial energy of approximately 0.6 MeV. The measured $\bar{z}_1$ is somewhat lower than the stopping power of electrons of the corresponding energy probably because of the relatively narrow beam irradiation geometry. The beam diameter is limited by the detector geometry to about four times the detector diameter. Thus, some delta rays (slowed electrons) that would normally produce larger events escape the detector and a compensating number of events are not produced by tracks outside the site. This may also account for the observed increase in $\bar{z}_1$ with increasing site size.

Calculation of Energy Deposition and Ionization in Very Small Volumes

W. E. Wilson and H. G. Paretzke

The randomness that is due to the spatial distribution of the radiation interactions within a medium in the deposited energy in a microscopic absorber is of current interest in explaining radiobiological phenomena. Experimental methods for measuring energy deposition distributions have concentrated on the use of proportional counters to magnify the microscopic site dimensions to experimental dimensions by lowering the molecular density. Physical limitations effectively restrict the experimental technique to equivalent volumes of greater than about 0.1 μm dia; therefore, it is attractive to consider calculating the statistical distributions for very small sites (<0.1 μm dia). Presently, the only tractable method that retains the inherent stochastics for handling particle transport in charged particle track structure is the Monte Carlo method.

Accurate secondary electron data is required if the Monte Carlo method is to be useful in a quantitative sense. The most abundant and most accurate data for source terms come from experimental measurements in a gaseous phase. Therefore, the validity of calculations for condensed phase based on such source terms must be carefully established.

A new Monte Carlo code (MOCA13) has been developed. The code makes extensive use of experimental ionization cross sections and recent improvements in electron transport that are based on the critical evaluation of data on electron interactions (see the article, "Calculation of Ionization Distributions in Condensed Phase").

We have used the code to calculate energy deposition and ionization frequency distributions in spherical sites ranging from 1 to 200 nm dia for 0.25 to 3 MeV protons. The distributions are obtained for individual proton tracks intersecting spherical sites at specific impact parameters. Figure 2.23 presents a typical result for the mean energy imparted for a site of 100 nm dia for 1 MeV protons.

The quotient of the mean imparted energy and the site dia (mean event size) is plotted as a function of the position of the proton path and is compared with the product of expected LET energy deposition and the path length through the site.

For tracks passing through the site, the mean event size is less than the product of LET and path length because some energy is transported beyond the site boundary for energetic δ-rays. Likewise, δ-rays transport energy into the site from proton tracks passing outside the site; hence, the mean event size is not zero for impact parameters greater than the site radius. The quotient of the mean number of ionizations and the site diameter uses the ordinate scale at the right. The quotient of imparted energy and ionization is plotted as open circles in the lower part of the figure. A constant value of about 32 eV/ion pair is observed for tracks through the site. The value abruptly increases near the site boundary to over 36 eV/ion pair and then decreases slowly for

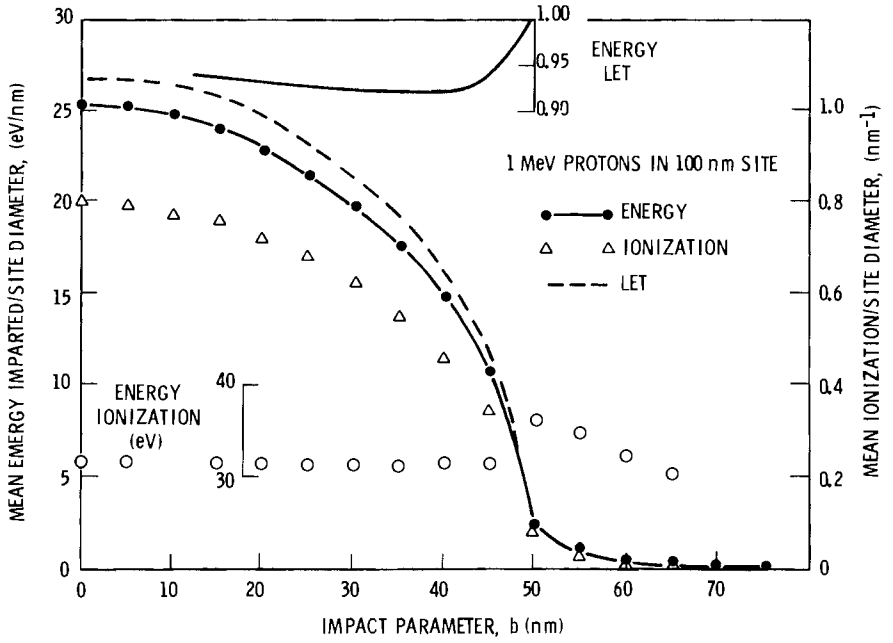

FIGURE 2.23. Calculated Mean Event Size for 1.0 MeV Protons Passing Through and Near a 100 mm Diameter Spherical Site at Distances b from the Center of the Site to Ionization; ---Ratio of Energy Imparted to LET Times Path Length.

—·—· Imparted Mean Energy
ΔΔΔΔ Mean Ionization
– – – – LET times relative path length
——— Ratio of energy imparted to LET times path length
oooo Ratio of energy imparted to ionization.

tracks passing beyond the site. The value of 32 is reasonable for tracks inside the site because it is close to typical W-values. The somewhat larger value outside the site but near its boundaries is attributed to the energy distribution of delta rays that are dominated by the large number of sub-ionization electrons. These electrons are able to contribute their energy to the site but do not themselves create much additional ionization.

Another interesting quantity is the quotient of mean event size and the LET-path product, (the ratio of the solid curve to the dashed curve). That ratio as a function of impact parameter is indicated in the upper portion of Figure 2.23. The ratio is almost constant at approximately 0.94 for the 100 nm site. It decreases slightly with increasing impact parameter out to about 0.8 of the site radius and then increases because the mean event size remains positive but the path length goes to zero at the site boundary.

These methods are providing us with quantitative data for energy deposition and ionization for sites too small (< 0.1 μm dia) for actual experimental determinations.

• Microdosimetry of Internal Sources

The purpose of this study is to develop practical methods for calculating microdosimetric distributions of plutonium or other alpha-emitting elements that are deposited especially as particulates in soft tissue and lung tissue. This study will aid the correlation and extrapolation of radiation effects measured at different levels of exposure and in different species. Computational methods will be developed and tested in the Radiological Physics Section. Concurrently, the Radiological Health Section will develop cell and tissue models in which those methods will be applied.

Calculations for Microdosimetry of Internal Sources

W. C. Roesch

The detailed theory behind the microdosimetry of internal sources was presented some time ago (Roesch 1977). It is mathematical and complicated. This year a simplified version was prepared for the 6th Symposium on Microdosimetry. This version is for those who are interested in using the technique but do not wish to become specialists in the details (W. C. Roesch in press). Essentially the same material was submitted to the task group on microdosimetry of the International Commission on Radiation Units and Measurements.

The new treatment proceeds by analogy with conventional microdosimetry and draws on the basic paper by reference for proofs. Conventionally, theoretical microdosimetry constructs densities in specific energy by adding the energies deposited in individual events while allowing for the stochastics in both the number of events and the energy deposited in each event. For application to internal sources, the same calculational methods are used to add energies. However, these energies correspond to individual occurrences of something else that is Poisson distributed, not to individual events. For example, the something else might be the number of particulates in the vicinity. Finding the energy depositions in individual occurrences requires a sequence of calculations of the same type. The sequence is the same as that used for the computer programs that perform the detailed calculations.

Many of the computer programs prepared for the microdosimetry of internal sources were rewritten in ASCII Fortran because of the change at Hanford from a CYBER to a UNIVAC computer. Subprogram calling arguments were left unchanged so that no revision is necessary when using the system.

Soft Tissue Modeling for Microdosimetrical Application

D. R. Fisher and J. L. Daniel

Work has proceeded in two phases on the development of a mathematical representation of deep lung tissue. This representation should lend itself well to descriptions of the specific alpha particle energy distribution. The project includes: analysis methodology development and data extraction from alpha track simulations.

The scanning control equipment for the "Quantimet" quantitative image analyzer was programmed to automatically measure the frequency distribution of cytoplasm, nuclei, and free air space encountered by simulated alpha particles. To prevent operator bias, the Zeiss Universal microscope automatically performed observations at random locations on specimen sections. Future programming will specify points of particle origin randomly along the interface of the alveolar lumen and the epithelium.

The probability of an alpha particle transecting a biologically sensitive nucleus and imparting a specific energy will be computed. This will be accomplished by incorporating information on the proportionate volume of the nucleus within the cell and the relative distribution of critical cell nuclei as a function of total nuclei in the field of view.

As the operational methodology is improved, a new series of data will be generated from slide specimens of healthy canine pulmonary tissue. This tissue was obtained under rigidly controlled pressure fixation and

staining conditions to permit characterization of tissue shrinkage. Multiple alpha particle track simulations should provide a statistical model of cell types and spatial distributions appropriate for microdosimetry calculations.

• Dosimetry of Internal Emitters

This program provides radiological and dosimetric guidance and support to radiobiological studies at PNL. The program considers radiological design of experiments and materials and includes theoretical and experimental dosimetry to various tissues and organs. These data are then related to observed biological effects. In particular, absorbed dose was calculated and measured in experiments that are attempting to develop dose-effect relationships for ^{238}Pu particle exposures in beagle dogs and ^{85}Kr gaseous exposures to rats.

Dosimetric Support of Radiobiology Studies

R. L. Roswell,* G. W. R. Endres,*
F. T. Cross** and D. W. Murphy*

Work on the calibration of thermoluminescent dosimeters (TLDs) to measure ^{85}Kr was continued from last year in support of the Toxicology of Tritium and the Noble Gases Program. Previous experiments comparing the dosimetry of ^{85}Kr and ^{36}Cl solutions did not show consistent agreement, although they should have because they have nearly identical beta energies and spectral shapes. These experiments were performed with suitably prepared solutions of ^{85}Kr and ^{36}Cl and measured with a phoswich detector consisting of a NaI crystal and a thin CsI crystal.

Calibration experiments were then continued using several modes of exposure. TLDs were left bare, wrapped in plastic film or in aluminum foil. Some were back-shielded with lead. Exposures to ^{85}Kr gas were made in the center of a 6-ft (1.8 m) dia plastic enclosure that simulated an essentially infinite beta cloud. The TLDs were suspended in the cloud in a 2 in. x 2 in. (5.1 cm x 5.1 cm) matrix. These experiments established a good comparison between the bare, unshielded TLD measurements in the ^{85}Kr air mixture and the TLD measurements in a ^{36}Cl solution.

The TLDs may sometimes have to be implanted in animals, and therefore have to be covered. Further experiments are being pursued that explore the effects on TLD response by covering them with various materials. The bare or unshielded TLD calibration for ^{85}Kr was successfully used to determine surface dose to rats in geometries not simulating the infinite cloud exposure.

*Occupational & Environmental Safety Department
**Biology Department

Dosimetry support was also provided to a study investigating the effects of single, large ^{238}Pu particles in beagle dogs' lungs. When the animals died, after approximately ten years exposure, μCi amounts of the isotopes in the particles were determined. Also, the effect on dose, dose rate, and change in photon spectra as a function of tissue thickness was measured.

To determine the effect of tissue thickness on dose, dose rate, and photon spectra, experiments were performed with a variety of detectors in several geometries. First, the lung lobe containing the particle was placed on a matrix of TLDs. An estimate of the dose rate for that tissue depth and the particle position were obtained. Second, the 60 keV ^{241}Am energy peak was measured at specific tissue thicknesses with a NaI detector as the lobe was dissected to obtain the ^{238}Pu particle. The NaI detector was again used to study shielding effects with and without interposed phantom tissue sections. The results from these two experiments proved to be comparable with the same ^{238}Pu particle in a glass vial. Third, the photon spectrum of the particle was measured with a high resolution Ge(Li) detector. Tissue equivalent plastic (TEP) was interposed in 5-mil increments up to 100 mils (~2.5 mm) between the detector and the particle, which was in a glass vial. The results of the experiments demonstrated that L x-rays were heavily absorbed in the 0.1 in. (2.5 mm) radius sphere surrounding the particle and thus were the reason for the necrosis of tissue observed in the animal. In a final experiment, the particle was placed in a beagle dog phantom at the position corresponding to its location in the dog lung. TLDs were placed throughout nearby lung and liver tissue. The dose rate measured immediately adjacent to the particle was 3.2 mrad/hr while at approximately a one-in. (2.5 cm) tissue depth the dose rate was 0.03 mrad/hr, or approximately twice background.

The NaI detector was used to determine the amount of ^{241}Am in the ^{238}Pu particle. One such particle contained approximately 0.075 μCi of ^{241}Am by this measurement. In addition, spectral data obtained from several Ge(Li) detectors were used to determine isotopic amounts of ^{238}Pu and ^{241}Am in the particles. These data yielded 55.5 μCi ^{238}Pu and 0.063 μCi ^{241}Am for the above case.

• Real-Time Measurement of Pu in Air at Below-MPC Levels

A direct-inlet mass spectrometer is being developed for monitoring low-level airborne plutonium on a real-time basis. The instrument will be capable of measuring plutonium concentrations below the maximum permissible concentration (MPC) level. Modifications to the instrument have reduced hydrocarbon background. A technique for electropolishing the bore of the direct-inlet capillary tube has been developed. Particle bouncing from the ionizing filament has been encountered while calibrating the instrument to provide particle size information.

Direct-Inlet Mass Spectrometer Development

J. J. Stoffels

Current techniques for monitoring airborne plutonium are limited by the rate of radioactive decay which, for ^{239}Pu, amounts to only one disintegration per second for every 10^2 atoms present. A new technique using direct-inlet mass spectrometry is being developed. It will measure one ion count for approximately every 10^2 atoms of ^{239}Pu present and will do this on an individual particle basis. The direct-inlet mass spectrometer (DIMS) and the direct-inlet mass spectrometric technique we have developed are described in previous PNL Annual Reports.

Work that is aimed at defining and controlling the parameters that affect the performance of different inlet capillary tubes has been continued. Examination of the capillary bore showed that its surface is quite rough (see Figure 2.24a). It is possible that this surface roughness induces turbulence in the air flow through the capillary. To eliminate this possibility, a technique for electropolishing the 0.013-in. diameter bore has been developed.

A special electropolishing fixture has been designed and built. It holds the stainless steel capillary tube straight, supports a 0.004-in. dia cathode wire on the axis of the tube, and provides for continuous pumping of electrolyte through the annular space between the cathode and tube. After experimenting with various electrolytes, a mixture of 80% acetic acid and 20% nitric acid was found to be best. It was necessary to pulse the current on and off to obtain uniform electropolishing action along the length of the tube. The polished bore has a surface that is uniformly smooth and bright (Figure 2.24b) with only microscopic flaws.

Further work to minimize hydrocarbon spectral interferences in the mass spectrometer has been completed. The turbomolecular pump on the ion source chamber was a major source of hydrocarbon contamination in the spectrometer. Backstreaming of the lubricating oil from the turbopump occurred whenever the pump was stopped to vent the ion source chamber. A gate valve was installed that allows the turbopump to run continuously under vacuum while the ion source chamber is vented. Also, the hydrocarbon lubricating oils that were used in the vacuum pumps have been replaced by fluorocarbon fluids.

Instrument calibration to measure particle sizes revealed an important problem. Some of the particles bounce when they strike the ionizing filament. This effect was observed while performing efficiency measurement with large (5-15 μm physical diameter) UO_2 particles. The measured efficiency (ions detected/atoms in the particle) for such particles that entered via the capillary inlet was five to six orders of magnitude lower than the efficiency for particles preloaded directly on the filament.

Particle bouncing on impact with the hot filament appears to be related to particle size and melting point of the material. The efficiency for 0.3 μm diameter CeO_2 particles entering via the inlet was 10 to 100 times greater than the efficiency for the large UO_2 particles, even though the melting point of CeO_2 is higher. Studies with 0.1 μm diameter Fe_2O_3 particles showed that a visible layer of this material, which has a considerably lower melting point, would accumulate on the hot filament.

We shall continue to investigate the extent of the particle bounce problem and, if necessary, shall devise methods to overcome the problem.

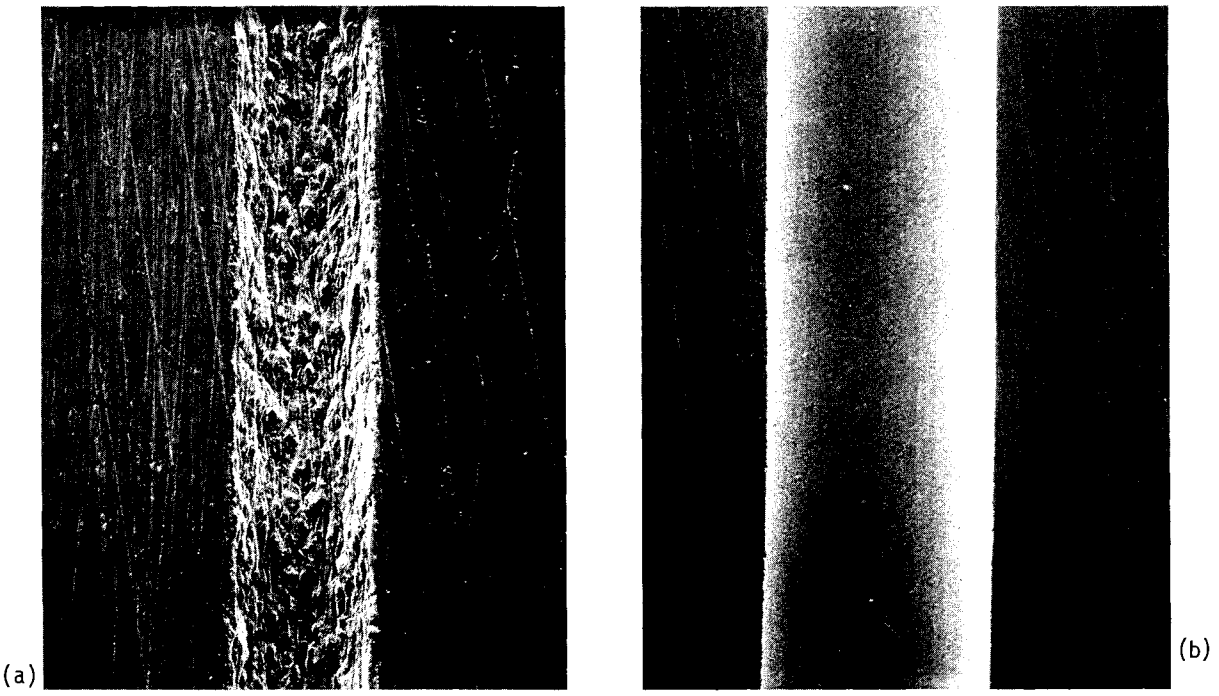

FIGURE 2.24. Bore of Stainless Steel Capillary Tubing: a) before electropolishing, 0.20-mm ID; b) after electropolishing, 0.30-mm ID.

• Analytical Techniques for Measurement of ^{99}Tc in Environmental Samples

Three new methods have been developed for measuring ^{99}Tc in environmental samples. The most sensitive method is isotope dilution mass spectrometry, which allows measurement of about 1×10^{-12} grams of ^{99}Tc. Results on analysis of five samples by this method compare very well with values obtained by a second independent method, which involves counting of beta particles from ^{99}Tc and internal conversion electrons from ^{97m}Tc. A third method involving electrothermal atomic absorption has also been developed. Although this method is not as sensitive as the first two techniques, the cost per analysis is expected to be considerably less for certain types of samples.

Ultrasensitive Measurement of ^{99}Tc

J. H. Kaye

From an environmental and hazard viewpoint, ^{99}Tc is one of the most troublesome radionuclides produced through nuclear fission. This is due to its long half-life (2.13×10^5 years), the volatile nature of the heptoxide, the mobility of the pertechnetate ion in aqueous solution, the high fission yield (over 6%), and the affinity of several organs of the human body for this element. Furthermore, technetium is almost impossible to detect at very low levels by direct counting methods because its half-life is long, and because it emits only low-level beta radiation.

The main purpose of this study is to develop more sensitive methods for the detection of ^{99}Tc than are currently available. We have made a great deal of progress. We can now measure as little as 1×10^{-12} g of ^{99}Tc by isotope dilution mass spectrometry in vegetation samples. We have also developed a quantitative counting method, and have evaluated use of the electrothermal, graphite-furnace atomic absorption technique for measuring ^{99}Tc.

This year we have successfully developed and evaluated a chemical procedure for isolating technetium in high purity from vegetation samples. Overall chemical yields of about 50 percent were obtained for technetium loaded onto a mass spectrometer filament. Analysis of a reagent blank yielded a value of less than 0.1 picograms (pg) of ^{99}Tc, as determined by mass spectrometry. However, measurements of ^{99}Tc by mass spectrometry for samples containing less than 1 pg of ^{99}Tc are not yet reliable. This is because we do not yet understand how the counting rate at the mass 99 position varies with time for samples that contain very small amounts of ^{99}Tc. This problem needs further study.

In addition to the mass spectrometric method, a counting method for measuring ^{99}Tc was also developed. This was done after it was discovered that the ^{97}Tc isotopic tracer contains a measurable amount of the 89-day isomer, ^{97m}Tc. By taking two counts on each sample after electrodeposition of the technetium onto an iridium foil, with and without a 13.9 mg/cm^2 aluminum absorber, both the chemical yield and the amount of ^{99}Tc in the sample can be determined. The electrodeposition step is already an integral part of the mass spectrometric analysis procedure, so if the ^{99}Tc level is above the detection limit of the counting technique (15 pg), it is possible to obtain two independent ^{99}Tc measurements on the same sample. This counting method may also be used as a screening technique to determine whether the more sensitive mass spectrometric method is required. If not, the man-hours required for the analysis are cut approximately in half.

A graphite-furnace, electrothermal atomic absorption technique for detecting ^{99}Tc was also evaluated. A detection limit of about 6×10^{-11} g was obtained for this method. This study used a special hollow cathode containing 4.5 mg of ^{99}Tc and a commercially available, demountable hollow cathode lamp employing neon fill gas. The results of this study are being published (Kaye and Ballou in press).

Seven samples have been analyzed for technetium content using both the counting and

mass spectrometric techniques. These samples included one standard containing 100 pg of ^{99}Tc, one reagent blank, one pre-atomic-age alfalfa sample and four samples taken from the vicinity of the Hanford fuel reprocessing facilities (200 Area). An additional standard, a second pre-atomic-age alfalfa sample and six more samples from the 200 Area, were analyzed by the counting method only. The results and the good agreement obtained between the counting method and the mass spectrometric method are illustrated in Figure 2.25.

A paper on the mass spectrometric method was presented at the Third International Conference on Nuclear Methods in Environmental and Energy Research, held in Columbia, Missouri October 10-12, 1977 (Kaye, Rapids, and Ballou 1978). Two additional papers were presented at the 22nd Conference on Analytical Chemistry in Energy Technology held October 10-12, 1978 Gatlinburg, Tennessee (Kaye, Ballou, and Rapids 1978a and 1978b).

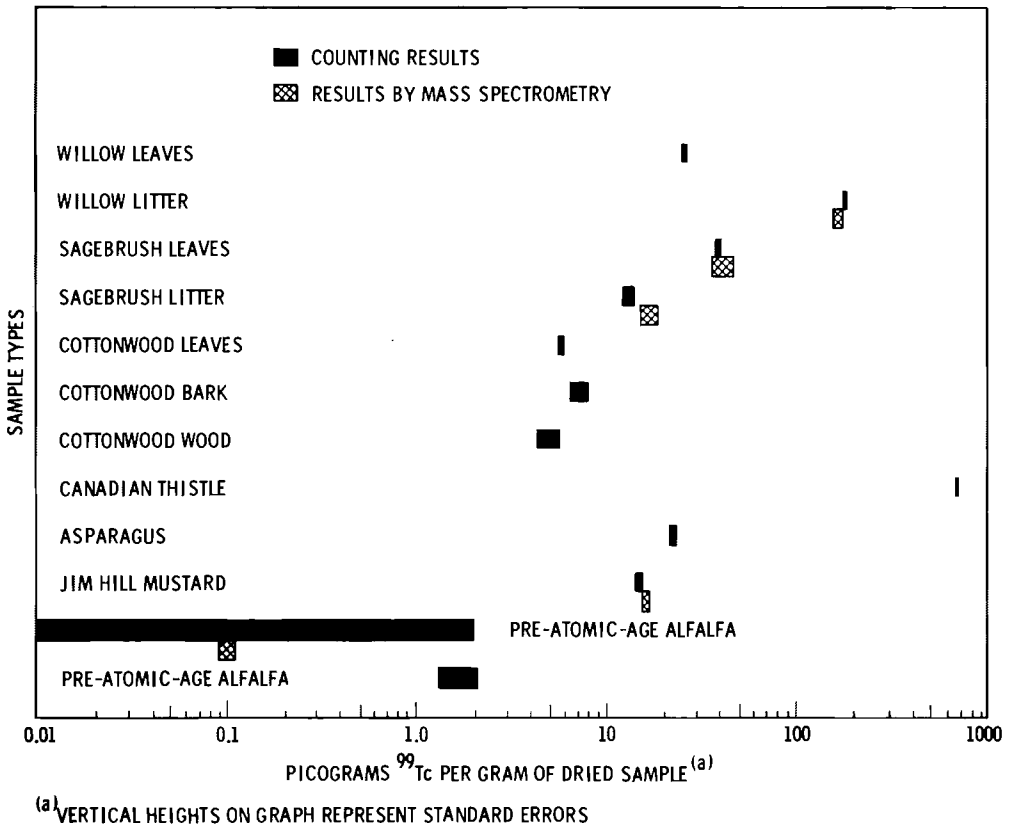

FIGURE 2.25. ^{99}Tc Levels in Vegetation Samples from the Hanford 200 Area.

• Radiation Instrumentation—Radiological Chemistry

Program efforts were concentrated in the following areas: development of low-level radiochemical laboratory techniques, in-situ monitoring techniques, and activation analysis technology.

Computer-Controlled Cyclic Activation Analysis with a $^{252}Cf/^{235}U$ Subcritical Multiplier

N. A. Wogman and H. G. Rieck, Jr.

A computer-controlled cyclic ^{252}Cf activation analysis facility has been developed for routine multielement analysis of a wide range of solid and liquid samples. The radiation facility contains six sources of ^{252}Cf totaling about 80 mg. These sources are placed in a 93% ^{235}U-enriched uranium core which is subcritical with a K effective approaching 0.985. The system produces thermal and fast fluxes shown in Figure 2.26. The thermal and fast neutron fluxes are relatively constant over a 25 cm vertical distance from the center of the core. This allows bulk samples to be irradiated with a constant flux. A computer-controlled pneumatic rabbit system which enters the center of a flux trap permits automatic irradiation, decay, and counting regimes to be performed on samples. The activated isotopes are analyzed through their photon emissions with solid state and NaI(Tl) gamma-ray spectrometers. Two Ge(Li) diodes with a combined efficiency of 50% record coincidence photons and act as a total absorption spectrometer for the cyclic activation analysis. A TN 11/10 system controls the number of cycles, decay periods, counting

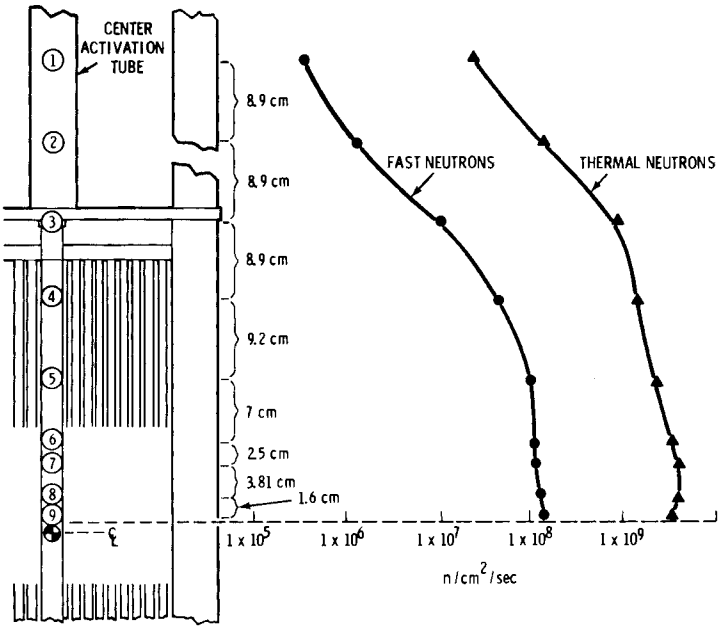

FIGURE 2.26. Flux Map for Computer-Controlled Cyclic Activation Facility, March 10, 1978.

times and samples that are to be inserted into the irradiation or counting system per user definition. The flow chart for the simultaneous counting and irradiation control of the pneumatic samples is shown in Figure 2.27. The cyclic approach to activation analysis is particularly useful for short-lived radionuclides whose half-lives are in the range of seconds to minutes. Computer programs involving a comparison of standards and unknown spectra are used in a PDP 11/35 to determine the quantity of each element present in the indicated material.

case, the radioactivity produced by the primary element is maximized with respect to the radioactivity induced in all elements present. With the existing computer system and irradiation analysis facility, the first irradiation cycle provides an indication of the elements and concentrations present in the sample. These data are then used to determine for a specific element the best irradiation time, analysis time, decay time, and number of cycles. This irradiation analysis program should provide increased capability to the subcritical system with its computer control.

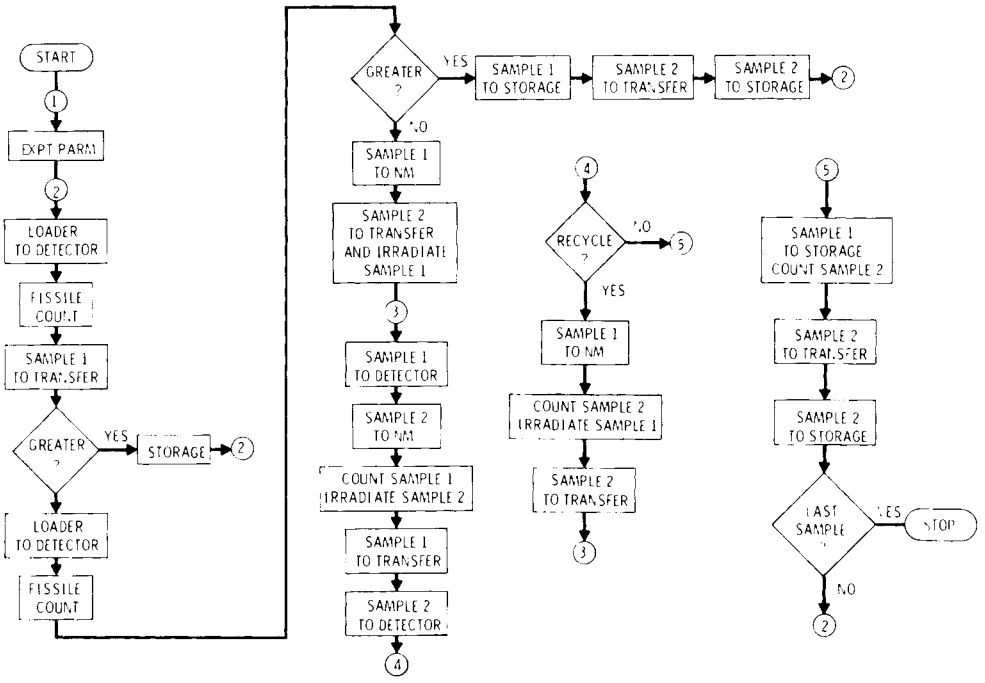

FIGURE 2.27. Flowchart for Simultaneous Count/Irradiation Control of Neutron Multiplier Pneumatic Sample Transfer System.

The subcritical multiplier has also been standardized for matrices and elements of interest. This allows a direct calculation of the desired elements in a sample matrix without a specific standard being used in the irradiation. This approach is used in cyclic activation analysis where the number of cycles involving irradiation-decay-count periods may be as high as 100.

The present computer program is being modified to include a complex program similar to the program called "Aardvark" written by Eisenhower et al. (1964, 1965). The modified program allows the analyst to determine the optimum conditions for irradiation and decay time for single and multiple cycles. In this

Trace Rare Earth Analysis by Neutron Activation and Gamma-Ray/X-Ray Spectrometry

J. C. Laul, K. K. Nielson and N. A. Wogman

Studies of rare earth element (REE) behavior in biological materials are important because such studies may provide information on the long-term behavior of transuranic analogs of the rare earth elements in the natural environment. The rare earth element concentrations in biological samples are at or below the parts-per-billion level. Detection at such low levels requires a rare earth element group separation scheme, followed by photon energy analysis using Ge(Li) and intrinsic germanium detectors. Table 2.3 summarizes

the most favorable counting techniques for rare-earth analysis.

The data shown in Table 2.4 were obtained using USGA samples BCR-1, W-1, AGV-1, G-2, GSP-1, and PCC-1; IAEA soil 5; and NBS orchard leaf and bovine liver standards. Precision for this group of elements based on duplicate analyses of BCR-1 is about 5%. Estimated errors based on counting statistics are from 1-5% for geological samples and 1-10% for biological samples.

The rare earth separation scheme, in conjunction with a selected detector system for each rare earth element, allows studies to be pursued on the rare earth patterns in orchard leaf and other plants, in biological material, and in geological media.

TABLE 2.3. Counting Techniques for Rare Earth Analysis.

Counting Technique	Rare Earth
Ge(Li) X-Ray and Gamma-Ray	^{140}La, ^{141}Ce, ^{142}Pr, ^{153}Sm, ^{171}Er, ^{177}Lu
Intrinsic Germanium Gamma-Ray	^{143}Ce, ^{147}Nd, ^{160}Tb, ^{166}Ho
Intrinsic Germanium X-Ray	^{152}Eu, ^{175}Yb
Ge(Li) Gamma-Ray or Intrinsic Germanium Gamma-Ray	^{153}Gd, ^{170}Tm

A Low Background Summing Gamma-Ray Spectrometer

N. A. Wogman

An anticoincidence shielded gamma-ray spectrometer has been constructed using a 24 cm diameter x 23 cm thick NaI(Tl) activated crystal. It has a well of sufficient size to accommodate a 500 ml polyethylene bottle. This crystal was fabricated from low background materials. The NaI(Tl) material was proven to be free from uranium and thorium at the sub-ppb level. The calcium carbonate that was used as packing and reflector material was proven to be free of potassium, thorium, and uranium at the ppb level. The iron that was used to encase the crystal system was from pre-World War II oil

TABLE 2.4. Rare Earth Abundances (ppm) in USGS Geological, IAEA Soil-5, and NBS Orchard Leaf and Bovine Liver Samples.

		La	Ce	Pr	Nd	Sm	Eu	Gd	Tb	Ho	Er	Tm	Yb	Lu
USGS														
BCR-1	(52/19)[a]	26.0	53.7	7.3	29.7	6.61	2.00	6.7	1.05	1.30	3.7	0.60	3.46	0.52
		25.5	55.0	7.1	30.3	6.58	1.95	7.0	1.04	1.21	3.5	0.54	3.43	0.53
W-1		10.9	24.4	3.0	13.6	3.30	1.10	4.3	0.61	0.75	2.4	0.37	2.10	0.31
AGV-1	(74/19)	37.1	70.3	9.9	32.8	5.30	1.51	5.4	0.63	0.60	<2	0.25	1.70	0.24
G2	(108/15)	89.1	155	21.4	57.4	7.24	1.40	4.6	0.42	0.34	<2	0.23	0.80	0.10
GSP-1	(17/22)	180	395	44.4	187	25.0	2.20	14.6	1.20	1.20	<5	0.40	1.78	0.23
PCC-1	(2/1)	0.034	0.075	7.0E-3[b]	<0.04	5.4E-3	1.0E-3	<0.01	1.3E-3	2.9E-3	<0.05	4E-3	0.025	4.8E-3
IAEA														
Soil-5		26.7	59.0	6.9	28.0	5.30	1.20	5.0	0.71	0.75	2.2	0.34	2.30	0.34
NBS														
Orchard Leaf SRM #1571		1.0	0.90	0.23	0.57	0.10	0.021	0.10	0.013	0.013	<0.1	<0.01	0.025	3.3E-3
Bovine Liver		0.017	0.021	<3E-3	<0.02	1.5E-3	3.0E-4	<3E-3	1.9E-4	2E-4	<5E-4	<2E-4	2.9E-4	3.8E-5
SRM #1577		0.017	0.022	<5E-3	9.0E-3	1.7E-3	4.0E-4	1.8E-3	1.7E-4	<3E-4	<5E-4	1E-4	2.8E-4	3.9E-5

[a] (Split/Position)
[b] E is base to 10.
Upper limits are based on 3σ value.

tanks and contained only ppb levels of uranium, thorium, and less than 1 disintegration per minute (dmp) ^{60}Co per kg iron.

The crystal was attached to a 24 cm dia x 5 cm thick NaI light pipe that was also encased in the same high purity iron. Four glass phototubes were coupled to the crystals with 5 cm dia x 30 cm quartz light pipes. This quartz was free of thorium, potassium, and uranium at the ppb level. The entire crystal assembly was enclosed in a 90 cm dia x 90 cm thick plastic phosphor* which served as the anticoincidence annulus. A 10 cm thick 5 wt% boron paraffin shield that reduced background contribution from external radiation and cosmic-produced neutrons was located between the plastic phosphor and the 10 cm lead shield. The lead shield reduced background contribution from external radiation.

The use, in Figure 2.28, of low background construction materials has reduced threefold the background in the energy region 0.1 to 4 MeV over that of a normally manufactured NaI(Tl) crystal (Wogman, Robertson and Perkins 1969). This threefold reduction over the entire energy spectrum indicates that internal radioactive species have been deleted from the crystal assembly. Internal radiation provides an energy smear from a variety of beta and alpha energies produced by the contaminating radionuclides.

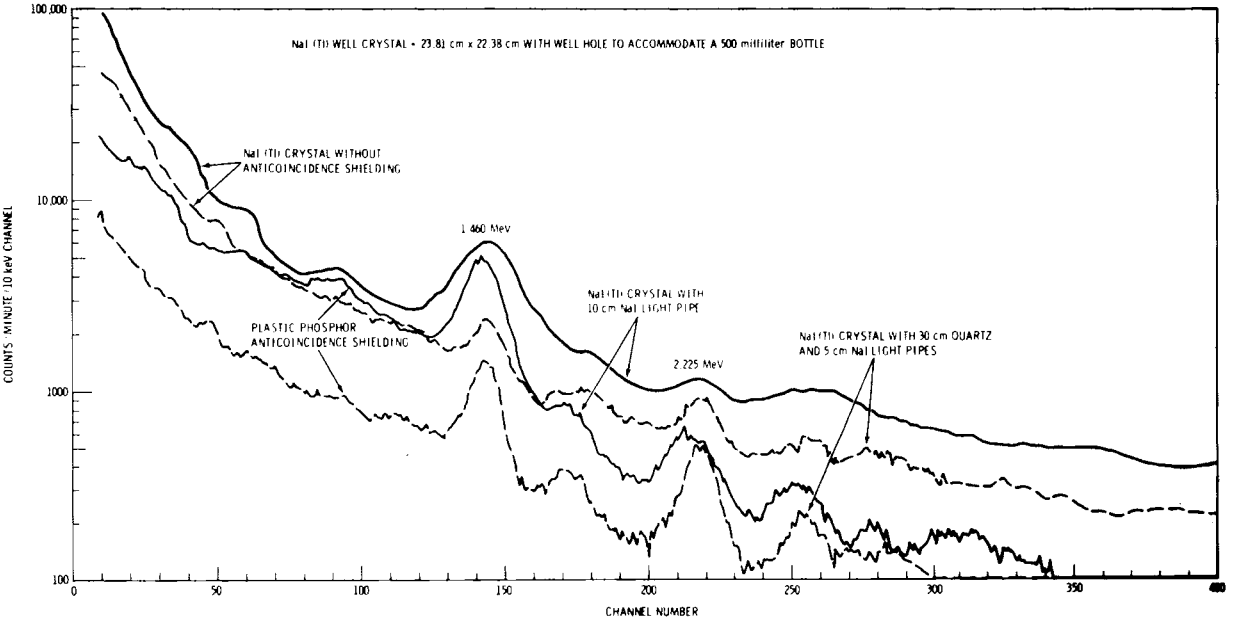

FIGURE 2.28. A Comparison of Background Observed by a NaI(T1) Well Crystal as a Function of its Shielding.

In Situ Quantitative Determination of Transuranics in Areas of High-Level Gamma Radiation

R. L. Brodzinski and N. A. Wogman

Accounting for transuranics in waste effluents is a formidable monitoring responsibility for the nuclear fuels reprocessing industry. Frequently, process streams generate gamma radiation fields so intense that electronic instruments will not operate, much less make accurate determination of the waste contents. Because grab sampling followed by laboratory analysis is an expensive and time-consuming analytical technique, an alternative in situ method to quantify the plutonium concentrations in high-level wastes was developed.

Basically, this technique uses metal flux monitors in or near the media to be analyzed. Neutrons emitted by the spontaneously fissioning transuranic isotopes and from (α,n) reactions on light elements, such as oxygen and fluorine in the medium, initiate nuclear reactions in the exposed metals. Subsequent low-background instrumental analysis of the metals is used to determine the radioactive transmutation products. From this the number and energy spectra of neutrons striking the metals are determined, and the quantity of transuranics required to emit that number of neutrons is calculated. Because some of these nuclear reactions have characteristic minimum neutron energy

* Nuclear Enterprise, 110.

thresholds, the fluence of neutrons above any chosen energy can be determined. Reactions currently being used are ^{63}Cu (n,γ), ^{64}Cu for thermal neutrons, ^{63}Cu cadmium-covered (n,γ), ^{64}Cu for epithermal neutrons, and ^{64}Zn (n,p) ^{64}Cu and ^{24}Mg (n,p) ^{24}Na for fast neutrons. The zinc reaction has a threshold of about 2 MeV and is responsive to fast neutrons produced both by (α,n) reactions and spontaneous fission. The magnesium reaction has a threshold of about 6 MeV and is responsive only to high energy spontaneous fission neutrons.

Mitigating factors affect the neutron spectrum emitted by any system containing transuranics. Obvious factors include the moderating capacity of the media, the relative amounts of oxygen and fluorine present, and the isotopic composition of the transuranics. Some of these factors are known from a general knowledge of the waste system. Others can be determined by appropriate choice of metal detectors that are calibrated against known standard sources of transuranic metals, oxides, and fluorides.

This technique has been applied to measure in situ plutonium concentrations in high-level liquid waste tanks at Hanford at a sensitivity of 7 nCi/cm^3. Similarly, a plutonium concentration as low as 4 nCi/cm^3 has been measured in semi-dry soils within controlled waste burial areas. The technique has also been applied to plutonium measurements in underground cribs and trenches, in settling tanks, in contaminated buildings, and in decommissioned process equipment. In another example, the technique was used to locate and identify hidden pockets of plutonium in a process hood. When the hood was breached, the predicted quantity of plutonium with the predicted oxide/metal ratio was recovered from within 3 in. (7.6 cm) of the predicted location.

Thus far field data have demonstrated the ultimate sensitivity of the technique to be approximately 1 nCi/g. The method is capable of determining transuranics in gamma radiation fields in excess of megarads/hr, and measurements can be completed in a few hours.

In Situ Analysis of Transuranics

K. K. Nielson

We have compared various instruments such as proportional counters, scintillation detectors, and solid state gamma-ray systems for use in surveying areas of suspected transuranic contamination with high sensitivity and specificity. See K. K. Nielson, C. W. Thomas and R. L. Brodzinski (1976).

A portable 19 cm^2 planar intrinsic germanium detector with an adjustable position coupling to its cryostat was fitted with an annular lead collimator to reduce background radiation to and define the detector's field of view. Surveys using this detector demonstrated its superior ability when compared to other transuranic radiation detection techniques to specifically detect ^{241}Am from its 59.5 keV photopeak, plutonium from UL x-rays, and specific plutonium isotopes from other x-ray peaks.

Sensitivity was greatest for ^{241}Am, which was detectable at levels of 0.005 nCi/cm^2 in ten-minute counts in concrete cells that were being decontaminated. Although plutonium detection limits were higher at 0.5 nCi/cm^2, the characteristic occurrence of ^{241}Am in transuranic contamination makes it the best indicator nuclide for surveying large areas. We estimate that a 1000 m^2 area could be surveyed at the 0.01 nCi/cm^2 level for ^{241}Am in $\sim$25 hours of survey time by placing the detector 1 m from the surface and making 476 individual 2.2 minute counts covering 2.1 m^2 each. Lower detection limits would be possible with longer counting times. None of the other techniques considered yielded sensitivities as low as the planar detector.

An Instrument for Monitoring the Transuranic Content of Chopped Leached Hulls from Spent Nuclear Fuel Elements*

N. A. Wogman and R. L. Brodzinski

Transuranic accountability is a significant problem in the processing of spent nuclear fuels, and many difficult determinations are required in the analysis of process effluents and solid wastes. Transuranic residuals may be embedded in the cladding material or as undissolved fuel after the leaching process. If the concentration of these transuranics exceeds the allowable limit, the hulls must be releached or placed in retrievable storage. We have designed a monitor that accepts a 5-gallon can of leached hulls. These hulls will be highly radioactive because of induced activities and residual fission products in the fuel cladding. The only distinctive radiations emitted by the small quantities of transuranics that can be characteristically identified in this high gamma field are neutrons emitted by spontaneous fission or from (α,n) reactions on light isotopes such as ^{17}O or ^{18}O. These neutrons could normally be detected by ^3He counters, $^{10}BF_3$ counters, or fission chambers. However, for this application, fission detectors are too inefficient, and ^3He counters are too sensitive to gamma radiation. Therefore $^{10}BF_3$ counters have been chosen.

The monitor design uses a 10-cm thick lead shield located between the sample

*Not funded by OER programs.

cavity and an annular detector array as shown in Figure 2.29. This thickness has been experimentally determined to be an optimum trade-off between gamma-ray attenuation and loss of geometry/efficiency for neutron detection. It is expected to reduce the radiation dose on the $^{10}BF_3$ tubes from about 10^4 R/hr to about 7 R/hr. Also, the $^{10}BF_3$ neutron detectors are shielded from excessive external gamma radiation and from external neutron sources by a 15-cm thick modular tank filled with a saturated aqueous solution of boric acid. The water acts as a bulk shield for gamma radiation and is a moderator for fast neutrons. Once thermalized, extraneous neutrons are eliminated by the boric acid with high efficiency.

scalers, one of which records single events and the others record double, triple, quadruple, etc., coincidence events. A variable time-delay window is used to define coincidence. Pulses are stored for counting periods ranging from 100 to 10,000 seconds. After appropriate background corrections are made, the net scaler readings are used to estimate the quantities of transuranics remaining in the hulls.

Background radiation is not constant because the majority of extraneous pulses are from temporally fluctuating cosmic particle neutron production in the massive lead shield surrounding the central cavity. However, these events are large multiple

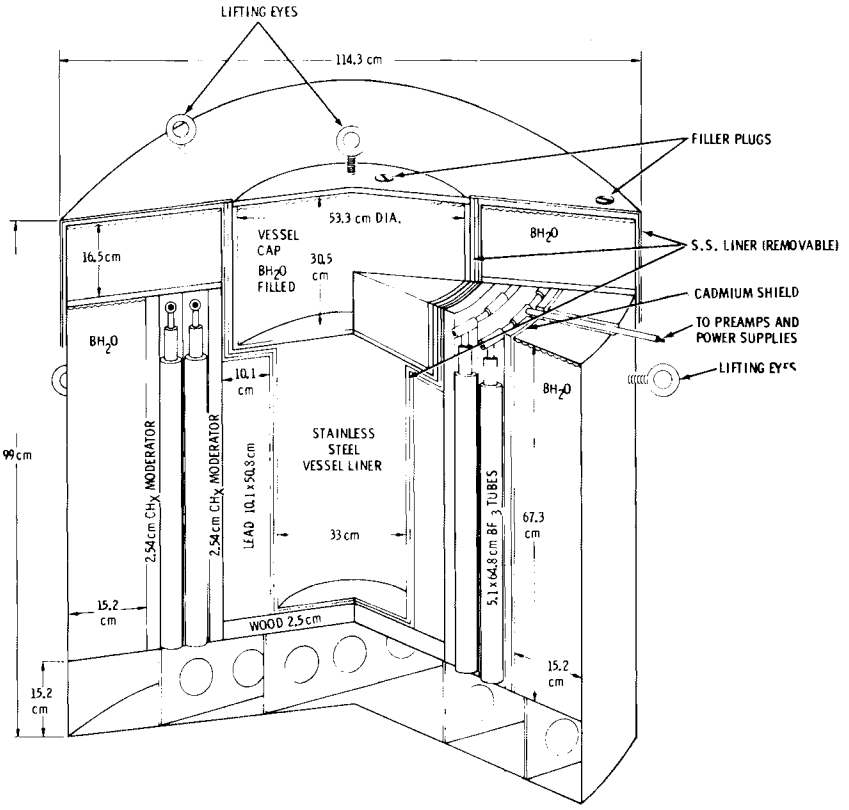

FIGURE 2.29. Transuranic Monitor for Chopped Leached Hulls.

The system is operated by remotely placing a bucket of chopped leached hulls in the central cavity. Neutrons emitted by the residual transuranics pass through the lead shield and enter the counter/moderator module. This module consists of one hundred 5-cm dia, 65-cm long $^{10}BF_3$ proportional counters surrounded by a minimum of 2.5 cm of polyethylene that acts as a thermalizer for the neutrons. Neutrons detected by the $^{10}BF_3$ tubes generate pulses that are stored in a series of ten

coincidence events, whereas the transuranic-produced neutrons are virtually exclusively single or double coincidence events. The multiple scaler counting system allows a rather precise definition of the single and double coincidence events of cosmic origin to be inferred from the measured higher order events. In this fashion, the necessary background correcting data are obtained at the same time the actual measurement is being made. Quantitative system calibration is accomplished with transuranic sources of

varying size, distribution, and chemical and isotopic composition.

Computer Methodology and its Application to Geological and Environmental Matrices

J. C. Laul, C. L. Wilkerson and V. L. Crow

We have developed a computer program for gamma-ray spectrometry that does not involve spectrum stripping, smoothing operations, spectrum unscrambling, etc., where shaping of a photopeak is involved. Our approach to the gamma-ray spectrum analysis is based on the principle of manual selection of a photopeak area and Compton background channels of the identified photopeaks of interest in a spectrum.

Gamma-ray spectra obtained from several Ge(Li) detectors are transferred directly from multichannel analyzers to the PDP-11/35 computer. Sample and detector identifications, and other parameters such as end of irradiation, date and time of counting, count time, dead time, and geometry position, are assigned to each gamma-ray spectra. These parameters and the gamma-ray spectra are stored on DEC tape by the PDP-11/35 computer. Up to fifty 2048-channel spectra can be stored on a single DEC tape.

A reference library for data reduction of up to 40 photopeaks in a spectrum is prepared. This library contains a given set of information including the desired radionuclide, half-life, peak channel, width of the photopeak (always odd number), Compton background channels on each side of the photopeak, total background channels, and concentration of the element in the standard. The computer program first searches and locates the photopeak by an iterative maxima summing process around the assigned peak channel. Subsequently, it integrates the photopeak according to the assigned width in the reference library. The computer program by the iterative process can allow a shift of 1 to 6 channels usually proportional to the peak width. When there is an integer shift in the peak channel, the program also shifts those background channels that correspond to the shift in the peak channel. The program also allows an additional shift of one channel by the minimum iterative process in the specified background channels on either side of the photopeak.

The program then compares samples to standards and lists the elemental concentrations in ppm, the associated error (%), and other parameters such as gross, net, and background counts; counting errors caused by the sample and standard; decay corrections during counting and from the end of irradiation; corrected counts/min/g, etc., that are used by the PDP-11/35 computer. The program also lists peak channel and any peak shift, peak width, any background channel shifts, and other tagged parameters that were initially assigned to each gamma-ray spectrum.

The program has been tested on five identical synthetic spectra that were comprised of ^{241}Am, ^{57}Co, ^{60}Co, ^{137}Cs, ^{203}Hg, and ^{46}Sc radionuclides. Each spectra consisted of 35 photopeaks of different intensities in the range of 60 to 1600 keV. The photopeak channels in the first spectrum were precisely calibrated, whereas the photopeak channels in the second and third spectra were shifted by two channels to the right and left, respectively. The peak channels in the fourth and fifth spectra were disproportionally shifted (2 to 6 channels) by a small to a large gain shift. In each case, 0.3, 0.5, 0.7, and 0.9 fractions of the photopeak width shifts were allowed. The program worked extremely well. The results by computer program in greater than 95% of the cases agreed precisely with those by manual calculations.

The computer program has been further tested in the analyses of geological and environmental matrices. We have analyzed the USGS standards BCR-1, W-1, and PCC-1, IAEA Soil-5, and NBC coal, fly ash, orchard leaf, and bovine liver for 34 major, minor, and trace elements (Al, As, Ba, Br, Ca, Ce, Cl, Co, Cr, Cs, Eu, Fe, Hf, K, La, Lu, Mg, Mn, Na, Nd, Ni, Rb, Sb, Sc, Se, Sm, Sr, Ta, Tb, Th, Ti, V, Yb, and Zn) in duplicate by Neutron Activation Analysis gamma-ray spectrometry. Our results within the precision (1σ) in the vast majority of cases agree very well with the recommended reported values.

3.0 Geothermal

• Heavy Metal and Noxious Gas Emissions from Geothermal Resource Development

Although geothermal energy is generally considered a relatively clean source of power, the high temperature processes that create the hydrothermal provinces mobilize some undesirable constituents. In this section, we report on a general effort underway to characterize and compare effluents from a number of different geothermal sites.

Chemical Characterization of Gases and Volatile Heavy Metals in Geothermal Effluents

D. E. Robertson, J. D. Ludwick,
C. L. Wilkerson and J. C. Evans

The rapidly increasing number of successfully drilled geothermal production wells is a good indication that geothermal energy development may meet or exceed projected forecasts of its potential as a cheap, clean source of energy. However, geothermal energy is not without some environmental impact. The very hot geothermal processes that create the steam or hot water used for energy production can also mobilize volatile and hot-water leachable chemical constituents and bring them to the surface from great depths in the earth. Noncondensable gases such as hydrogen sulfide, ammonia, radon, carbon dioxide, methane, and other volatile elements such as mercury, boron, arsenic, and selenium are vented to the air when geothermal resources are tapped. Thermal waters reaching the earth's surface contain very high concentrations of a wide variety of dissolved chemical constituents, some of which are toxic in relatively low concentrations (H_2S, NH_3, Hg, As, Cu, Zn, Se, Pb, Ag, Sn, Sb, and Cd). It is essential that the effluents from each specific site be characterized to define and quantify the releases of undesirable materials.

During the past three years, we have been engaged in characterizing the noxious gases and heavy metals released in effluents from two geothermal power plants and several test facilities. These areas include The Geysers, California; Cerro Prieto, Baja California; Raft River, Idaho; Tigre Lagoon, Louisiana; and the Imperial Valley, California sites at Niland, East Mesa, and Heber.

Samples of incoming steam were condensed and the condensates and noncondensable gases were sampled in order to chemically characterize and quantify the geothermal gases and trace elements in geothermal well effluents, and to establish mass balances of these constituents entering and leaving the power plants. The power plant effluents, which consisted of cooling tower waters, cooling tower exhaust air, ejector off-gases, and brine waters, were also collected for analyses.

When steam-brine separators were not available at the new well heads, a small portable separator was used to separate the steam from the brine phase. A specially designed nonmetallic steam condenser was used to condense the steam and separate the noncondensable gases.

A number of difficult-to-preserve constituents and several chemical parameters were measured immediately after sampling in a mobile laboratory. These included H_2S, NH_3, F^-, and dissolved $S^=$, and pH, oxidation-reduction potential (Eh), and various chemical forms of mercury. Samples of liquids and gas scrubber solutions were collected and preserved for laboratory analyses of a variety of other major and trace constituents.

Neutron activation analysis, atomic absorption spectrometry, plasma emission spectrometry, and x-ray fluorescence techniques were used in these analyses.

A summary of the constituents of the greatest environmental concern is presented below and in Table 3.1.

Hydrogen Sulfide

Hydrogen sulfide is the most notorious geothermal effluent because of its objectionable odor and toxicity. The H_2S concentrations in noncondensable gases were extremely variable at the geothermal sites that were studied, and ranged from as high as 5.7% (by volume) at The Geysers Unit 11 to as low as 0.5 ppm at the Tigre Lagoon geopressured well site. The Imperial Valley sites exhibited quite variable H_2S concentrations, and all sites

TABLE 3.1. Concentrations of Various Constituents in Geothermal Noncondensable Gases, Steam Condensates and Brine.

Noncondensable Gases	The Geysers[a]	Raft River[b]	Vermilion Bay[c]	East Mesa[d]	East Mesa[e]	Niland[f]	Niland[g]	Heber[h]	Cerro Prieto[i]
H_2S (ppm) Vol.	28,400-57,400	215	0.5-5	580-630	380	1,390-1,620	4,670	—	15,000-20,000
Hg (µg/ℓ)	1.8-5.8	0.039	<0.001	2.3-3.6	3.3	0.8-1.6	1.8	<0.03	0.3-0.4
NH_3 (µg/ℓ)		—	130	108	—	45	—	—	17.8
Rn (pCi/ℓ)	3,820-27,800[j]	—	10-40	280-305	1,095-1,262	830-1,150	535-644	3,200-4,300	—
As (µg/ℓ)	<0.003	—	—	—	—	—	—	—	<0.016
Steam Condensate									
H_2S (mg/ℓ)	49-225	0.66	—	2.8	0.09	5.5	9.5	—	36-71
NH_3 (mg/ℓ)	157-818	1.8	—	98	15.5	331	360	—	88-163
Hg (µg/ℓ)	2.8-10	0.13	—	14.4	1.45	2.20	3.12	3.9	3.8-5.4
B (mg/ℓ)	6.4-76	<0.1	—	<0.1	—	5.9	—	<0.1	<0.1
As (mg/ℓ)	0.0014-0.092	0.012	—	—	—	—	—	—	0.006
Flashed Brine									
NaCl (‰)	—	0.13	10.4	1.77	—	16.5	—	—	2.27
H_2S (mg/ℓ)	—	0.1	—	0.33	0.07	—	—	—	0.16
NH_3 (mg/ℓ)	—	0.27	90	6.5	1.4	394	400	—	127
Hg (µg/ℓ)	—	0.022	0.007	0.003	<0.001	0.020	0.11	0.44	0.049
B (mg/ℓ)	—	0.13	40	9.8	—	340	—	—	19
As (mg/ℓ)	—	0.028	0.045	—	—	—	10.0	—	0.50-2.3
Ratio: Noncondensables (ℓ) Steam (kg)	1.96-4.46	0.25	1.6[k]	17.7	4.54	8.8	9.27	—	9.5
Brine Flow (kg/hr)	—	—	—	10,600	—	109,000	—	7,500	1.58×10^6
Steam Flow (kg/hr)	—	—	—	860	—	13,600	—	—	7.37×10^5
Temperature (°C) (Incoming)	—	—	—	151	—	165	204	161	—

[a]Units 3, 4, 7, 8 and 11 — sampled October 1975 and May 1976
[b]DOE Well — sampled September 14, 1976
[c]DOE Geopressured Well near Delcambe, LA — sampled May 26, 1977
[d]BLM Well 6-2 — sampled March 30-31, 1977
[e]Republic Geothermal Well 38-30 — sampled September 7, 1977
[f]Woolsey Well — sampled May 5, 1977
[g]Magmamax #1 Well — sampled September 9, 1977
[h]Nowlin Well — sampled March 2, 1977
[i]Main Steam Header — sampled May 12, 1976
[j]Radon data from The Geysers by Stoker and Kruger, 1973 and by Anspaugh, et al., 1977
[k]No steam was produced. This is the ratio of noncondensable gas to brine in ℓ/kg.

were substantially lower in H_2S compared to the Cerro Prieto geothermal field located only about 30 km south of the California border. The noncondensable gas concentration in the steam phase at the Raft River site was very low compared to all other areas, and the H_2S levels in the gas were only 215 ppm. The H_2S levels in the flashed brine at all hot water dominated sites were always very low, indicating that most of the H_2S follows the steam phase, when superheated brines flash into steam as the pressure is lowered at the well heads.

Mercury

Mercury is an extremely volatile element in geothermal fluids because of its high vapor pressure, and exists in elevated concentrations in the gas and steam phases. Mercury concentrations in noncondensable gases ranged from 0.03 µg/ℓ at Heber to 5.8 µg/ℓ at The Geysers Unit 3.

These mercury concentrations at most sites were 10^5 to 10^6 times higher than mercury levels in the ambient air. Mercury concentrations in the ejector off-gases at The Geysers and Cerro Prieto were considerably lower than in the noncondensable gases in the incoming steam. The ejector off-gases are scrubbed by cooling tower water during the steam condensation in the power plants, and some of the mercury is removed. Mercury levels in cooling tower exhaust air ranged from 0.18 to 1.3 ng/ℓ, compared to ambient air levels of approximately 0.001 to 0.010 ng/ℓ of air at most sites.

The dominant form of volatile mercury in all gaseous samples was elemental Hg^0 vapor, which was determined by using selective mercury vapor sorption traps. These traps were designed and tested to quantitatively separate and trap Hg^0 vapor, mercury chloride vapor, methyl mercury chloride vapor, and dimethyl mercury vapor.

An unanticipated discovery was the observation of mercury in the incoming noncondensable gases and in the ejector off-gases as Hg^0 vapor when H_2S levels in these gases were

so high, frequently ranging from 1.0 to 5.7%. Apparently, the elevated temperatures and reducing environment, together with the high vapor pressure of Hg^0, permit the mercury to exist even with the high sulfide levels.

With the condenser systems used in geothermal installations, roughly one-third to one-half of the mercury condenses when the steam is condensed. The mercury concentrations in steam condensates ranged from 0.13 µg/ℓ at Raft River to 14.4 µg/ℓ at the BLM East Mesa Well #6-2. These levels are about 100 to 10,000 times the mercury concentrations in uncontaminated fresh or ocean waters.

At the hot water dominated sites, the mercury follows the steam phase during brine flashing, which results in very low mercury concentrations in the flashed brine.

Arsenic

Unlike mercury, the arsenic in geothermal effluents predominantly remains with the flashed brine and only a very small fraction follows the steam phase. Arsenic vapor was undetectable (less than 0.003 to 0.016 µg/ℓ) in the noncondensable gases. Arsenic concentrations in steam condensates ranged from 0.001 to 0.09 mg/ℓ. In the flashed brines, the arsenic concentrations were much higher and ranged from 0.028 mg/ℓ at Raft River to 10 mg/ℓ in the high salinity brine at Niland. The chemical forms of the arsenic in the condensates and brines are partitioned between inorganic As^{+3} and As^{+5}. The As^{+3} form is more prevalent in fresh condensate and brine exhibiting a reducing Eh, but as these waters become exposed to the atmosphere, the As^{+3} gradually oxidizes to As^{+5}, the least toxic of the inorganic forms.

Boron

Boron concentrations in steam condensates at The Geysers ranged from 6.4 to 76 mg/ℓ. Cooling tower waters contained considerably higher boron levels because of the concentrating effect by evaporation of water in the cooling towers. The amount of boron entering Geyser power plant units is listed in Table 3.2. Most of this boron is reinjected. At the hot-water dominated sites, boron was found in the steam condensate only at Niland, at a concentration of 5.9 mg/ℓ. The boron concentrations in the flashed brine phases ranged from 0.13 mg/ℓ at Raft River to 340 mg/ℓ in the highly saline Niland brine. At Cerro Prieto, 30 kg/hr of boron are released with the flashed brine to the evaporation pond, and less than 0.07 kg/hr goes to the power plant with the steam phase.

TABLE 3.2. Amount of Boron Entering Power Plant Units at The Geysers.

Power Plant Unit	Boron, kg/hr
3	2
4	5.8
7	11
8	35
11	5.2

Ammonia

Ammonia is found in all geothermal effluents; it is present in the noncondensable gas, steam condensate, and brine. Ammonia concentrations in steam condensates ranged from 1.8 mg/ℓ at Raft River to as high as 818 mg/ℓ in several Geysers wells that supply steam to Unit 11. At Raft River and East Mesa, the ammonia concentrations in the steam condensates were much higher than the concentrations in flashed brine, but at Niland and Cerro Prieto the ammonia levels were about the same in the brine and condensate. At Cerro Prieto 92 kg/hr and 0.1 kg/hr of ammonia enter the power plant as condensable and noncondensable ammonia, respectively, while 200 kg/hr are released to an evaporation pond with the flashed brine. Most of the ammonia leaving the power plant in steam condensate is released to the atmosphere from the cooling towers.

Radon

Radon-222 gas concentrations were highly variable in the noncondensable gases from the various sites, ranging from 10 pCi/ℓ at the Tigre Lagoon geopressured site to 4300 pCi/ℓ at Heber. By comparison, the ^{222}Rn concentrations measured by other investigators at The Geysers ranged from 3820 to 27,800 pCi/ℓ. The ^{222}Rn follows the noncondensable gas phase and is essentially all released to the atmosphere.

4.0 Oil Shale

• Oil Shale and Tar Sand Research

Oil shale and tar sands in the United States represent a potential supply of nearly one trillion barrels of crude oil for the country's future use. The renewed commercial interest in developing these reserves has increased the need for studies that would help developers assure that conversion processes are carried out in an environmentally acceptable manner. A vital part of this environmental research program is the physical and chemical characterization of the effluents from the various proposed conversion schemes. Characterization studies are important and should begin at an early stage of development, preferably at the pilot plant or semiworks stage. Because of the complex nature of the effluents, new sampling, analysis, and chemical separation procedures have had to be developed. In this section, new and improved techniques for organic, inorganic, and speciation analysis are presented with applications for oil shale research. Also reported is the progress of a program to provide representative and well-characterized fossil fuel samples for environmental and health effects studies and for interlaboratory comparisons to ensure accuracy of the data.

Organic Analysis of Oil Shale Samples

D. M. Schoengold and M. R. Petersen

This study is an investigation of the organic composition of potential effluents from an operating shale oil retort. The ultimate objective is to predict what compounds may find their way into the environment because of the development of the shale oil industry. The pilot facility that was selected for this study was the Paraho Semiworks plant at Rifle, Colorado. A variety of samples was collected during sampling trips to this facility, including samples of recycle gas, thermal oxidizer off-gas, retort waters, and product oil. Sample compositions were investigated using several different techniques. A qualitative description of the organic compounds and compound types are given below for each sample.

Gas samples were analyzed by gas chromatography and gas chromatography/mass spectrometry (GC/MS). In the thermal oxidizer off-gas, only carbon dioxide was detected. In the Paraho recycle gas, carbon dioxide, two series of n-alkanes and n-alkenes up to C11, aromatics to xylene, branched chain aliphatics, and acyclic hydrocarbons were found.

A methylene chloride extract of a Paraho recycle water sample was analyzed by glass capillary column GC/MS. A large number of nitrogen and oxygen substituted compounds were found, including pyridines, furans, tetrahydroquinolines, cyanobenzene, piperidines, pyrolidines, caprolactams, piperidones, pyrazine, quinoline, carboxylic acids, phenols, and pyridenes. No pyrroles, indoles, or carbazoles were detected.

The whole shale oil samples were separated into neutral, acidic, and basic fractions and were then analyzed by glass capillary column GC/MS. The neutral fraction showed alkanes and alkenes to at least C22, alkyl benzenes substituted to at least C9 (including the homologous series n-hexyl to n-nonyl alkyl benzenes), naphthalenes, di- and tetrahydronaphthalenes and a few polynuclear aromatics.

The acidic fraction of the shale oil contained mainly substituted (to at least C6) phenols, substituted naphthols, and a large number of alkanes, alkenes, and alkylbenzenes.

The basic fraction was primarily alkyl substituted pyridines. A pyrrole and several alkyl substituted quinolines were also found.

Reconstructed single ion chromatograms were used to find pyrroles, indoles, and carbazoles in both the basic and neutral fractions. Except for the single pyrrole peak found in the basic fraction, none of these compounds was found in either of the fractions.

The composition of the oil sample fractions is extremely complex. Current studies are underway to find the most promising

quantitation procedures. This program has been closely coordinated with biological testing efforts. Samples that are provided to the PNL biology group are the same samples on which extensive chemical analyses are conducted. As biological information is obtained, refined chemical analyses and separations are made of the most interesting fractions. In this manner, a realistic analytical chemistry program has evolved that is directly responsive to the biological and ecological study requirements.

Comparative Elemental Abundances in Shale Oil and Natural Crude Oils

C. L. Wilkerson

The elemental abundance of sulfur and six trace metals (arsenic, iron, nickel, selenium, vanadium, and zinc) is compared for a surface-retorted shale oil and for a group of 88 North American crude oils. The data for the North American crude oils are those presented by Hitchon, Filby, and Shah (1975); the data for the shale oil were determined in this laboratory. All elemental analyses were obtained by instrumental neutron activation analysis. The data are presented in Figure 4.1 which shows comparisons of the ranges, maximum concentrations, average concentrations, and detection limits.

The concentration of S in the shale oil is essentially the same as the average value determined for the 88 natural crude oils, namely 0.8%. The elemental abundance of Fe, Ni, and Zn is within a factor of 2-3 of the average values reported for the natural crude oils. Iron is slightly more concentrated in the shale oil, while Ni and Zn are more abundant in North American petroleum. The most significant comparison is for the elements arsenic, selenium, and vanadium. Vanadium was measured in 84 of the 88 natural crude oils investigated. The average concentration of vanadium in these natural crude oils is two orders of magnitude greater than that for the shale oil. Conversely, the concentrations of As and Se are significantly higher

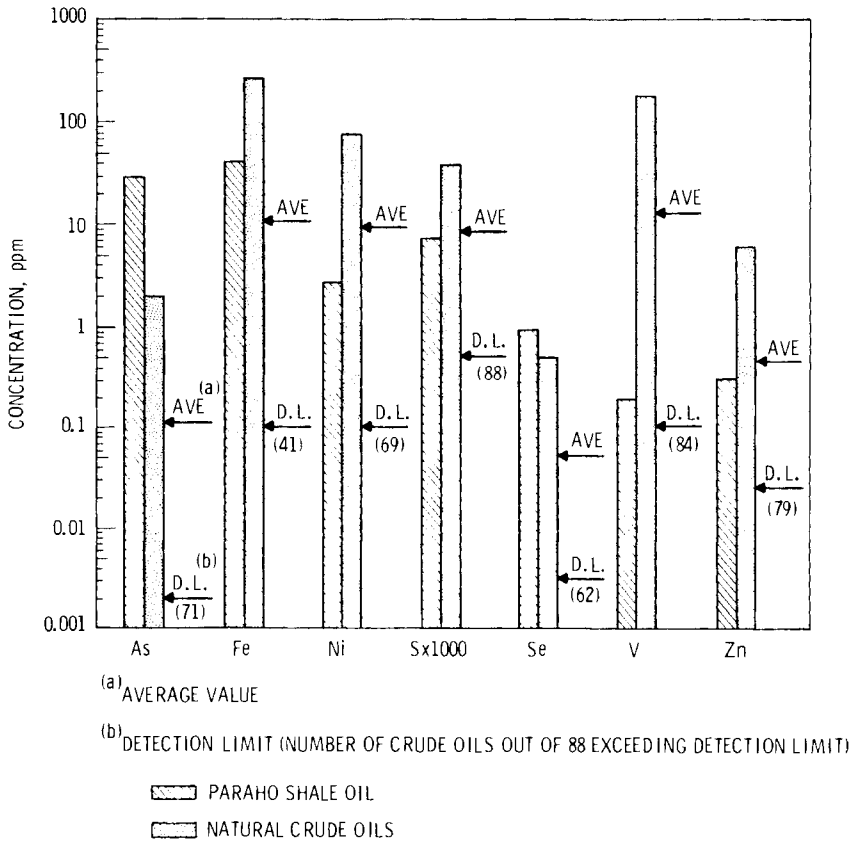

FIGURE 4.1. Elemental Abundances in a Surface-Retorted Shale Oil Compared to Natural Crude Oils.

in the shale oil where their abundance exceeds the maximal values reported for the crude oils. The As and Se abundance in shale oil is approximately 1.5 to 2.5 orders of magnitude greater than those reported for crude oil.

The high level of As and Se in the shale oil is a significant problem for environmental protection and engineering development of potential oil shale technologies. For example, As poisons many industrial catalysts used in upgrading or refining the crude shale oil. An alternative to upgrading the shale oil is to burn it directly in a conventional oil-fired boiler. This strategy is currently being investigated by the Electric Power Research Institute (EPRI) and others. Because the volatilization of As and Se in the firebox could produce significant environmental problems, appropriate control technology would be required.

X-Ray Fluorescence Analysis of Shale Oil Samples

J. S. Fruchter
Technical Assistance: R. W. Sanders

Techniques for accurate and sensitive elemental and trace metal analysis of oil are important for determining the fate of various trace contaminants during refining procedures and fuel combustion. Because of renewed interest in synthetic fuel production from oil shale, development of dependable analytical methods has become even more important. Many traditional analytical methods are inapplicable to the complex shale oil matrix. To resolve this problem, we have adapted the x-ray fluorescence (XRF) technique to the analysis of shale oil and other oil samples.

Sample preparation is straightforward. A one ml oil sample is pipetted onto a prepared slide, which has a 0.0032 mm polypropylene seal on the flush side. The mounted sample is placed in a laminar flow hood and allowed to reach a highly viscous state. This normally requires about a day with a resultant 5 to 15% weight loss for most crudes. Samples prepared this way generate very little outgas when exposed to the vacuum in the x-ray system.

To prevent loss of volatile inorganics, the sample can be processed in air, eliminating the evaporating step. This procedure, however, requires the use of a prepared multielement standard to compensate for backscatter and absorption, which are caused by air. Sensitivities for the low atomic number elements are diminished by a factor of 5 or 6 for air. Volatilization losses of trace elements do not seem to be significant for most crude and shale oil samples.

Analysis requires a 60-min x-ray exposure using a tungsten x-ray primary beam with a filtered Zr or Ag secondary source.

Figure 4.2 illustrates a computer plot of the Zr source spectra of Wilmington, California crude and Paraho 8-25-77 shale oil. The shaded areas represent the integration of the element peak.

Table 4.1 presents a comparison of neutron activation analysis (NAA) and XRF analysis of a crude oil from Wilmington, California and a Paraho shale oil.

The XRF method provides data on a number of elements not easily obtainable by other methods. Comparison of XRF and NAA analyses shows that, except for arsenic, the results are in good agreement, which provides an indication of the accuracy of the XRF method. It is possible that some volatile forms of arsenic are lost during the XRF sample preparation.

XRF Analysis of Shale Oil Process Waters and Associated Aqueous Samples

J. S. Fruchter
Technical Assistance: R. W. Sanders

Process waters produced with shale oil are chemically complex. This complexity causes interference with many traditional methods for metal analysis of these waters. We have, therefore, developed and validated three x-ray fluorescence procedures for analysis of shale oil process waters. One method evaporates a small volume 0.1 ml of solution in a 1 cm diameter area and places the sample in the constant flux area of the x-ray beam. This method is rapid but requires a homogeneous sample. It also presents difficulties with low atomic number elements when there is mass absorption caused by organics.

Another method freezes the solution into a thin wafer and exposes it to x-rays in a vacuum for a short period. This application has the advantage of no volatile loss. However, the major disadvantage is the relatively high scattering resulting from the mass of water.

The most useful and versatile procedure is adding a known weight of solution (10 to 50 gm) to 50 mg of cellulose. The sample is evaporated to dryness in a laminar flow hood at ambient temperature, homogenized, and pressed into a 3.18 cm diameter wafer, and its weight is determined. Counting time is 60 min at 40 kV 13.5 mA using a Zr or Ag secondary source. The resultant spectra are reduced using a computer program that corrects for peak overlap, mass absorption, and elemental enhancement. Differences in spectra using the three techniques for the same process water sample are illustrated in Figures 4.3, 4.4 and 4.5.

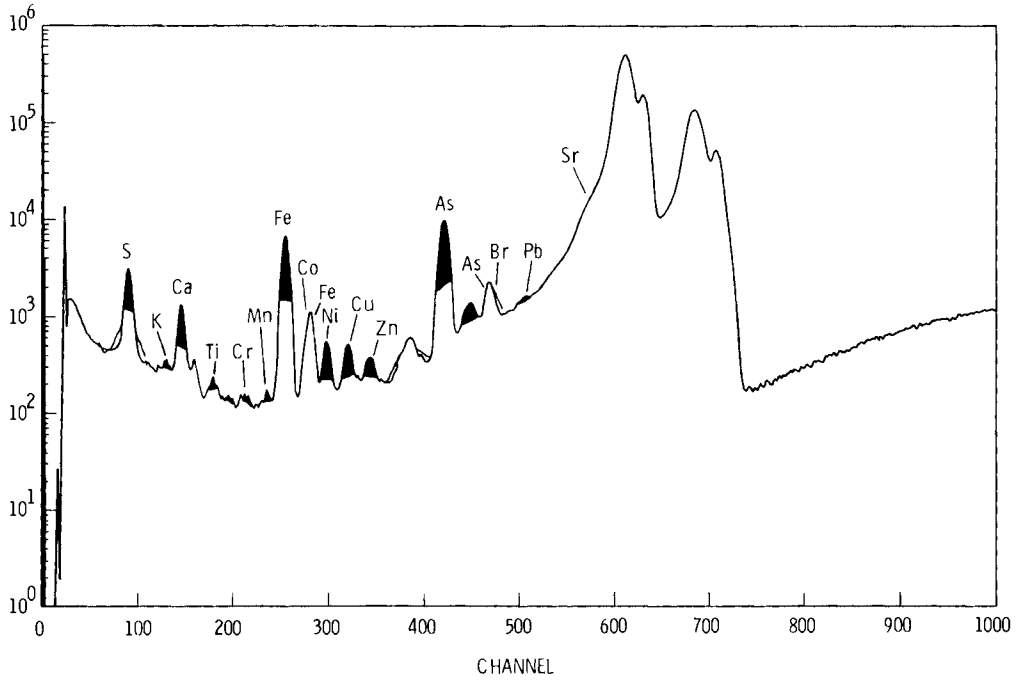

(a)

FIGURE 4.2a. X-Ray Fluorescence Spectrum—Paraho Shale Oil—Zr Secondary Source.

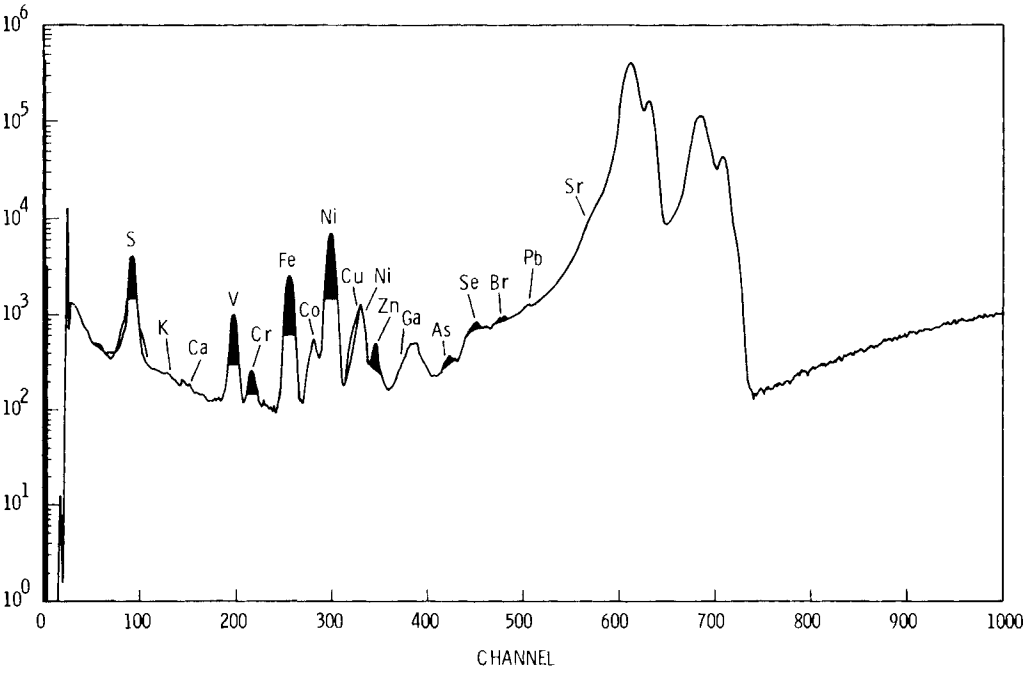

(b)

FIGURE 4.2b. X-Ray Fluorescence Spectrum—Wilmington Crude Oil—Zr Secondary Source.

TABLE 4.1. Comparison of Neutron Activation Analysis and X-ray Fluorescence Analysis of Wilmington Crude and Paraho Oil Samples.

	Wilmington Crude Petroleum			Paraho Oil Collected 8-25-78		
	Method			Method		
Elements, ppm	NAA	XRF-Air	XRF-Vac	NAA	XRF Air	XRF-Vac
	10% Error					
As	0.25	0.08 ± 0.04	0.14 ± 0.07	31 ± 2	23 ± 2	19 ± 2
Br	<1	0.11 ± 0.06	0.27 ± 0.09	<0.2		<0.14
Ca			<10			245 ± 29
Cl	6		<126	3.0 ± 0.9		<140
Co	1.21	1.31 ± 0.21	1.79 ± 0.36	1.39 ± 0.08		1.44 ± 0.42
Cr	0.15	<1.0	<1.47			1.55 ± 0.66
Cu	<10	1.50 ± 0.2	0.48 ± 0.27	1.1 ± 0.04	0.83 ± 0.12	0.97 ± 0.23
Fe	32	37 ± 3	40 ± 4		59 ± 5	74 ± 8
Ga		<0.08	<0.14			<0.11
Hg		<0.3	<0.51			
K			<20			41 ± 15
Mn	<0.2	<0.38	<0.67	0.4 ± 0.05	0.45 ± 0.25	<0.51
Mo		<0.19		<3		
Nb		<0.17				
Ni	54	58 ± 4	62 ± 6		2.72 + 0.20	2.76 ± 0.36
Pb		<0.4	<0.60		<0.40	<0.40
Rb		<0.13	<0.17		<0.19	<0.14
S, %	1.58		1.63	0.99 ± 0.08		0.89 ± 0.10
Se	0.37	0.37 ± 0.07	0.38 ± 0.10		0.92 ± 0.07	0.71 ± 0.12
Sr		<1.2	<1.6		<1.3	<1.2
Ti			<2.5	2.6		4.1 ± 1.9
V	47	46 ± 3	56 ± 6	0.29 ± 0.01		<1.29
Y		<0.14				
Zn	1.07	1.4 ± 0.1	1.7 ± 0.2	<0.70	0.57 ± 0.09	0.55 ± 0.13
Zr		<0.16				

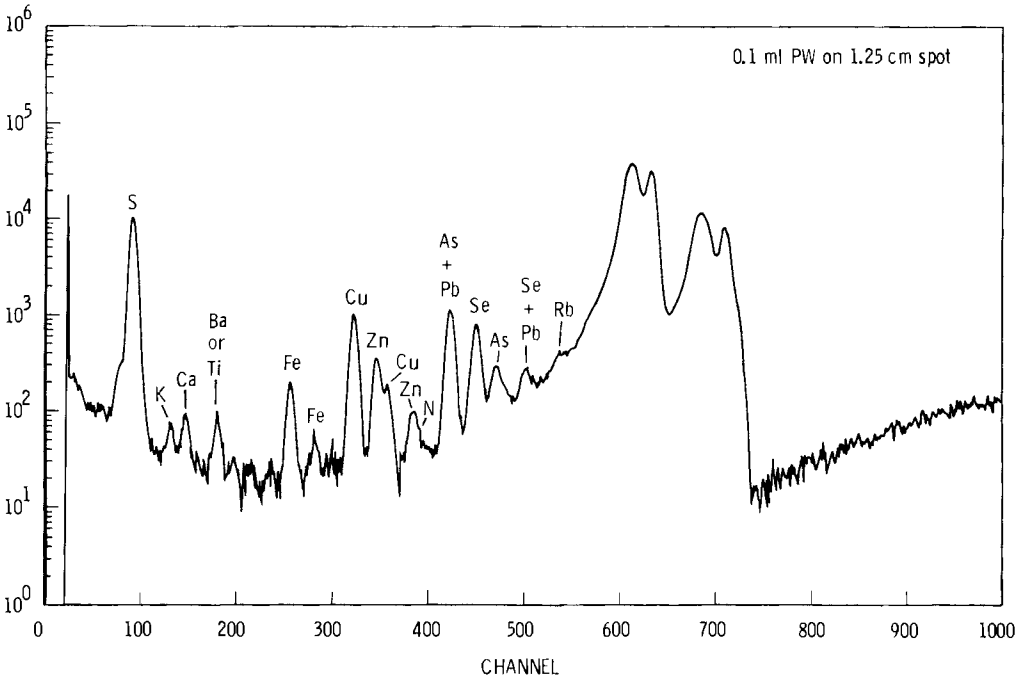

FIGURE 4.3. X-Ray Fluorescence Spectrum—Oil Shale Process Water (0.1 ml spot technique)—Zr Secondary Source.

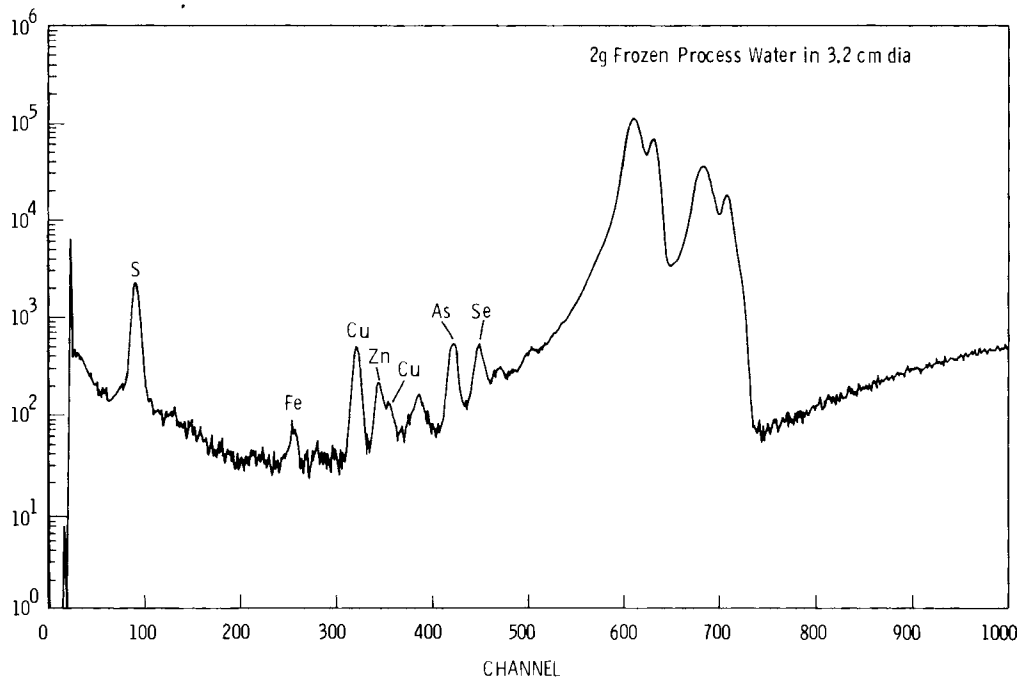

FIGURE 4.4. X-Ray Fluorescence Spectrum—Oil Shale Process Water (frozen sample method).

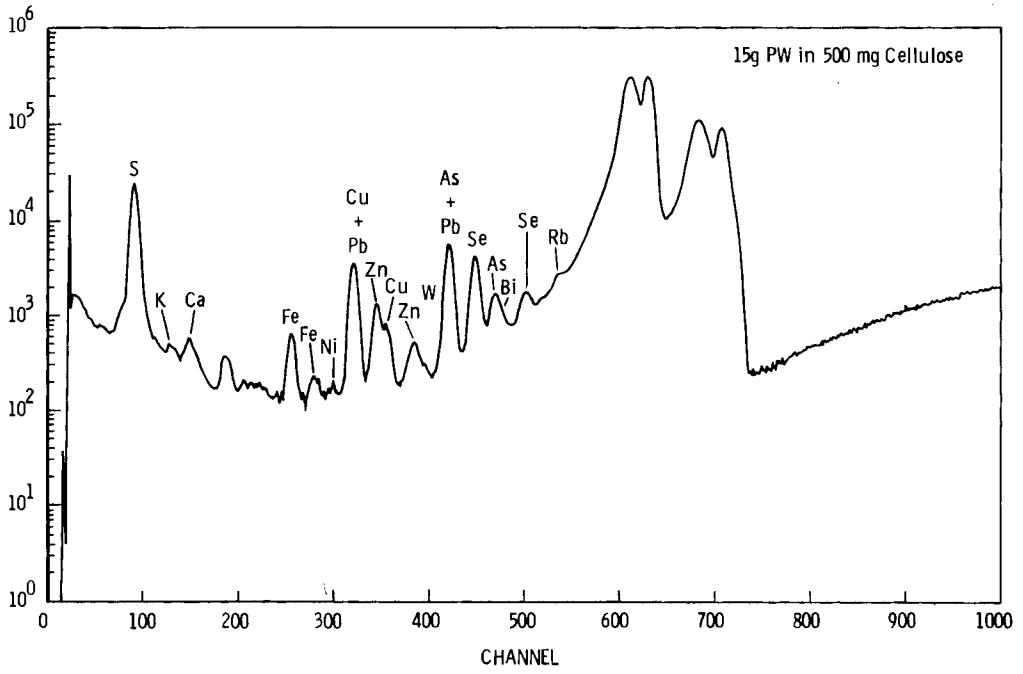

FIGURE 4.5. X-Ray Fluorescence Spectrum—Oil Shale Process Water (cellulose wafer method).

Agreement in the reported values was generally good when compared with available results from other reliable methods. The difference between methods was usually less than 10%.

Radiochemical Analysis of Cd, Se, Te, U and Zn in Oil Shale Samples

J. C. Laul

The elements Cd, Se, Te, and Zn are of considerable interest in fossil fuel research areas because these elements are volatile and potentially toxic in environmental and health related areas, and because their elemental concentrations are not well known in oil shale materials. These elements are not always reliably determined in various oil shales, products, and wastes using techniques such as atomic absorption (AA), instrumental neutron activation analyses (INAA), and x-ray fluorescence (XRF). Therefore, we have developed a radiochemical neutron activation analysis scheme that is rather simple and enables us to easily achieve the accuracy and sensitivity desired for these elements. The elements Cd, Se, Te, and Zn were determined from their neutron activation products; U was determined from its fission product ^{132}Te. We tested our radiochemical procedures on a raw oil shale, retorted oil shales, the USGS BCR-1 geological standard, and on the well-characterized Allende meteorite. Our results for BCR-1 agree very well with the literature values, giving us confidence in our values for the oil shale matrices.

Known fractions of sample materials and appropriate standard materials were irradiated in a reactor at a neutron flux of $\sim 6 \times 10^{12}$ n/cm^2/sec for $\sim$8 hours. After about two days' delay, the samples were transferred into Ni crucibles containing carriers for Cd, Se, Te, and Zn ($\sim$20 mg each), and the samples were fused with a mixture of Na_2O_2-NaOH. The fused cake was decomposed with H_2O, neutralized with HCl, and finally adjusted to 3 N HCl solution. The 3 N HCl solution (150 ml) was loaded onto an anion exchange column (1 x 10 cm), AG 1-X10 resin, 100-200 mesh, chloride form. The Se was collected as an effluent, and Cd, Te, and Zn were retained on the column. The Te was eluted with 30 ml 0.25 N HCl. The Zn was next eluted with 150 ml of 0.1 N HCl, and finally the Cd with 0.002 N HCl. Following this preliminary separation, each fraction was further purified, weighed, and counted on a Ge(Li)/NaI(Tl) detector system.

The Se fraction was adjusted to 6 N HCl and SO_2 gas was passed through the solution to reduce Se to its metallic state. The 136 or the 265 keV gamma ray of ^{75}Se ($t_{1/2}$ = 120 d)* was used for the Se measurement. Tellerium fractions were adjusted to 3 N HCl and SO_2 was passed through to precipitate Te as metal. The 159 keV gamma ray of ^{123m}Te ($t_{1/2}$ = 120 d) was used for the Te determination. The 228 keV gamma ray of ^{132}Te ($t_{1/2}$ = 3.25 d) was used for the U determination.

Holdback carriers of Fe, Cr, Sc, and Co were added to the Cd fraction and the solution was evaporated until dry. The residue was dissolved in 15 ml of 1 N HCl. A few drops of $TiCl_3$ were added to reduce Fe^{+3} to Fe^{+2} and Cr^{+6} to Cr^{+3} states, and the solution was again loaded onto another ion exchange column. The Fe, Cr, Sc, and Co passed through the column and were rejected as washings. The column was washed with 100 ml each of 1 N HCl and 0.1 N HCl. The Cd was eluted with 100 ml of 0.002 N HCl. The solution was reduced in volume, and Cd precipitated as $Cd(NH_4)PO_4$. The 336 keV gamma ray of ^{115m}In ($t_{1/2}$ = 4.5 h) daughter in secular equilibrium with ^{115}Cd ($t_{1/2}$ = 56 h) was used for analysis of the Cd.

Holdback carriers of Fe, Cr, Sc, and Co were added to the Zn fraction and the solution, like the Cd fraction, was treated with $TiCl_3$ and loaded onto an ion exchange column. The column was washed with 100 ml of 1 N HCl and Zn was eluted with 100 ml of 0.1 N HCl. The solution was reduced in volume and Zn was precipitated as $ZnHg(SCN)_4$. The 1115 keV gamma ray of ^{65}Zn ($t_{1/2}$ = 240 d) was used for analysis of the Zn. Results of the determinations in the various samples are shown in Table 4.2. Where reliable determinations of these elements by other methods were available, the agreement was generally good. The values obtained for measured standards also agreed well with accepted values.

Arsenic Analysis of Oil Shale Process Water--An Example of the Multitechnique Approach

J. C. Evans, C. L. Wilkerson and
J. S. Fruchter
Technical Assistance: R. W. Sanders

The analysis of oil shale process water poses some unusual analytical problems because of the complex nature of the matrix. A multitechnique approach to inorganic analysis provided an opportunity to assess the strengths and weaknesses of various techniques. An intralaboratory study was recently completed using arsenic analysis as an example of the multitechnique approach. The sample chosen for analysis was an oil shale process water collected from a storage tank at the Paraho Semiworks retort. The sample was known to be relatively high in arsenic and thus did not tax the sensitivity limit

*halflife

TABLE 4.2. Determination of Several Potentially Toxic Trace Elements in Oil Shale Samples[a] by Radiochemical Neutron Activation Analysis, ppm by weight.

Sample	Cd	U	Se	Zn	Te	
Raw Shale, Run 01 Sample 02 Batch 07, 11/16/77	0.630	4.78	1.94	63.1	0.12	(30%)
Spent Oil Shale, Run 01 Sample 04 Batch 08, 11/16/77	0.921	5.93	2.44	80.3	0.10	(40%)
Raw Oil Shale, Run 02 Sample 14 Batch 10, 5/23/77	0.622	4.70	1.86	93.8	0.12	(40%)
Raw Oil Shale, Run 01 Sample 11 Batch 05, 8/24/77	0.643	4.64	2.00	63.0	0.15	(30%)
Retorted Oil Shale, Run 01 Sample 04 Batch 05, 8/24/77	0.900	4.90	2.30	77.3	0.15	(25%)
Spent Oil Shale, Run S-11 Sample 20 Batch 1, 11/27/77 LLL Small Retort	0.760	5.88	1.28	149	0.16	(26%)
BCR-1	0.150	1.75	0.089	130	<0.08	
Allende Meteroite	0.500	0.016	8.20	113	0.770	(6%)

[a]Errors for the Cd, U, Se, and Zn values range from 3% to 8% (1σ). Errors for Te are shown in parentheses.

of any of the methods. Seven techniques were chosen for comparison. Instrumental neutron activation analysis (INAA) using the californium subcritical assembly was considered to be the most reliable technique and was used as the reference technique. Other techniques included x-ray fluorescence (XRF), D. C. arc plasma emission spectroscopy, flame atomic absorption, graphite furnace atomic absorption, hydride generation, and the American Society for Testing and Materials (ASTM) colorimetric method using silver diethyldiothiocarbonate. The method of standard addition was used when applicable. The first set of results from this intercomparison showed a spread of about 60%. Even the INAA results varied by 30% on triplicate samples. This problem was traced to particulate matter in the sample bottle despite prior filtering of the process water at the time of collection. The analyses were rerun on freshly filtered samples with much better agreement results, which are shown in Table 4.3.

Good agreement with INAA was obtained for XRF, D. C. plasma emission, hydride generation, and graphite furnace atomic absorption. The flame atomic absorption result is somewhat high. This is probably due to the large background correction required because of flame absorption at the chosen analytical wavelength.

The ASTM standard method did not yield any results. Evolution of a large amount of H_2S during the arsine generation step rendered the technique unusable on this type of sample without substantial technique modification. This problem was not encountered with the

TABLE 4.3. Arsenic Values in an Oil Shale Process Water as Determined by Seven Different Analytical Techniques.

Technique	Concentration, μg/gm
Instrumental Neutron Activation	8.8 ± 0.3
X-Ray Fluorescence	9.4 ± 0.5
Plasma Emission Spectroscopy	10.2 ± 0.3
Atomic Absorption	12.6 ± 0.4
Graphite Furnace Atomic Absorption	9.7 ± 1.6
Hydride Method	9.5 ± 1.0
Colorimetric Method	No Result

arsine method in routine use by our laboratory because the much greater sensitivity of the plasma emission detector makes it possible to use much less sample.

Elemental Mass Balance for the Paraho Semiworks Retort

C. L. Wilkerson and J. S. Fruchter
Technical Assistance: R. W. Sanders

During the past year, a mass balance for sulfur and ten metallic elements was completed for the Paraho Semiworks retort located near Rifle, Colorado to determine the amounts of various species released during the retorting phase of shale oil production. Representative samples of raw shale, retorted shale, product shale oil, retort water, and product off-gas were collected at the plant site and analyzed for elemental abundances by several modern analytical techniques. The observed concentrations of Al, As, Co, Fe, Hg, Mg, Ni, S, Se, V, and Zn, and the retorting parameters that were provided by the Paraho plant management were used to determine elemental mass balances. The Fischer assay of the raw shale was reported to be 23.8 gal of product oil/ton of raw shale. Table 4.4 summarizes the concentration of each element in the raw shale, the resulting elemental mass balances and the observed mass imbalances.

The computed elemental mass balances show that 1% or greater fractions of As, Co, Hg, Ni, S, and Se are released during retorting and are redistributed into the product shale oil, retort water, or product off-gas. The fraction of these six elements released ranged from 1% for Co and Ni to 50-60% for Hg. Approximately 20-30% of the S and 5% of the As, and Se are released. The mass redistribution for Al, Fe, Mg, V, and Zn was observed to be no greater than 0.05%.

Determination of Mercury and Mercury Species in Flared Product Gas of Paraho Semiworks Retort

C. L. Wilkerson

Table 4.4 shows that a significant fraction of the mercury entering the Paraho Semiworks retort is released during retorting and redistributed into the product shale oil and the product gas. Because a portion of the product gas is eventually flared to the atmosphere, this effluent gas stream must be characterized for the concentration and chemical form of mercury released. This characterization was completed during field trips to the plant site in August and November 1977. Representative data are given in Table 4.5.

The total mercury concentration in the flared product gas was sampled by using an in-stack quartz sampling probe and absorption tubes containing 80-100 mesh gold-coated beads. Samples of the effluent gas were pumped from the thermal oxidizer stack and passed through the gold-coated bead traps to remove total vapor mercury. The chemical forms of mercury in the gas stream were isolated by pumping additional sample fractions through selective sorption beds which absorb $HgCl_2$, CH_3HgCl, Hg^0 and $(CH_3)_2HgCl$. After collection, all traps containing mercury were

TABLE 4.4. Elemental Mass Balances for the Paraho Semiworks Retort.

		Weight % Element in Products and Effluents				
Element	Elemental Abundance in Raw Shale, ppm	Retorted Shale	Oil	Retort Water	Product Gas	Imbalance
Al	38,800	101.8	<0.01	<0.01	<0.01	+1.8%
As	48	100.5	5.5	0.05	0.07	+6.1%
Co	8.9	102.0	1.0	<0.01	<0.02	+3.0%
Fe	20,500	98.0	0.02	<0.01	<0.01	-2.0%
Hg	0.079	41.4	33.7	0.03	15.6	-9.3%
Mg	35,900	96.8	<0.01	0.01	<0.01	-3.2%
Ni	25	100.3	1.0	0.01	<0.04	+1.3%
S	6,000	81.6	10.8	2.6	22.6	+17.6%
Se	2	94.0	3.8	1.4	<0.01	-0.8%
V	86	103.6	0.02	<0.01	<0.01	+3.6%
Zn	66	104.1	0.05	<0.01	<0.01	+4.2%

TABLE 4.5. Mercury and Mercury Species in the Paraho Thermal Oxidizer Gas.

	Paraho Thermal Oxidizer Gas		
Date	Total Hg, $\mu g/m^3$	Hg Species, $\mu g/m^3$	
8-24-77	9 ± 3		
8-25-77	6.7 ± 0.8		
8-26-77	4.5 ± 1.3	as $HgCl_2$	<0.3
		as CH_3HgCl	<0.2
		as Hg°	4.5
		as $(CH_3)_2HgCl$	<0.1
11-15-77	7.2 ± 0.9		
11-16-77	12 ± 2	as $HgCl_2$	<0.1
		as CH_3HgCl	<0.4
		as Hg°	9.4
		as $(CH_3)_2HgCl$	<0.4

analyzed by flameless atomic absorption spectrometry.

The range of total mercury observed in the Paraho thermal oxidizer gas was 4.5 to 12 $\mu g/m^3$. The speciation measurements indicate that the mercury is emitted to the atmosphere as the metal (Hg^0). This is expected because almost all mercury compounds decompose to Hg^0 at high temperatures.

Sulfur Speciation in Oil Shale Retort Off-Gases and Process Waters

J. D. Ludwick and J. S. Fruchter

The chemical form of sulfur in oil shale retort off-gases and waters has a considerable influence on the ultimate fate and effects of these effluents. Therefore, we have been developing methods to determine sulfur species.

Gases from process lines at the Paraho Semiworks retort were either directly fed or fed through volume dilution systems into analytical instrumentation for measurements. Hydrogen sulfide levels were measured. Mercaptan levels were measured potentiometrically in an Interscan sulfur analyzer. Sulfur dioxide concentrations were determined by the loss in potentiometric sulfur response when this species was selectively scrubbed from the process or diluted air stream. Results of these analyses of samples are shown in Table 4.6.

Sulfur speciation methods for retort process waters are in a somewhat less developed

TABLE 4.6. Sulfur Species at Paraho Semiworks Retort, November 15-16, 1977.

	Sulfur Species,[a] ppm					
Techniques	SO_2	H_2S	Mercaptans	H_2S + RSH	RSH	$S^=$
Thermal Oxidizer			Off-gas Samples			
Dilution Technique	276	<0.4	<0.4			
Direct	256					
Recycle Gas Concentration						
November 15						
Dilution-trap						
From November 16 Ratio		930		2800	1870	
November 16						
Trap-dilution						
Direct-dilution		802[b]				
By Difference in Techniques					1064[b]	
			Process Water Sample			
November 15						9.9
Total S 4.6%						

[a] All samples were analyzed with an Interscan sulfur analyzer except for those noted in the table.
[b] Sample was analyzed with a Del-Mar Colorimeter.

state; a number of widely recognized sulfur analysis methods are not applicable for these complex waters. Table 4.6 also shows a sulfide analysis of a Paraho process water that was performed with a selective ion electrode; total sulfur values were obtained by neutron activation and x-ray fluorescence. The large differences indicate that most of the sulfur in this water sample is not in the form of sulfide. The bulk of the sulfur may be present as a combination of sulfur dioxide, sulfur, and thiosulfate, but we have not confirmed this. Work is continuing on this aspect of sulfur speciation.

Fossil Fuel Research Materials

J. S. Fruchter and M. R. Petersen

The purpose of this program is to obtain, store, prepare, and distribute homogeneous and chemically analyzed synthetic fossil fuel samples for characterization, environmental, and health effects studies. A number of samples from oil shale retorts and coal conversion processes that are available in our refrigerated repository were listed in last year's Annual Report. Additional samples collected this year include a crude oil and a process water from a true in-situ oil shale retort in northeastern Utah, and light distillate, heavy distillate, and vacuum bottoms from the Solvent Refined Coal-II process. PNL, under its DOE contract, has provided a number of chemical fractions and bulk samples to biologists, ecologists, and waste treatment specialists at PNL. Fractions included Solvent Refined Coal-I liquids, fractions from Solvent Refined Coal-II liquids and vacuum bottoms, samples of several crude petroleums, fractions from Paraho shale oil and Livermore L-OI shale oil, and spent shale and retort water from Paraho. Studies conducted on these samples include characterization studies, intercomparison studies, Ames mutagenicity assays, mammalian cell assays, skin painting tests, acute toxicity tests, and spent-shale leaching studies.

Listed below are reference materials that are currently available.

1. Solvent-Refined Coal Process-I
    a. Solvent-refined coal
    b. Mineral residue
    c. Light oil (naphtha)
    d. Recycle solvent
    e. Wash solvent
2. Lawrence Livermore 125 kg Retort
    a. Mahogany Zone raw shale (24 gal/ton)
    b. Spent shale (Run S-11)
3. Lawrence Livermore 7 Ton Retort
    a. Spent shale (Run L-1)
    b. Crude shale oil (Run L-1)
    c. Process water (Run L-1)
4. Geokinetics In Situ
    Process water
5. Crude Petroleums
    a. Wilmington (high N)
    b. Gato Ridge (high metals, high N, high S)
    c. Prudhoe Bay (low N, low S)
6. Paraho Semiworks Retort*
    a. Raw shale
    b. Retorted shale
    c. Crude shale
    d. Product water
    e. Raw shale crushing fines from filter baghouse
    f. Retorted shale fines from filter baghouse
7. CO_2 Acceptor
    a. Ash
    b. Spent acceptor
8. Solvent-Refined Coal Process II
    a. Light distillate
    b. Middle distillate
    c. Heavy distillate (product)
    d. Vacuum bottoms
9. Vernal, Utah In-Situ Retort
    a. Crude shale oil
    b. Retort water

Preparation and Multielement Characterization of a Colorado Oil Shale Reference Material

C. L. Wilkerson and J. S. Fruchter

Renewed commercial interest in developing the nation's oil shale reserves has required numerous studies to evaluate the environmental and health impacts associated with potential oil shale mining and retorting operations. The successful implementation of many of these programs depends on the availability of research materials that can be used for the development of analytical technology and

*Use of any materials from Paraho requires approval from Development Engineering, Inc. (operators of Paraho retort) on a case-by-case basis.

for use in environmental and biological exposure studies. To help meet this need for research materials, our laboratory has started preparing and chemically characterizing a Colorado oil shale reference material.

A 25-kg quantity of raw oil shale was obtained from the Anvil Points Mine near Rifle, Colorado. The material has been ground to -140 mesh, mixed, split into subsamples of approximately 200 g, and stored in a manner that inhibits chemical degradation. The Fischer assay of the raw shale is 23.8 gal of product oil per ton of raw shale. The material is being characterized for major minerals and for approximately 50 major, minor, and trace element constituents. To assure a high level of confidence in the analytical measurements, the characterization is based on the use of multiple analyses, interlaboratory comparisons, and verifications among several analytical techniques including instrumental neutron activation analysis, flame and flameless atomic absorption spectrometry, and D. C. coupled plasma emission spectrometry.

Preliminary analyses from two different splits of the proposed reference material show it to be quite homogeneous for all elements that have been investigated. Acceptable homogeneity has been verified for material fractions as small as 0.1 g. The water content of the oil shale was investigated by freeze-drying several preweighed fractions to a constant weight. The results show the raw shale to be essentially anhydrous; no significant weight loss was observed. The major minerals identified by x-ray diffraction analysis are dolomite (∿50%), quartz (∿25%), analcime (∿10%), calcite (∿5%), feldspar (∿5%) and illite (∿5%).

Neutron Activation Analysis of Coal and Oil Shale Materials with a ^{252}Cf-235U Fueled Subcritical Multiplier Facility

C. L. Wilkerson

A detailed chemical characterization of the liquid products and effluents from oil shale retorting processes is necessary for assessing environmental impacts and for aiding engineering design and process control. PNL recently developed a ^{252}Cf neutron multiplier facility for use in trace element analysis by neutron activation analysis to help provide the analytical capability for these detailed chemical characterizations. During the past year, this facility's analytical applications to oil shale retort waters and crude shale oils have been evaluated. Other applications included analyses of liquid products derived from coal.

A significant advantage of the ^{252}Cf facility over most conventional research reactors is that relatively large (10-100 ml) volumes of oily water, shale oils, and other organic liquids may be irradiated directly with no sample pretreatment. Danger of sample leakage or explosion is reduced. These advantages and the inherent advantages of neutron activation analysis, including multielement characterization capability and its relative independence from sample matrix effects, makes the ^{252}Cf facility an extremely valuable analytical tool.

Multielement analysis of sample materials (typically 10 ml volumes) based on 10-, 100-, and 1000-min irradiations has been used with oil shale and coal-derived liquids. A large group of major and minor elements can be quantitatively measured in very complex environmental matrices with this sequential irradiation procedure and a thermal neutron flux level of $\sim 10^{10}$ n/cm^2/sec. Elements typically observed and quantified include Al, As, Br, Ca, Cl, Co, Cu, Fe, Mg, Mn, Mo, Na, Ni, S, Se, V, and Zn. A representative gamma-ray spectra for neutron-activated crude shale oil is shown in Figure 4.6.

Program CANGAS Applied to Oil Shale Matrices

J. C. Laul, C. L. Wilkerson and V. L. Crow

We have developed a computer program, CANGAS, (Computer ANalysis for GAmma-ray Spectrometry), that is used for quantitative multielement analysis by neutron activation analysis/gamma-ray spectrometry. CANGAS is based on a manual selection approach of a photopeak area and Compton background channels of the identified photopeaks of interest in a spectrum. The program first checks for any shift in the assigned peak center (channel) in an allowable shift range (1 to 6 channels) with an iterative maxima summing process and a peak symmetry value. A shift of 0.5 channels is allowed each iteration in the direction that causes the value of peak symmetry to decrease. Iterations continue until the peak symmetry value changes sign. At this iteration, the smaller absolute value between the two peak symmetry values determines the final peak shift, and thus the peak center. After locating the peak center, the program integrates the photopeak according to the assigned width in the reference library. The program also shifts the assigned Compton background channels according to the integral shift in the peak center, and the program also allows an additional shift of one channel by a minimum summing iterative process.

The program compares a sample to a standard for final computation of results and lists the elemental concentration in ppm and the associated error (%). The program also lists gross, net and background counts, counting errors caused by the sample and standard, decay corrections from the end of irradiation and during counting, upper limit values based

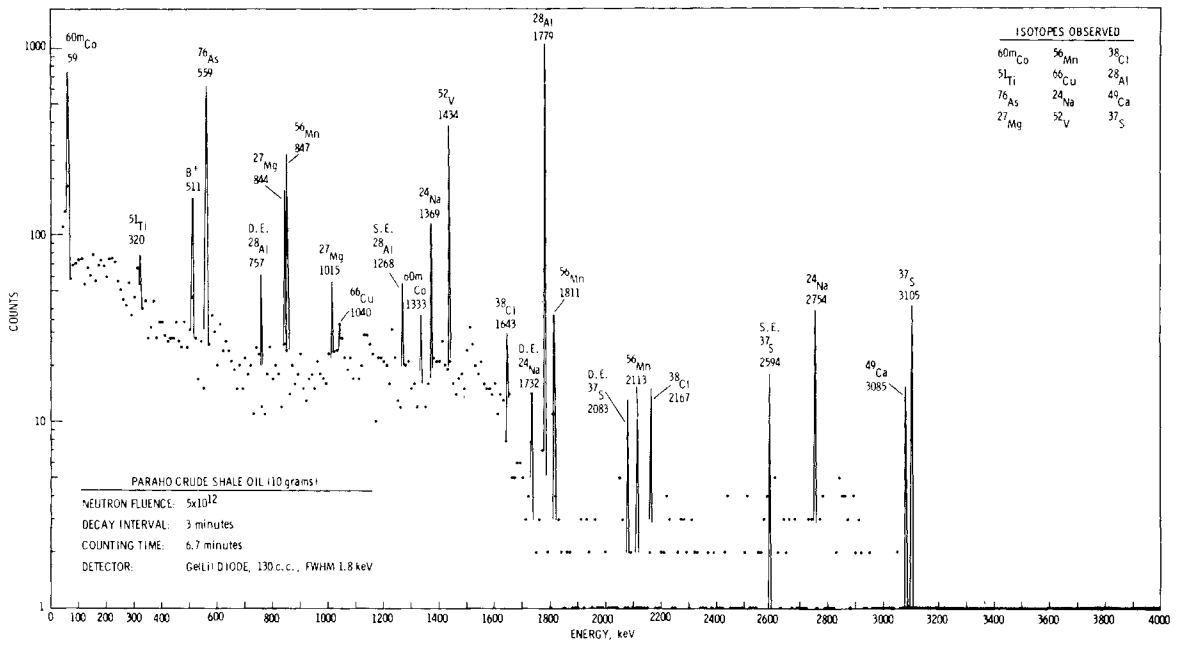

FIGURE 4.6. Representative Gamma-Ray Spectra of a Neutron-Activated Crude Shale Oil.

on 3σ of the gross counts and background counts, and corrected count/min/gm. The program lists peak center and any peak shift, peak width taken, any shift in background channels, and other descriptive parameters that were initially assigned to each gamma-ray spectrum.

We satisfactorily tested CANGAS on five TEST synthetic spectra, which consisted of 36 photopeaks of different intensities in the 60-1500 keV energy range. These spectra had variable shifts in photopeaks, and the relative intensities among photopeaks varied as much as by factors of ∿1000; the peak-to-Compton ratios varied from ∿1.5 to 100. About 90% of the values agreed within ±2%, all within ±5%, with manual computations. We also successfully applied CANGAS to the analysis of 33 elements by instrumental neutron activation analysis in NBS coal, fly ash, and recently prepared different oil shale standards. Our values in the vast majority of cases agreed very well with reported values for NBS coal and fly ash. In the case of oil shale matrices, whenever comparison values existed, our values agreed well with those obtained by other analytical techniques and/or other laboratories.

5.0 Multitechnology

• Environmental Pollution Analysis Instruments and Methods Development

Assessment of energy-related pollutants, their sources, and their transport through the environment requires reliable analytical instrumentation and methods. Analysis methods have been developed for measurement of the chemical form and quantity of mercury in fresh water, geothermal water, and sea water by precipitation and x-ray fluorescence. Improved peak analysis methods and computer programs to handle scattered radiation have been developed to improve the matrix correction and accuracy of x-ray fluorescence analysis. Liquid and gas chromatography methods have been developed in conjunction with activation analysis and plasma emission spectroscopy for the measurement of organometallic species in synthetic fuels.

Technique Development for Ultra Low-Level Analysis of Mercury in Water

E. A. Crecelius

Research in this laboratory has shown that natural waters sometimes contain less than one nanogram of mercury per liter of water. Because existing analytical techniques were not sensitive enough for these levels, work was directed toward extending the detection limit down to the 0.1 ng/ℓ level.

In the previous technique, mercury was reduced to Hg^0 in solution by $SnCl_2$, then purged from solution with nitrogen gas and collected on gold before detection by flameless cold vapor atomic absorption. That analysis system was checked for absorption losses using a ^{203}Hg radioactive tracer. The magnesium perchlorate water vapor trap used between the gold trap and the detector absorbed significant amounts of mercury.

To eliminate the need for a drying agent, the gold traps are now dried by flushing with 40°C mercury-free nitrogen before the trap is analyzed. A chromatographic grade aluminum oxide trap (1/2 x 4 cm), which is located between the gold trap and the detector, is used to absorb organic vapor that could cause an interference in the spectrophotometer.

The newly developed technique consists of adding 30 mℓ of 10% $SNCl_2$ in 10% H_2SO_4 to a 1 ℓ water sample that has been acidified to pH of 1-2. The water sample is purged with mercury-free N_2 gas at a flow of 1 ℓ/min for 30 min using a glass frit. The Hg^0 vapor is then trapped on a gold bead and analyzed by cold vapor atomic absorption as it was in the earlier methods. The detection limit is 0.1 ng/ℓ.

X-Ray Fluorescence Peak Analysis Method

K. K. Nielson

A Battelle-developed direct method for calculating net peak areas in energy dispersive x-ray fluorescence (XRF) spectra has now been evaluated for a wide variety of experimental conditions to assure its accuracy under anticipated XRF applications. The method, detailed previously (Nielson 1978a, Nielson and Wogman 1978), uses the area above a pseudo "background" which connects the intensities at the integration window boundaries. This area is a constant fraction of the net peak area as long as the detector resolution is constant.

Failure to locate peaks is completely avoided by this method because integration windows are placed in expected positions according to peak energy rather than according to spectral features. The required energy calibration is determined for each spectrum from fiducial peaks. This accommodates the small gain shifts resulting from variable high count rates. Experiments covering 0-95% dead time for a given sample have demonstrated complete compensation for the resulting gain shift. The peak broadening which occurs at high count rates was also shown to cause less than 1% intensity loss at 40% dead time and less than 5% loss at 65% dead time. Usual operations have less than 30% dead time.

The direct peak areas are independent of background intensity and linear background slope. Sharply curving background such as that adjacent to a large interfering peak causes systematic errors, but they are easily corrected by applying peak overlap factors directly measurable from the single element calibration spectra. The accuracy of such

corrections has been demonstrated over wide intensity ranges by successful analyses of a large number of National Bureau of Standards (NBS), U.S. Geologic Survey (USGS), and International Atomic Energy Agency (IAEA) standard reference materials. Because no assumptions are made regarding peak shape, the many non-gaussian doublets in XRF spectra are easily handled. About 3 s are required for the PDP-11/35 computer to analyze 26 peaks, and no operator intervention is necessary. Once created, a set of peak calibrations can be used indefinitely with only occasional checks on detector resolution.

Use of Backscattered X-Rays in X-Ray Fluorescence Matrix Corrections

K. K. Nielson

A review of XRF matrix correction methods that use scattered radiation (Nielson 1978b) has provided a systematic evaluation of their capabilities and has clarified their relation to a method developed at Battelle (Nielson 1977 and 1978b). Most scatter-based matrix corrections have relied on relative intensity measurements and simply replace the calibration of analyte fluorescent intensities with a calibration of fluorescent/scatter intensity ratios. The ratios are independent of excitation intensity and analysis time, and are less sensitive to varying sample compositions, densities, and geometries. Thus, they are especially useful in field measurements where careful sample geometry and instrumental control is often difficult. Coherent, incoherent, and combined scatter have been used in these applications. The relative methods are limited, however, in that they are quantitative only for thick samples that have similar absorption coefficient ratios to standards at the analyte and scatter peak energies.

Correction methods that use absolute scatter intensities require accurate control of instrumental parameters but potentially permit quantitative analysis of samples without similar standards. The multielement method developed at Battelle (Nielson 1977) is the only one of the absolute methods that uses scattering cross sections to numerically solve for all significant elements and their resulting matrix effects. This method is based on the isolated atom model of x-ray scattering and separately considers coherent and incoherent scattering in characterizing a sample's constituents and its thickness. Thus, the method makes use of two extra degrees of freedom that are neglected in relative intensity methods. From these parameters, self-absorption, enhancement, and particle size corrections are explicitly calculated from fundamental constants. This permits analysis of samples of varying thickness and composition and does not require preparation of similar standards. Therefore, by maximizing use of spectral information, prior knowledge of sample composition or subjective assumption of its similarity to a standard is avoided.

Minimization of Sample Preparation for X-Ray Fluorescence Analysis

K. K. Nielson

A matrix correction method recently developed for XRF analysis has been extended to accommodate samples of non-standard geometry and thickness. The new method permits quantitative analysis of samples such as oils, hair, radioactive materials, and other materials that cannot be prepared by conventional methods such as pelletizing. Such samples are sealed between thin polypropylene films in a sandwich configuration and need not be weighed or otherwise handled. By this simplified procedure, cost and contamination are greatly reduced, and the quantitative XRF method is extended to a much greater variety of samples.

The new method determines the average mass or thickness of the samples in the x-ray beam from the backscattered x-ray intensities, and the effective absorption characteristics are computed from the ratios of coherent and incoherent scatter and from the analyte fluorescent intensities. Sample mass must be large compared to the $\sim$0.5 mg (6 μm) thick plastic film containing it in order for the backscatter to accurately represent sample composition. Relative uncertainties of 1-3% have been obtained for S, Ca, and Zn in replicate hair analyses, and accuracies have been verified for both oil and hair samples by other analytical methods. The method is still being investigated for potential application to unconsolidated powder samples, where particle size estimates may become the major source of uncertainty.

Identification of Organometallic Species in Effluents from Advanced Fossil Fuel Facilities

J. A. Campbell and W. C. Weimer

Molecular speciation studies to characterize organometallic substances that may be found in the environment as by-products of several advanced fossil fuel processes are underway. Because of the very small concentrations at which these constituents are present, the detection and identification of organometallic compounds in the environment present several challenging analytical problems in collection, separation from natural matrices, and quantitative identification.

Research activities thus far have emphasized characterization of two types of

effluents from oil shale retorting processes. Preliminary results from pyrolysis experiments of well-characterized raw shale indicate small concentrations of Ni, Zn, and Cu present in the condensed volatile product gases. All of these elements are known to form organometallic complexes. High-performance liquid chromatography (HPLC) analysis of this condensate has shown a very complex mixture of organic moieties, several of which have been tentatively identified. Capillary column GC/MS has been used to analyze the product gases and the oil produced by this pyrolysis of raw shale. The results of these characterizations show high concentrations of short-chain alkanes and alkenes, some higher aliphatic compounds up to C19 in length, as well as several fused ring and aromatic compounds that may form organometallic complexes.

Ultrafiltration investigations of oil shale process waters have identified Fe, Cr, Co, Cu, Ni, and Se present in a high molecular weight fraction of the organic portion of these waters. Further research employing HPLC and an electrochemical detector system that is highly sensitive to organometallic species is continuing on both the condensate from the oil shale pyrolysis and the process waters.

• Environmental Pollutant Characterization by Direct-Inlet Mass Spectrometry (DIMS)

The utility of direct-inlet mass spectrometry for the detection, characterization, and monitoring of important particulate airborne pollutants that arise as by-products of energy production and other industrial activities is being experimentally determined. The direct-inlet mass spectrometer system previously constructed has been interfaced to a digital computer, a particle generator has been constructed, and initial calibration experiments of the entire system have been performed. The materials to be studied in this program have been selected through a review of important airborne particulate pollutants.

Characterizing Environmental Pollutants by DIMS

C. R. Lagergren and R. L. Gordon

The purpose of this program is to experimentally determine the utility of direct-inlet mass spectrometry (DIMS) as an analytical technique for the detection, characterization, and monitoring of important particulate airborne pollutants that enter the environment as by-products of energy generation or other industrial activities.

In the DIMS technique, airborne particles are introduced as a jet directly into the ion source of a surface ionization mass spectrometer. Particles striking the hot filament form bursts of ions that are then mass analyzed and measured. Burst rates are related to particle concentration in sampled air while the total charge per burst is a measure of particle size. Ionization efficiencies by surface ionization for a wide range of elements are sufficiently high so that submicrometer size particles of compounds of these elements can be detected.

To determine the utility of DIMS as a sensitive, species-selective, and real-time analytical technique for measuring airborne pollutants, the nature of the ionization produced by surface ionization of specific pollutant materials of interest must be established. The ionization efficiency, cracking pattern (ion spectrum), and time characteristics of the signals that are produced are not only functions of the molecular and physical form of the pollutant material, but are also functions of the nature and temperature of the filament surface. These quantities and relationships are unknown and need to be determined for successful application of the technique.

A DIMS system for these studies had been designed and constructed previously. The system, which consists of a direct inlet for airborne particles, a surface ionization filament, and a quadrupole mass filter, has been interfaced to a digital computer, which permits the rapid accumulation of data (total charge per burst of ions). In addition, computer programs have been written to collect and analyze data and to report the results of analyses, and a jet-mill type particle generator has been constructed to produce suitable aerosols of the materials to be studied in this program.

Initial performance tests of the DIMS system showed that refinements were necessary to improve the transmission of ions from the surface ionization filament to the quadrupole. Therefore, an additional ion lens that provided a stronger electrical draw-out field for ions produced at the filament surface was added. The overall transmission, including that of the quadrupole, was greater than 15 percent.

An initial calibration experiment was performed using $CsNO_3$ as a sample material. Aerosols were generated in the jet-mill and introduced into the inlet system. Ion bursts of approximately 10 msec durations were produced at a filament temperature of 1000°C. The total ion charge collected for each of 4096 bursts was stored in a computer memory for subsequent determination of pulse size distribution.

To determine the size distribution of particles that react with the surface ionization filament, the filament was cleaned by heating and then maintained at room temperature so that particles could be collected on its surface. Photographs of particles collected on the filament were taken with a scanning

electron microscope and sized using a IIMC particle-measurement apparatus.* The particles were found to be confined within a circle of approximately 1.6 mm in diameter, which indicates the inlet system operates properly. Analysis of the particle size data revealed that the collected particles could be characterized by a log-normal distribution that had a count median diameter of 0.23 micrometers and a geometric standard deviation of 1.65.

Figure 5.1 summarizes the particle size and total charge data in a log-probability plot. The lower line is a fit to the particle size data points (logarithm of diameter versus cumulative particle area percent) represented by (□), and the upper line is the corresponding particle area distribution (logarithm of diameter versus cumulative particle area percent). The total charge per burst data, represented by (o), are also log-normally distributed. When these data are plotted as logarithm of square root of charge versus cumulative charge percent, they fit well to the area distribution curve. It was expected that the DIMS data would fit a mass distribution data curve, i.e., logarithm of cube root of charge versus cumulative charge percent. These data are preliminary, and the reason for their unexpected behavior is still under investigation. However, an important result is that with calibration, DIMS can provide particle size information.

* Manufactured by Millipore Corporation.

A brief survey was conducted to identify those elements that could serve as promising candidates to determine the suitability of direct inlet mass spectrometry for real-time monitoring of their elemental concentrations in the atmosphere. The survey used the reference Toxic Metals, Pollution Control and Worker Protection (Sittig 1976), which compiles the results of an extensive survey of available literature on the toxic metals and their compounds. Three criteria were used to select the elements for DIMS investigations:

1. Particulates containing the element must be toxic.

2. The element must possess an ionization potential less than 8.0 eV so that a reasonable ion signal from surface ionization could be expected.

3. The material must be sufficiently hazardous to warrant real-time atmospheric monitoring.

In all selected cases, successful application of DIMS would offer real-time measurements as well as significant simplification over conventional methods of sampling and analysis for the elements being investigated. The elements selected for evaluation include V, Cr, Mn, and Pb.

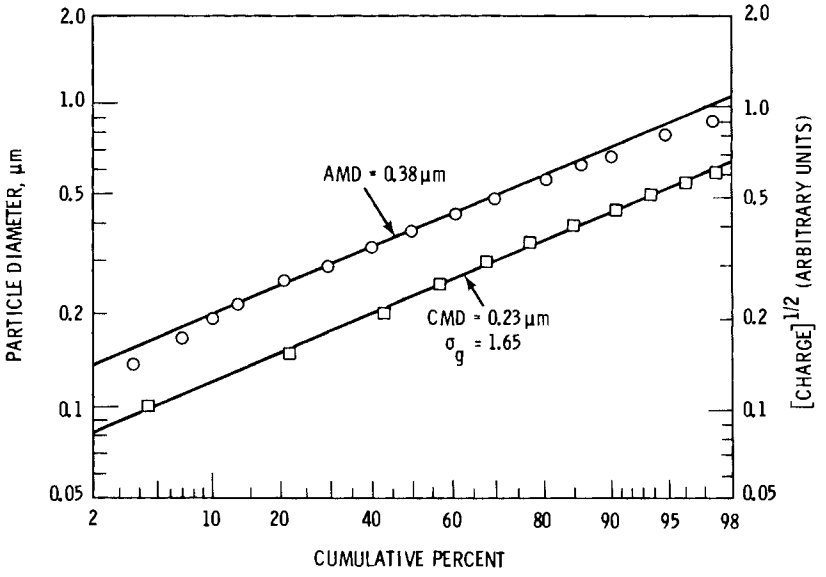

FIGURE 5.1. Comparison of Cesium Nitrate Particle Size Distribution with the Corresponding Charge Distribution of Ion Bursts Measured by DIMS.

• Trace Analysis by Laser Excitation

The identification and measurement of low-level environmental pollutants remain high priority problems associated with energy production from both nuclear and fossil fuels. Studies of the environmental behavior and hazards of a variety of radionuclides, stable elements, and organic pollutants could be greatly simplified by the development of new analytical techniques that have greater sensitivities and real-time capabilities.

The purpose of this program is to develop laser excitation techniques for the detection of low-level pollutants. The high photon fluxes available with laser radiation may allow the detection of many species at concentrations orders of magnitude lower than those achieved by conventional methods. This capability has been dramatically demonstrated at ORNL, where laser excitation has been used to detect single cesium atoms. While such results are optimistic for all species, it is reasonable to expect detection limits on the order of 10^4 to 10^7 atoms for atomic species and concentrations in the parts-per-trillion to parts-per-billion range for molecular species.

This year, efforts have included studies of polynuclear aromatic hydrocarbon detection by laser fluorescence and development of an improved two-photon laser excitation scheme. We have also participated in a significant effort with the comparable laser group at ORNL.

Oxygen Quenching of Gas Phase PNA Fluorescence

B. A. Bushaw and T. J. Whitaker

Previous studies examined the effects of sample conditions on the fluorescence analysis of pyrene vapor. We have now extended those studies to a number of other gas-phase polynuclear aromatic hydrocarbons (PAHs). Stein-Volmer analysis of fluorescence intensity as a function of varying partial pressure of O_2 allows the determination of the rate constants and quenching efficiencies for 15e deactivation process:

$$M^* + O_2 \xrightarrow{kg} M + O_2$$

where M represents the PAH of interest. The determination of the quenching efficiencies is important for trace analysis under atmospheric conditions because the quenching efficiencies will determine ultimate sensitivities and also affect actual quantitative measurements.

We have found strong correlations between excited state lifetime and quenching efficiency of a series of PAHs ranging in size from naphthalene to perylene, (Figure 5.2). As expected, the species with longest lifetimes are those that are quenched most efficiently. There also appears to be a correlation between the energy gap between the

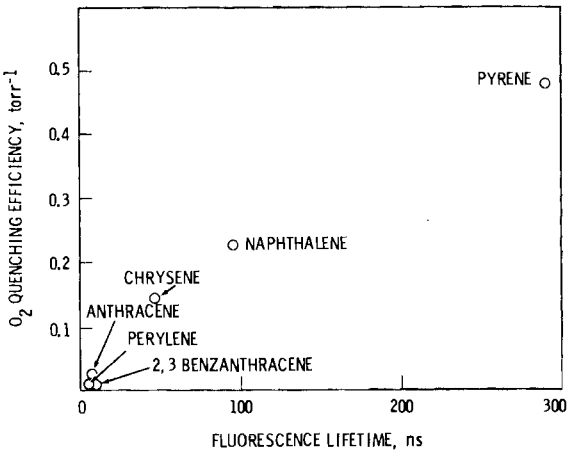

FIGURE 5.2. Oxygen Quenching Efficiency Versus Fluorescence Life-Time.

first excited singlet and the first excited triplet states in the PAHs. When this energy gap is near the energy of either of the first excited singlet states of oxygen, the quenching becomes more efficient. This can be explained by a quenching mechanism that involves a spin-conserving collision. The excited singlet PAH and the triplet ground-state oxygen undergo energy and spin exchange during collision to produce a triplet PAH and an excited singlet oxygen. The triplet PAH then decays by nonradiative processes.

Laser System Development

B. A. Bushaw and T. J. Whitaker

Resolution of the N_2 laser-pumped dye laser has been improved in a continuing effort to obtain isotopically selective two-photon excitation of xenon. The oscillator can now be used in single-mode operation with the output bandwidth nearly transform-limited to 120 MHz. Continuous tuning of the oscillator cavity by grating rotation has not been performed because the output frequency "hops" through successive cavity modes, which are separated by approximately 375 MHz as determined by the cavity length. This type of operation precludes the possibility of obtaining Doppler-free two-photon spectra that exhibit the resolution of the single-mode bandwidth. Instead, the resolution is limited in a stepwise fashion to the mode separation, and when the output is frequency doubled and two photons are absorbed, the effective resolution is then limited to four times the mode spacing (about 1500 MHz). Spectra that show isotopic hyperfine structure with this resolution have been obtained; however, further peak separation is required to allow isotopically selective analysis.

Oak Ridge National Laboratory Computer System for Laser Research

B. A. Bushaw and T. J. Whitaker

Because of similarities in data acquisition requirements for experiments in our program and some of the experiments in another DOE-sponsored program at Oak Ridge National Laboratory (ORNL), a cooperative effort was begun that has resulted in a considerable financial savings to the ORNL program. The ORNL group, headed by G. S. Hurst, has installed a mini-computer based data acquisition system that is identical to the one in the laser program funded at PNL. The ORNL group has been able to take advantage of software expertise developed here, which has resulted in significant savings in time and funds for the ORNL program. Cooperation with ORNL resulted in a paper soon to appear in Chemical Physics Letters on the diffusion of highly reactive species.

• Applications of Holography

Holography that uses short laser pulses is being studied to determine its usefulness for examining environmental problems. We have designed and built a simple portable holo-camera that would have applications in the field and laboratory for characterizing the physical properties and behavior of aerosols, particulates, and underwater organisms.

Applications of Holography to Environmental Studies

B. P. Hildebrand

Holography is a photographic technique that records a scene in three dimensions. This record or hologram can be used to reconstruct the scene for later study. The reconstruction is so perfect that it can be used for making precise measurements by means of interferometry, for example. The invention of the laser in the 1960s resulted in a rapid expansion of holography research and application. The pulsed laser, in particular, moved research efforts in the direction of particle holography that could record transient events which could later be studied in the laboratory. Commercial pulsed-ruby lasers are expensive and cumbersome and usually require an outside source of power. For these reasons, holography has not reached its full potential in any but the most specialized applications. Therefore, our research has focused on developing a more useful holographic process. Last year we succeeded in building a small battery-powered ruby laser developed from a Metz 402 photographer's flash unit. We also adapted a 35 mm Pentax camera body to hold the Kodak SO-173 film that records the Gabor holograms.

Measurements indicate that full output of the laser is 12-15 millijoules, enough to overexpose the film. Therefore, an existing circuit in the flash unit was modified to shorten the length of the pulse and provide optimum exposure. The sensor that measures the light on the scene was removed from the flash unit and incorporated into the camera in such a way that it reads the amount of light striking the film. This assures correct exposure even if the laser output varies or the aerosol cloud thickens.

The pulse length of the laser is about 1.5 msec. Small particles (5-10 μm) with velocities greater than 1-2 mm/sec will cause a blurred image. Therefore, we have put a lot of effort this year into designing a Q-switch that can shorten the pulse to 30-100 nsec. A pulse this short will allow particle velocities of 5-10 m/sec, which is certainly adequate. We tried a number of techniques before deciding to use a simple electro-mechanical method to bend the laser rod. When the flash-lamp is fired, the rod is released. Natural resilience of the ruby rod causes it to flex through its normal straight configuration with a resulting Q-switched output. A simple electromagnet powered by the flash unit bends the rod.

We had planned to proceed with a motion picture holo-camera this year. However, the company that promised a repetitively-pulsed, air-cooled Nd-Yag laser was unable to produce it as advertised. At the present time, we cannot obtain a repetitively-pulsed laser without cumbersome water cooling, and a water-cooled laser is not useful for meeting our program's objective of a portable self-contained system.

• Certified Research Materials

In all of the environmental and biological programs, analytical standards are essential so that the accuracy of measurements can be known. We have employed the IAEA standard fish homogenate MA-A-2 as a test material in this intercomparison to determine the reliability of the various measurement methods employed within our laboratory. Our research establishes the actual concentrations of trace elements in this material, and thus certifies it as a research material for use by other laboratories.

Elemental Characterization of the IAEA Standard Fish Homogenate MA-A-2

C. L. Wilkerson, K. K. Nielson and
L. A. Rancitelli

Studies in marine pollution chemistry have often been limited by an inadequate comparability of measurements of trace elements in marine environmental materials. Because this problem affects marine science at both national and international levels, the International Atomic Energy Agency's Laboratory of Marine Radioactivity, Principality of Monaco, is currently coordinating a program of interlaboratory comparisons in trace element analysis of marine environmental samples.

The primary objective of this program is to render a service to countries and their laboratories by supplying the means for analytical quality control needed in marine pollution monitoring and marine research in general. This is being accomplished in two ways: 1) Problem areas are being identified in trace element characterization of marine environmental materials. These areas include relative performance of participating laboratories; relative performance of analytical techniques; and problems in sampling, pretreatment, and storage of marine samples. 2) Reference materials that have acceptable homogeneity and well documented elemental abundances are being made available. To date the Monaco Laboratory has developed and distributed several marine reference materials including oyster homogenate, copepod tissue, and sea plant powder. Other materials to be developed are marine sediments and sea water.

To help achieve a successful intercalibration program, the IAEA asked Pacific Northwest Laboratory (PNL) and a few other reputable analytical laboratories to collaborate in the intercomparison studies. The data contributed by this select group serve both as input to each characterization exercise and as a check on the overall quality of analyses submitted by other participating laboratories.

PNL recently participated in a multielement characterization of the newly circulated IAEA reference material Fish Homogenate MA-A-2. Two splits of this material were analyzed for 53 major, minor, and trace element constituents by instrumental neutron analysis (INAA) and x-ray fluorescence analysis (XRF). Six or 7 samples from each split were analyzed by each analytical technique. All samples were analyzed as received and then corrected for a 4% water content, which was determined by a freeze-drying experiment. The resulting "dry weight" data were tabulated, Chauvenet's criteria were applied to anomalous values, and average elemental abundances were then computed. The average elemental abundances ($\pm 1\ \sigma$) are summarized in Table 5.1.

The results show that Fish Homogenate MA-A-2 is quite homogeneous for the majority of elements measured. The excellent agreement between the two analytical techniques for As, Br, Fe, K, Rb, Se, and Zn verify that the reference material is generally homogeneous for samples as small as 0.25 g (sample weight for INAA). The few elements observed to be inhomogeneous are Ag and Cr, which were identified by INAA at 0.25 g, and Cr and Ti, which were identified by XRF at 0.5 g.

TABLE 5.1. Summary of Elements Determined in IAEA Fish Homogenate MA-A-2, ug/g dry wt

	Split 021			Split 022		
	Method of Analysis			Method of Analysis		
Element	INAA	INAA	XRF	INAA	INAA	XRF
Ag		0.089 ± 0.002			0.092 ± 0.012	
Al	22.3 ± 2.1			21.2 ± 3.2		
As		2.96 ± 0.09	2.7 ± 0.2		2.85 ± 0.08	2.6 ± 0.3
Ba		<10	3.7 ± 1.1		<9	2.6 ± 1.2
Br		22.0 ± 0.3	22.4 ± 0.6		22.1 ± 0.1	22.2 ± 0.5
Ca		<3000	502 ± 80		<3000	525 ± 106
Cd			<2			<2
Ce		<0.1	<3		<0.1	<3
Cl	2990 ± 110		3040 ± 130	2990 ± 170		2870 ± 240
Co		0.043 ± 0.001	<0.8		0.044 ± 0.002	<0.8
Cr		1.01 ± 0.05	1.4 ± 0.5		1.42 ± 0.41	1.4 ± 1.1
Cs		0.119 ± 0.003	<2		0.115 ± 0.003	<2
Cu	<20		3.6 ± 0.6	<20		3.3 ± 0.2
Dy	<0.1			<0.1		
Eu		0.009 ± 0.001			0.008 ± 0.001	
Fe		48.2 ± 2.9	51.1 ± 3.1		47.5 ± 1.4	52.4 ± 6.0
Ga			<0.3			<0.3
Hf		<0.006			<0.006	
Hg		0.36 ± 0.02	<1		0.37 ± 0.02	<1
I			<2			<2
In			<2			<2
K		17,100 ± 200	16,600 ± 500		17,500 ± 300	16,400 ± 400
La		<0.05	<3		<0.04	<3
Lu		<0.01			<0.01	
Mg	1160 ± 60			1470 ± 310		
Mn	<0.7		0.9 ± 0.6	<0.7		1.2 ± 0.6
Mo			<0.6			<0.5
Na	1890 ± 90	1910 ± 20		1900 ± 140	1910 ± 10	
Nb			<0.5			<0.5
Nd		<2			<2	
Ni		<1	0.91 ± 0.30		<1	0.87 ± 0.13
P			9200 ± 150			9540 ± 530
Pb			<1			<0.9
Rb		6.8 ± 0.3	7.3 ± 0.4		6.6 ± 0.4	7.2 ± 0.3
S			10,430 ± 450			10,560 ± 350
Sb		0.009 ± 0.001	<2		0.011 ± 0.002	<3
Sc		0.0011 ± 0.0003			0.0009 ± 0.0004	
Se		1.22 ± 0.01	1.09 ±0.07		1.13 ± 0.02	1.04 ± 0.11
Si			<3000			<3000
Sm		<0.006			<0.007	
Sn			<2			<2
Sr		<2	1.37 ± 0.30		<2	1.47 ± 0.34
Ta		<0.002			<0.002	
Tb		<0.003			<0.003	
Te			<2			<2
Ti	<20		3.7 ± 2.8	<20		7.4 ± 4.9
Th		0.007 ± 0.002			0.006 ± 0.002	
U			<1			<1
V	<0.2		<2	<0.2		<2
Y			<0.4			<0.4
Yb		<0.04			<0.04	
Zn		34.5 ± 0.04	33.2 ± 1.1		34.3 ± 0.8	32.5 ± 0.4
Zr			<0.5			<0.5

References

REFERENCES

1.0

Campbell, J. A., R. D. Smith, and L. E. Davis. 1978. Application of x-ray photoelectron spectroscopy to the study of fly ash. J. Appl. Spectro. 32:316.

Campbell, J. A. et al. 1978. Separation and chemical characterization of finely-sized flyash particles. Anal. Chem. 50:1032.

Davison, R. L. et al. 1974. Trace elements in fly ash: dependence of concentration on particle size, Environ. Sci. Tech. 8:1107.

2.0

Allison, S. K. 1958. Experimental results on charge-changing collisions of hydrogen and helium atoms and ions at kinetic energies above 0.2 keV. Rev. Med. Phys. 30:1137-68.

Booz, J. 1978. Mapping of fast neutron radiation quality. In Third symposium on neutron dosimetry in biology and medicine, eds. G. Burger and H. G. Ebert, pp. 499-514. Luxembourg: Commission of European Communities.

Braby, L. A. and W. H. Ellott. 1971. Ionization in microscopic volumes irradiated by energetic photons. Oregon State University Report AD 731 709.

Brady, L. A., J. M. Nelson and W. C. Roesch. 1978. Inactivation and recovery in Chlamydomonas reinhardi as a function of temperature. In Pacific Northwest Laboratory annual report for 1977 to the DOE assistant secretary for environment, PNL-2500, Pt 4. Richland, Washington: Pacific Northwest Laboratory.

Braby, L. A. and W. C. Roesch. 1978a. Noise-free measurement of <z> for fast electrons. Radiat. Res. 74:482.

Braby, L. A. and W. C. Roesch. 1978b. Direct measurement of f(z) for fast electrons. In Proceedings Sixth symposium on microdosimetry, J. Booz and H. G. Ebert, eds. pp 251-60. Holland: Harwood Academic Publishers, Ltd.

Braby, L. A. and W. C. Roesch. In press. Testing dose-rate models with Chlamydomonas reinhardi. Radiat. Res.

Braby, L. A., W. C. Roesch, and J. M. Nelson. 1977. Temperature effect on the production and repair of radiation damage in Chlamydomonas reinhardi. Radiat. Res. 70:684-5.

Bryant, P. E. 1970. The effect of hypoxia on recovery from sublethal damage in Chlamydomonas. Int. J. Radiat. Biol. 17:533-9.

Deering, R. A. et al. 1970. Gamma-ray-resistant and -sensitive strains of slime mold (Dicytostelium discoideum). Radiat. Res. 70:684-5.

Dodelet, J. P. and G. R. Freeman. 1972. Mobilities and ranges of electrons in liquids: effect of molecular structure in C_5-C_{12} alkanes. Can. J. Chem. 50:2667-79.

Eisenhower, T. L. and G. H. Morrison. 1964. A computer program to optimize times of irradiation decay and activation analysis. Anal. Chem. 36:1089.

Eisenhower, T. L., E. A. Evans and G. H. Morrison. 1965. Texas proceedings, Modern trends in activation analysis. p. 123.

Goppola, M. et al. 1976. Experimental evaluation of the spectral energy deposition in small volumes by low LET radiations. In Fifth symposium on microdosimetry, pp. 377-91. Luxembourg: Commission of European Communities.

Inokuti, M. 1971. Inelastic collisions of fast charged particles with atoms and molecules - the Bethe Theory revisited. Rev. Mod. Phys. 44:297-347.

Kaye, J. H. and N. E. Ballou. In press. Determination of technetium by graphite furnace atomic absorption spectrometry. Anal. Chem.

Kaye, J. H., N. E. Ballou and M. S. Rapids. 1978a. Measurement of ^{99}Tc in environmental materials by isotope dilution mass spectrometry. PNL-SA-7001-A (Abstract). Richland, Washington: Pacific Northwest Laboratory.

Kaye, J. H., N. E. Ballou and M. S. Rapids. 1978b. A quantitative radiochemical method for determination of ^{99}Tc. PNL-SA-7026-A, (Abstract). Richland, Washington: Pacific Northwest Laboratory.

Kaye, J. H., M. S. Rapids and N. E. Ballou. In press. Determination of picogram levels of technetium-99 by isotope dilution mass spectrometry. In Proceedings of Third international conference on nuclear methods in environmental and energy research, Columbia, Missouri.

Kellerer, A. M. and H. H. Rossi. 1972. The theory of dual radiation action. Current Topics in Radiat. Res. Qtrly. 8:85-158.

Kupperman, A. 1974. Diffusion kinetics in radiation chemistry: an assessment. In Physical mechanisms in radiation biology, eds. R. Cooper and R. Wood, pp. 155-83. USAEC Technical Information Service.

Laurie, J., J. S. Orr and C. J. Foster. 1972. Repair processes and cell survival. Brit. J. Radiol. 45:362-8.

Madison, D. and E. Merzbacher. 1975. Theory of charge-particle excitation. In Atomic inner shell processes, ed. B. Crasemann, pp. 2-72. New York: Academic press.

Manson, S. T. et al. 1975. Energy and angular distributions of electrons ejected from helium by fast protons and electrons: theory and experiment. Phys. Rev. A 12:60-70.

Miller, J. H. 1978. Effect of the spatial distribution of energy deposition on the radioluminescence of benzene in cyclohexane. Radiat. Res. 74:594-5.

Miller, J. H. In press. Inhomogeneous chemical kinetics in pulsed proton radioluminescence. Biophys. J.

Miller, J. H. and A. E. S. Green. 1973. Proton energy degradation in water vapor. Radiat. Res. 54:343-63.

Miller, J. H. and M. L. West. 1977. Quenching of benzene fluorescence in pulsed proton irradiation: dependence on proton energy. J. Chem. Phys. 67:2793-7.

Mozumder, A. and J. L. Magee. 1966. Model of tracks of ionizing radiations for radical reaction mechanisms. Radiat Res. 28:203-14.

Nelson, J. M. 1978a. Plateau phase Chinese hamster ovary cells. In Pacific Northwest Laboratory annual report for 1977 to the DOE assistant secretary for environment, BNWL-2500, Part 4, p. 2.20. Richland, Washington: Pacific Northwest Laboratory.

Nelson, J. M. 1978b. Culture conditions associated with production and maintenance of viable noncycling monolayers. In Vitro 14:380.

Nelson, J. M., L. A. Braby and W. C. Roesch. 1977. Determination of mean recovery time following split-dose or protracted irradiation. Radiat. Res. 70:708.

Nelson, J. M., L. A. Braby and W. C. Roesch. 1978a. Characterization of rapid recovery in Chlamydomonas reinhardi. Radiat. Res. 74:534.

Nelson, J. M., L. A. Braby and W. C. Roesch. 1978b. Rapid repair of ionizing injury in Chlamydomonas reinhardi. PNL-SA-7148, Richland, Washington: Pacific Northwest Laboratory.

Nielson, K. K., C. W. Thomas and R. L. Brodzinski. 1976. Development of plutonium-americium monitor for in-situ soil surface and pond bottom assay. Nucl. Instr. and Methods 138:227-37.

Paretzke, H. G. 1973. Comparison of track structure calculations with experimental results. In Proceedings of the Fourth symposium on microdosimetry, pp. 148-68. Verbania, Italy.

Paretzke, H.G. and M. J. Berger. 1978. Stopping power and energy degradation for electrons in water vapor. In Sixth international symposium on microdosimetry, eds. J. Booz and H. G. Ebert, p 749-58. Holland: Harwood Academic Publishers, Ltd.

Purdie, J. W. et al. 1974. Increased response of anoxic Bacillus megaterium spores to radiation at high dose rates. Int. J. Radiat. Biol. 26:435-43.

Roesch, W. C. 1971. Analysis of distributions produced by charged particles (and other compound-Poisson processes). Radiat. Res. 47:333.

Roesch, W. C. 1977. Microdosimetry of internal sources. Radiat. Res. 70:494-510.

Roesch, W. C. 1978a. Dose-rate and fractionation theory for multiple recovery processes. Radiat. Res. 74:535.

Roesch, W. C. 1978b. Models of the radiation sensitivity of mammalian cells. In Third symposium on neutron dosimetry in biology and medicine, eds. G. Burger and H. G. Ebert, pp. 1-27. Luxembourg: Commission of the European Communities.

Roesch, W. C. 1978. Internal microdosimetry. In Sixth symposium on microdosimetry, eds. J. Booz and H. G. Ebert. Holland: Harwood Academic Publishers, Ltd.

Rudd, M. E. and J. H. Macek. 1972. Mechanisms of electron production in ion-atom collisions. Case Studies in Atomic Phys. 3:49-126.

Schneiderman, M. H., L. A. Braby and W. C. Roesch. 1977. Division delay after low x-ray doses and treatment with cycloheximide. Radiat. Res. 70:130-40.

Spinks, J. W. T. and R. J. Wood. 1964. An introduction to chemistry. New York: John Wiley and Sons.

Toburen, L. H. 1971. Distributions of energy and angle of electrons ejected from molecular nitrogen by 0.3 to 1.7 MeV protons. Phys. Rev. A 3:216-28.

Toburen, L. H., S. T. Manson and Y. K. Kim. 1978. Energy distributions of secondary electrons. III. Projectile energy dependence for ionization of He, Ne, and Ar by protons. Phys. Rev. A 17:148-59.

Toburen, L. H., H. G. Paretzke and W. E. Wilson. 1976. Electron emission from proton bombardment of carbon foils. In Pacific Northwest Laboratory annual report for 1977 to the DOE assistant secretary for environment, BNWL-2000, Part 4, 2.48. Richland, Washington: Pacific Northwest Laboratory.

Toburen, L. H. and W. E. Wilson. 1977. Energy and angular distributions of electrons ejected from water vapor by 0.3 - 1.5 MeV protons. J. Chem. Phys. 66:5202-13.

Toburen, L. H. and W. E. Wilson. In Press. Differential cross sections for ionization of argon by He^{+} and He^{++} ions, PNL-SA-7141. Richland, Washington: Pacific Northwest Laboratory. Phys. Rev. A.

Toburen, L. H., W. E. Wilson and R. J. Popowich. In Press. Secondary electron emission in ionization of water vapor by helium ions and alpha particles. Richland, Washington: Pacific Northwest Laboratory. J. Chem. Phys.

von Foerster, H. 1959. Some remarks on changing populations. In The kinetics of cellular proliferation, ed. F. Stohlman, pp. 382-407. New York: Grune and Stratton.

Weitkamp, W. G. and F. H. Schmidt. 1974. The University of Washington three-stage tandem Van de Graaff accelerator. Nucl. Instr. and Meth. 122:65-9.

West, M. L. 1976. Quenching of benzene fluorescence in pulsed proton irradiation. J. Phys. Chem. 80:26-32.

West, M. L. and J. H. Miller. 1978. Quenching of benzene fluorescence in pulsed proton irradiation: temperature dependence. Radiat. Res. 74:594.

Wilson, W. E. 1972. Stopping power partition and mean energy loss for energetic protons in hydrogen. Radiat. Res. 49:36-50.

Wilson, W. E. and L. H. Toburen. 1978. Analytical expressions for cross section data. Pacific Northwest Laboratory annual report for 1977 to the DOE assistant secretary for environment, PNL-2500, Part 4, p. 2.7. Richland, Washington: Pacific Northwest Laboratory.

Wilson, W. E., L. H. Toburen and H. G. Paretzke. 1978a. Ionization and energy deposition in small sites. Radiat. Res. 74:481-2.

Wilson, W. E., L. H. Toburen and H. G. Paretzke. 1978b. Calculation of energy deposition spectra in small gaseous sites and its applicability to condensed phase. In Proceedings of the Sixth symposium on microdosimetry. eds. J. Booz and H. G. Ebert, pp 239-250. Holland: Harwood Academic Publishers, Ltd.

Wogman, N. A., D. E. Robertson and R. W. Perkins. 1969. A large well crystal with anticoincidence shielding. Health Physics 13:737-67.

4.0

Hitchon, B., R. H. Filby and K. R. Shah. 1975. Geochemistry of trace elements in crude oils, Alberta, Canada. In The role of trace metals in petroleum, ed. T. F. Yen. Ann Arbor, Michigan: Ann Arbor Science Publishers, Inc.

5.0

Nielson, K. K. 1978. Application of direct peak analysis to energy-dispersive-x-ray fluorescence spectra. X-Ray Spectrom. 7:15-22.

Nielson, K. K. and N. A. Wogman, ANS Transactions. 28-1:14.

Nielson, K. K. 1978. Proceedings, 27th Denver conference on applications of x-ray analysis. Denver, Colorado.

Nielson, K. K. 1977. Anal. Chem. 49:641-648

Sittlig, M. 1976. Toxic metals, pollution control and water protection. Park Ridge, New Jersey: Noyes Data Corporation.

Publications and Presentations

PUBLICATIONS

Abel, K. H., D. E. Robertson, E. A. Crecelius, and W. B. Silker. 1978. Speciation studies of radionuclides in low-level wastes and process waters from a pressurized water reactor. Amer. Chem. Soc. 339.

Braby, L. A. and W. C. Roesch. 1978. Noise-free measurement of z for fast Electrons. Radiat. Res. 74:482.

Braby, L. A. and W. C. Roesch. In press. Testing dose-rate models with Chlamydomonas reinhardi. Radiat. Res.

Brauer, F. P. and J. E. Fager. 1978. A minicomputer system for radiochemical analysis by coincidence spectrometry. ANS Transactions. 28-1:61.

Brauer, F. P., R. W. Goles, J. H. Kaye, H. G. Rieck. 1978. Sampling and measurement of long-lived radionuclides in environmental samples. In Proceedings of Fourth joint conference on sensing of environmental pollutants. pp 330-335. American Chemical Society.

Brauer, F. P. and W. A. Mitzlaff. 1978. Evaluation of well-type Ge(Li) detectors for low-level radiochemical analysis. In IEEE Trans. on Nucl. Sci. NS 25-1:398.

Brauer, F. P., J. E. Fager, J. H. Kaye, and R. J. Sorenson. 1978. A mobile computerized gamma-ray spectrometric analysis and data processing system. ANS Transactions 28-1:71-3.

Brauer, F. P. and J. E. Fager. 1978. Standard materials for iodine activation analysis. Proceedings of IAEA symposium on nuclear activation techniques in the life sciences, IAEA-SM-227/65:1-10. Vienna, Austria: IAEA.

Brodzinski, R. L., and N. A. Wogman. 1978. In-situ quantitative determination of transuranic elements in areas of high-level gamma radiation. Proceedings of the American Nuclear Society topical meeting, analytical methods for safeguard and accountability measurements of special nuclear materials. Williamsburg, Virginia.

Campbell, J. A., J. C. Laul, K, K. Nielson, and R. D. Smith. 1978. Separation and chemical characterization of finely-sized flyash particles. Anal. Chem. 50:1032-40.

Campbell, J. A., R. D. Smith, K. K. Nielson and K. H. Abel. 1978. Analysis of submicron flyash particles. American Chem. Soc. Environmental Chemistry Division. 18-2:610.

Campbell, J. A., R. D. Smith, and L. E. Davis, Jr. 1978. Application of x-ray photo-electron spectroscopy to fly ash. J. Appl. Spectro. 32:316.

Campbell, J. A., J. C. Laul, K. K. Nielson, and R. D. Smith. 1978. Separation and chemical characterization of finely-sized flyash particles. Anal. Chem. 50:1032.

Christensen, D. C., J. A. McNeese, G. W. Dawson, and W. C. Weimer. In press. Fixation of kepone contaminated wastes. In Stabilization/solidification options for hazardous waste disposal. ed. R. B. Pojasek, Ann Arbor Michigan: Ann Arbor Science.

Crecelius, E. A. 1978. Modification to the arsenic speciation techniques using hydride generation. Anal. Chem. 50:826-7.

Crecelius, E. A., G. Roesijadi and T. O. Thatcher. 1978. Errors in determination of residual oxidants in chlorinated seawater. Env. Sci. & Tech. 12-9:1088.

Dawson, G. W., W. C. Weimer, and S. J. Shupe. n.d. Kepone - Case Study of a persistent material. Accepted for publication by AIChE Journal.

Fitzgerald, A., J. A. Campbell, G. D. Smith, C. N. Caughlan and S. E. Cremer. 1978. Crystal and molecular structures of 2,2,3-Trimethyl-1-phenylphosphetane 1-Oxide and 2,2,3,3,4-Pentamethyl-1-phenylphosphetane 1-Oxide. J. Org. Chem. 43:3513.

Fruchter, J. S. and M. R. Petersen. n.d. Characterization of products, byproducts and effluents from coal conversion processes for environmental purposes. In Analytical methods for coal and coal products. Ch. 46. Morgantown, West Virginia: Morgantown Energy Technology Center (in preparation).

Gurtisen, J. M., E. A. Crecelius, K. H. Abel, and C. W. Philbrick. 1978. Copper complexing capacity of Pacific Northwest coastal waters. Amer. Geophys. Union Trans. 58:1165.

Laul, J. C., W. C. Weimer, and L. A. Rancitelli. 1978. Biogeochemical distribution of rare earths and other trace elements in plants and soils. In Proceedings of the Second symposium on the origin of the elements. Paris, France: UNESCO.

Laul. J. C., C. L. Wilkerson, and V. L. Crow. 1978. Computer methodology and its applications to geological and environmental matrices. Proceedings of the Conference on computers and activation analysis and gamma ray spectroscopy. Mayaguez, Puerto Rico: American Nuclear Society.

Laul, J. C., K. K. Nielson, and N. A. Wogman. 1978. Trace rare earth analysis by neutron activation and gamma/x-ray spectrometry. Proceedings of the Third international conference on nuclear methods in environmental and energy research.

Miller, J. H. 1978. Effect of the spatial distribution of energy deposition on the radioluminescence of benzene in cyclohexane. Radiat. Res. 74:594-5.

Miller, J. H. and M. L. West. In press. Nonhomogeneous chemical kinetics in pulsed proton radioluminescence. Biophysics J.

Miller, J. H. 1977. "Z^3 effect in the ionization cross section of argon by 1.2 and 2.0 meV alpha particles. Phys. Rev. A 16:2478-9.

Nelson, J. M., L. A. Braby and W. C. Roesch. 1978. Characterization of rapid recovery in Chlamydomonas reinhardi. Radiat. Res. 74:534.

Nelson, J. M. 1978. Culture conditions associated with establishment and maintenance of viable noncycling monolayers. In Proceedings of 29th Annual Tissue Culture Association (abstract).

Nelson, J. M. 1978. Culture conditions associated with establishment and maintenance of viable noncycling monolayers. In Vitro. 14-4:380.

Nielson, K. K. 1978. Application of direct peak analysis to energy-dispersive x-ray fluorescence spectra. X-Ray Spectrometry. 7:15-22.

Nielson, K. K. and N. A. Wogman. 1978. Direct Measurement of net peak areas in energy-dispersive x-ray fluorescence. ANS Transactions. 28-1:14

Nielson, K. K., R. L. Brodzinski, and N. A. Wogman. 1978. In-situ transuranic element measurement technique for wastes associated with power reactor fuels. In Proceedings of the American Nuclear Society topical meeting, analytical methods for safeguard and accountability measurements of special nuclear materials. Williamsburg, Virginia: American Nuclear Society.

Nielson, K. K., and D. R. Kalkwarf. 1978. Multielement analysis of urine using energy dispersive x-ray fluorescence. In Analytical electron microscopy and x-ray applications: environmental and occupational health 1, eds. P. A. Russell and A. Hutchings, pp. 31-39. Ann Arbor, Michigan: Ann Arbor Science Publishers,

Nielson, K. K., N. A. Wogman, and R. L. Brodzinski. 1978. X-ray fluorescence capabilities for uranium ore analysis. Advances in X-Ray Analysis 21:51-88.

Robertson, D.E., J. S. Fruchter, J. D. Ludwick, C. L. Wilkerson, E. A. Crecelius and J. C. Evans. 1978. Chemical characterization of gases and volatile heavy metals in geothermal effluents. Geothermal Resources Council Transactions. 2, July.

Robertson, R. G. H., R. A. Warner, P. Dyer, R. C. Melin and T. J. Bowles. 1978. Observation of the radioactive capture process $^{2}H(\alpha,\gamma)\ ^{6}Li$ (abstract). Bull. Am. Phys. Soc. 23:518.

Roesch, W. C. 1978. Dose-rate and fractionation theory for multiple recovery processes. Radiat. Res. 74:535.

Roesch, W. C. 1978. Internal microdosimetry. In Sixth symposium on microdosimetry, eds. J. Booz and H. G. Ebert. Holland: Harwood Academic Publishers, Ltd.

Saalfeld, F. E., J. J. DeCorpo, R. D. Smith, and J. R. Wyatt. 1978. Mass spectrometric studies of low temperature flames. II. Concentration profiles and reactions of additives in flames. Advances in Mass Spectrometry. 7A:707.

Smith, R. D., and J. H. Futrell. 1978. Carbon ion reactions with ethylene and propylene oxide. Chem. Phys. Letters. 54:273.

Smith, R. D., and P. W. Ryan. 1978. Chemical ionization mass spectrometry as a tool for the elimination of surface related phenomena in the spectra of unstable compounds. Anal. Chem. 50:371.

Smith, R. D., and J. H. Futrell. 1978. Internal energy effects in proton transfer reactions. Advances in Mass Spectrometry. 7A:326.

Smith, R. D., J. R. Wyatt, J. J. DeCorpo, and F. E. Saalfeld. An Investigation of the hydride impurity of $(SN)_x$. Inorg. Chem. 17:1639.

Smith, R. D. A mass spectrometric study of the thermal pyrolysis of S_4N_4. Chem. Phys. Letters. 55:590.

Smith, R. D., and G. B. Street. 1978. A mass spectrometric study of the vapor phase species of brominated polymeric sulfur nitride and tetrasulfur tetranitride. Inorg. Chem. 17:938.

Smith, R. D., J. A. Campbell, and K. K. Nielson 1978. Mechanisms for trace element enrichment in fly ash during coal combustion. American Chemical Society, division of fuel chemistry preprints. 23:196.

Smith, R. D., and J. Futrell. 1978. Reactions of Thermal energy $(^2P)C^+$ ions with several molecules. International J. of Mass Spectrometry and Ion Physics. 26:111-3.

Smith, R. D., and J. J. Decorpo. 1978. Secondary ion reactions in benzene. International J. of Mass Spectrometry and Ion Physics. 26:279-88.

Smith, R. D., J. A. Campbell K. K. Nielson, and J. C. Laul. 1978. Separation and chemical characterization of finely-sized flyash particles. Anal. Chem. 50:1032.

Stoffels, J. J., C. R. Lagergren and P. J. Hof. 1978. An ion detecting and measuring system with wide dynamic range. International Journal of Mass Spectrometry and Ion Physics. 28:159-69.

Styris, D. L., J. Leshuk, R. Zaworski and O. K. Harling. n.d. Solar pond stability experiments. Accepted for publication by Solar Energy.

Toburen, L. H., and W. E. Wilson. In press. Differential cross sections for ionization of argon by He^{++} and He^+ ions. Phys. Rev. A.

Toburen, L. H., S. T. Manson, and Y.-K Kim. 1978. Energy distributions of secondary electrons. III. Projectile energy dependence for ionization of He, Ne and Ar by protons. Phys. Rev. A, 17:148-59.

Toburen, L. H., R. J. Popowich, and W. E. Wilson. In press. Secondary electron emission in ionization of water vapor by helium ions and alpha particles. J. Chem. Phys.

Weimer, W. C., and J. C. Langford. 1978. Iron-55 and stable iron in oceanic aerosols: forms and availability. Atmospheric Environ. 12:1201-5.

Weimer, W. C., J. C. Laul, J. C. Kuh, and E. A. Bondietti. 1978. Plant uptake of Am, Cm, and the chemical analog Nd. In Proceedings of the Third international conference on nuclear methods in environmental and energy research. Columbia, Missouri.

West, M. L., and J. H. Miller. 1978. Quenching of benzene fluorescence in pulsed proton irradiation: temperature dependence. Radiat. Res. 74:595.

Wilson, W. E., L. H. Toburen, and H. G. Paretzke. 1978. Ionization and energy deposition in small sites. Radiat. Res. 74:481.

Wilson, W. E., L. H. Toburen and H. G. Paretzke. 1978. Calculation of energy deposition spectra in small gaseous sites and its applicability to condensed phase. In Proceedings Sixth symposium on microdosimetry, eds. J. Booz and H. G. Ebert, pp. 239-50. Holland: Harwood Academic Publishers, Ltd.

wogman, N. A., H. G. Rieck, and J. C. Laul. 1978. Computer-controlled cyclic activation analysis with a $^{252}Cf/^{235}U$ subcritical multiplier. ANS Transactions. 28-1:62.

Wogman, R. L. Brodzinski, and D. P. Brown. 1978. An instrument for monitoring transuranic content of chopped leached hulls from spent nuclear fuel elements. In Proceedings of the American Nuclear Society topical meeting, analytical methods for safeguard and accountability measurements of special nuclear materials. Williamsburg, Virginia: American Nuclear Society.

Wogman, N. A. 1978. In situ x-ray fluorescence and californium-252 neutron activation analysis for marine and terrestrial mineral exploration. In Proceedings of IAEA meeting: nuclear techniques and mineral resources 1977. pp 447-63. Vienna, Austria: IAEA.

Wogman, N. A., R. L. Brodzinski, L. Van Middlesworth. 1977. Radium Accumulation in animal thyroid glands: a possible method for uranium and thorium prospecting. J. Radioanalytical Chem. 41:115-25, December.

Wyatt, J. R., J. J. DeCorpo, R. D. Smith, and F. E. Saalfeld. 1978. Mass spectral studies of polymeric sulfur nitride. Advances in Mass Spectrometry. 7A:597.

PRESENTATIONS

Braby, L. A. and W. C. Roesch. Direct measurements of f(z) for fast electrons. Presented at Sixth symposium on microdosimetry. Brussels, Belgium. May 22-26, 1978.

Braby, L. A. and W. C. Roesch. Noise-free measurement of z for fast electrons. Presented at the Radiation Research Society meeting. Toronto, Canada. May 14-18, 1978.

Braby, L. A. and J. M. Nelson. Use of high dose rate electron beams to study cellular repair mechanisms. PNL-SA-6950, INVITED PAPER presented at Small accelerator conference. Denton, Texas. November 6-8, 1978.

Brauer, F. P., J. E. Fager, J. H. Kaye and R. J. Sorenson. A mobile computerized gamma-ray spectrometric analysis and data processing system. PNL-SA-6571A, presented at the American Nuclear Society topical conference, preliminary program computers in activation. Mayaguez, Puerto Rico. April 20-May 3, 1978. ANS Transactions. 28-1:71-3. May 1-4, 1978.

Brauer, F. P., J. E. Fager, J. H. Kaye, and R. J. Sorenson. A mobile nondestructive assay verification and measurement system. Washington, D.C. June 29-July 1, 1977. In Proceedings 18th annual meeting, Institute of Nuclear Materials Management, Inc. 6-3:680-94. December 1977.

Brauer,F. P., and J. E. Fager. A minicomputer system for radiochemical analysis by coincidence spectrometry. BNWL-SA-6562A, presented at the American Nuclear Society topical conference, computers in activation analysis and gamma-ray spectroscopy. Mayaguez, Puerto Rico. April 20-May 3, 1978. ANS Transactions. 28-1:61-2. May 1-4, 1978.

Brauer, F. P., and R. S. Strebin, Jr. Standard materials for iodine activation analysis. BNWL-SA-6566A, presented at Symposium on nuclear activation techniques in the life sciences. Vienna, Austria. May 22-26, 1978. IAEA-SM-227/65:1-10.

Brauer, F. P., W. A. Mitzlaff and J. E. Fager. U and Pu analysis with well-type germanium detectors. PNL-SA-6600A, presented at the Spring 1978 American Chemical Society meeting. Anaheim, California. March 12-17, 1978. (To be published in Anal. Chem.)

Campbell, J. A., R. D. Smith, and K. K. Nielson. Analysis of submicron fly ash particles. Presented at 176th national meeting, American Chemical Society. Miami Beach, Florida. September, 10-15, 1978.

Crecelius, E. A., K. H. Abel, J. C. Laul, S. R. Garcia, and L. A. Rancitelli. Characterization of emissions from the Colstrip coal-fired power plant. Presented at the EPA sponsored Workshop on Colstrip coal-fired power plant project. Corvallis, Oregon. January 17-19, 1978.

Crecelius, E. A. Detailed chemical characterization of coal fly ash leachates. Presented at Workshop on fly ash disposal. EPRI. Palo Alto, California. May 1978.

Dawson, G. W., W. C. Weimer, and S. J. Shupe. Kepone - case study of a persistant material. Presented at AIChE Conference on toxic substances: definition, legislation, and public protection. Philadelphia, Pennsylvania. June 6-8, 1978.

Fager, J. E., and F. P. Brauer. Rapid nondestructive plutonium isotopic analysis. PNL-SA-6601A, presented at ANS topical meeting, analytical methods for safeguard and accountability measurements. Williamsburg, Virginia. May 15-17, 1978.

Fruchter, J. S. As and Hg speciation in oil shale retort offgases. Informal workshop presentations at oil shale environment and health conference. Los Alamos, New Mexico. August 1978.

Fruchter, J. S. and M. R. Petersen. Characterization of oil shale materials for trace elements and organic constituents. PNL-SA-6589A, presented at the AAAS annual meeting. Feb. 12-17, 1978.

Fruchter, J. S. Suitability of standard methods for arsenic analysis in oil shale retort waters. Presented at the ASTM winter meeting of committee D19 on water. Fort Lauderdale, Florida. January 31, 1978.

Fruchter, J. S. Trace element and speciation analysis of effluents from two oil shale retorts. Presented at FACSS meeting. Boston, Massachusetts. November 1978.

Hildebrand, B. P. Applications of holography. Presented at DBER workshop on advanced laser technology for pollutant measurements. Oak Ridge, Tennessee. February 1978.

Kalkwarf, D. R. and J. C. Langford. Response of agarose solutions to magnetic fields. Proceedings of the Northwest regional ACS meeting. Seattle, Washington. June 14-16, 1978.

Laul, J. C., C. L. Wilkerson, and V. L. Crow. Computer methodology and its applications to geological and environmental matrices. Presented at the ANS topical conference, computers in activation analysis and gamma-ray spectroscopy. Mayaguez, Puerto Rico. May 1-4, 1978.

Miller, J. H. Effect of the spatial distribution of energy deposition on the radioluminescence of benzene in cyclohexane. Presented at Radiation Research Society meeting. Toronto, Canada. May 14-18, 1978.

Miller, J. H. and M. L. West. Nonhomogeneous chemical kinetics in pulsed proton radioluminescence. Presented at Arlie House conference. Arlie, Virginia. April 2-5, 1978.

Miller J. H. and M. L. West. Pulsed proton radioluminescence in binary liquid scintillators. PNL-SA-7122, presented at Small accelerator conference. Denton, Texas. November 6-8, 1978.

Nelson, J. M., L. A. Braby, and W. C. Roesch. Characterization of rapid recovery in Chlamydomonas reinhardi. Presented at Radiation Research Society meeting. Toronto, Canada. May 14-18, 1978.

Nelson, J. M. Culture conditions associated with establishment and maintenance of viable noncycling monolayers. Presented at 29th annual Tissue Culture Association meeting. Denver, Colorado. June 5-7, 1978.

Nelson, J. M. DNA-synthetic activity in density and nutritionally inhibited monolayers. Presented at Second annual meeting of Cell Kinetics Society. St. Louis, Missouri. March 17-19, 1978.

Nielson, K. K. and N. A. Wogman. Direct measurement of net peak areas in energy dispersive x-ray fluorescence. Presented at ANS conference, computers in activation analysis and gamma-ray spectroscopy. Mayaguez, Puerto Rico. May 1-4, 1978.

Nielson, K. K. and N. A. Wogman. In situ transuranium element measurement technique for wastes associated with power reactor fuels. Presented at ANS conference on analytical methods for safeguard and accountability measurements of special nuclear material. Williamsburg, Virginia. May 15-17, 1978.

Nielson, K. K. Progress in x-ray fluorescence correction methods using scattered radiation. Presented at 27th Denver conference on applications of x-ray analysis. Denver, Colorado. August 1-4, 1978.

Nielson, K. K. Use of Compton scattered radiation for correction of matrix effects. Presented at X-ray fluorescence spectrometry workshop. Denver, Colorado. August 1, 1978.

Nielson, K. K., N. A. Wogman, and R. L. Brodzinski. X-ray fluorescence capabilities for uranium ore analysis. Denver x-ray conference on advances in x-ray analysis. Denver, Colorado. 1977.

Robertson, D. E., J. S. Fruchter, J. D. Ludwick, C. L. Wilkerson, E. A. Crecelius, and J. C. Evans. Chemical characterization of gases and volatile heavy metals in geothermal effluents. Presented at the annual meeting of the Geothermal Resources Council. Hilo, Hawaii. July 25-28, 1978.

Robertson, D. E., J. S. Fruchter, J. D. Ludwick, C. L. Wilkerson, E. A. Crecelius, and J. C. Evans. A chemical characterization of pollutants released during geothermal energy development. Presented at the AAAS annual meeting. Washington, D.C. February 12-17, 1978.

Roesch, W. C. Dose-rate and fractionation theory for multiple recovery processes. Presented at Radiation Research Society meeting. Toronto, Canada. May 14-18, 1978.

Roesch, W. C. Internal microdosimetry. Presented at Sixth symposium on microdosimetry. Brussels, Belgium. May 22-26, 1978.

Roesch, W. C. Models of the radiation sensitivity of mammalian cells. INVITED PAPER in Proceedings Third symposium on neutron dosimetry in biology and medicine, eds. G. Burger and H. G. Ebert, pp. 2-27. Luxembourg: Commission of the European Communities.

Smith, R. D., J. A. Campbell, and K. K. Nielson. Mechanisms for trace element enrichment in fly ash during coal combustion. Presented at 175th National ACS meeting. Anaheim, California. March 1978.

Stoffels, J. J. Real-time measurement of plutonium and other particulates in air. Presented at 11th aerosol technology meeting. Davis, California. September 6-8, 1978.

Toburen, L. H. Differential cross sections for electron emission in heavy ion-atom collisions. PNL-SA-6086, INVITED PAPER presented at Small accelerator conference. Denton, Texas. November 6-8 1978.

Warner, R. A. and P. L. Reeder. Delayed neutrons from ^{98}Rb and ^{146}Cs. Presented at the American Physical Society, division of nuclear physics 1978 meeting. Asilonar, California. November 1-3, 1978.

Weimer, W. C., J. C. Laul, J. C. Kuh, and E. A. Bondietti. Plant uptake of Am, Cm, and the chemical analog Nd. Presented at the Third international conference on nuclear methods in environmental and energy research. Columbia, Missouri. October 10-13, 1978.

West, M. L. and J. H. Miller. Quenching of benzene fluorescence in pulsed proton irradiation: temperature dependence. Presented at Radiation Research Society meeting. Toronto, Canada. May 14-18, 1978.

Wilson, W. E., L. H. Toburen, and H. G. Paretzke. Calculation of energy deposition spectra in small gaseous sites and its applicability to condensed phase. PNL-SA-6681, presented at Sixth symposium on microdosimetry, Brussels, Belgium. May 22-26, 1978.

Wilson, W. E., and H. G. Paretzke, Calculation of proton ejection of electrons from foils. PNL-SA-7188, presented DEAP meeting, APS. Madison, Wisconsin. November 29-December 1, 1978.

Wilson, W. E., L. H. Toburen, and H. G. Paretzke. Ionization and energy deposition in small sites. Presented at Radiation Research Society meeting. Toronto, Canada. May 14-18, 1978.

Wogman, N. A. A $^{252}Cf/^{235}U$ subcritical multiplier computer-controlled cyclic activation analysis facility. Californium-252 utilization meeting. Atlanta, Georgia. October 3-5, 1978.

Wogman, N. A., H. G. Rieck, and J. C. Laul. Computer-controlled cyclic activation Analysis with a ^{252}Cf-^{235}U subcritical multiplier. Presented at ANS conference on computers in activation analysis and gamma-ray spectroscopy. Mayaguez, Puerto Rico. May 1-4, 1978. ANS Transactions 28-1:62.

Author Index

AUTHOR INDEX

Organization Charts Distribution

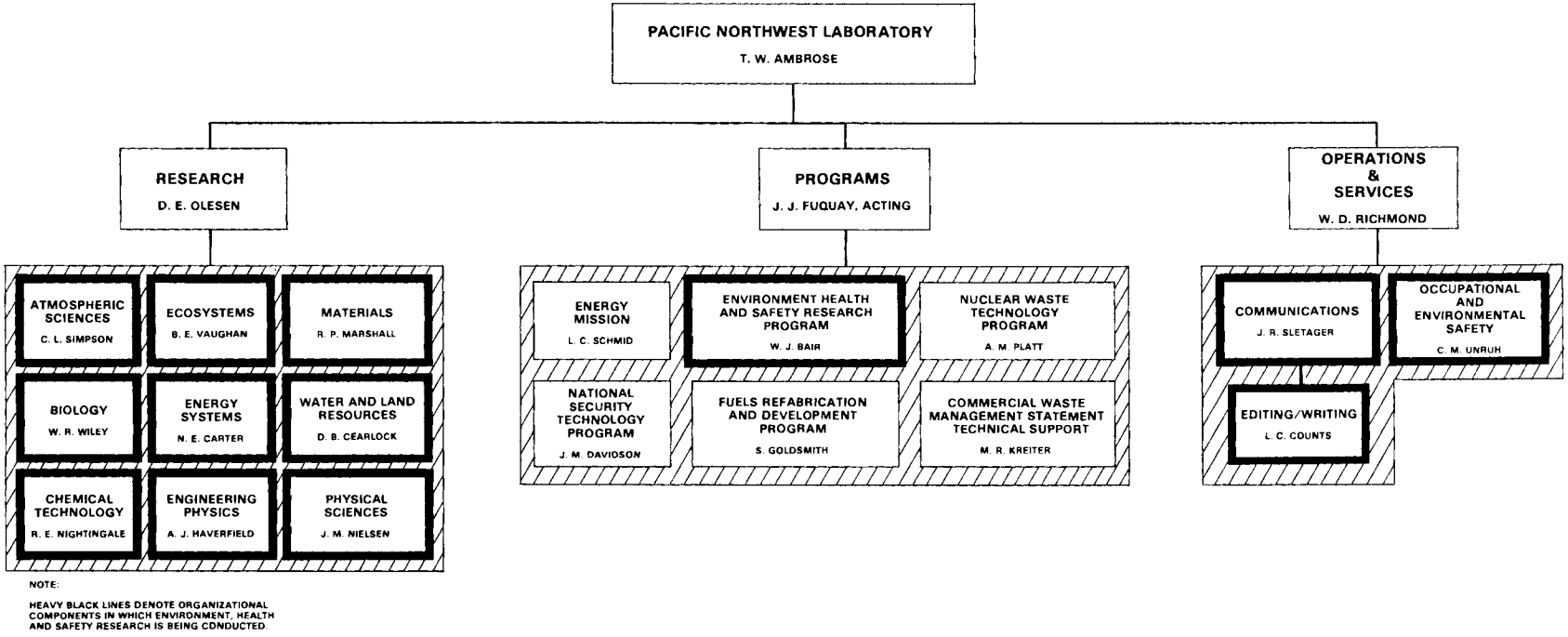

NOTE:

HEAVY BLACK LINES DENOTE ORGANIZATIONAL COMPONENTS IN WHICH ENVIRONMENT, HEALTH AND SAFETY RESEARCH IS BEING CONDUCTED.

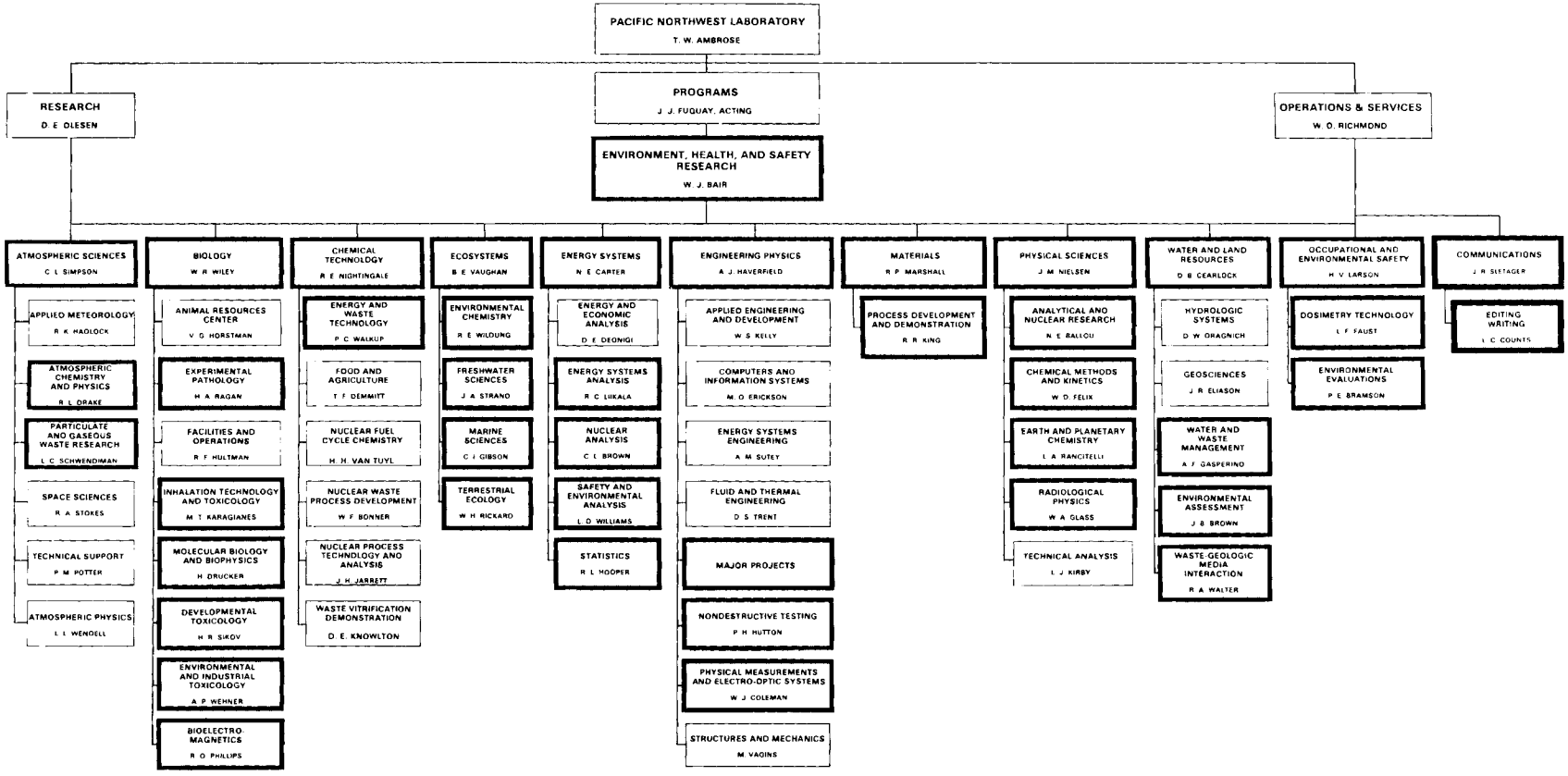

NOTE HEAVY BLACK LINES DENOTE ORGANIZATIONAL COMPONENTS IN WHICH ENVIRONMENT, HEALTH AND SAFETY RESEARCH IS BEING CONDUCTED

PHYSICAL SCIENCES DEPARTMENT
(7HA0)

December 1, 1978

JM (Julian) Nielsen, Manager
FL (Louise) Barton, Secretary

RW (Dick) Perkins, Assoc. Manager
RM (Rose) Garcia, Secretary

#WE (Bill) Gross, Financial Specialist

EI (Earl) Wandling, Specialist,

Radiological Physics
(7HA3)

WA (Bill) Glass, Manager
JA (Judy) Ewing, Secretary

Radiological Research Group

WC (Bill) Roesch, Technical Leader, Radiation Biophysics

LH (Larry) Toburen, Technical Leader, Radiation Physics

LA (Les) Braby
JH (John) Miller
JM (John) Nelson
LL (Lowell) Nichols
CA (Charlie) Ratcliffe
ML (Martin) West
WE (Walt) Wilson

***MS (Mike) Creek
MK (Marvin) Lein
R (Rudy) Rodriquez

Accelerator Facility
(7HA4)

Analytical and Nuclear Research
(7HA5)

NE (Nate) Ballou, Manager
GJ (Jean) Clark, Secretary
KM (Kathy) Barry, Secretary

FP (Fred) Brauer
+MW (Martin) Cole
JE (Jon) Fager
GM (Glen) Giacoletto
RW (Ron) Goles
RL (Dick) Gordon
DC (Doug) Hamilton
JH (Jim) Kaye
JM (Jim) Kelley
CR (Bob) Lagergren
WA (Bill) Mitzlaff
PL (Paul) Reeder
DM (Dean) Robertson
+BW (Brian) Smith
JJ (Jim) Stoffels
RS (Bob) Strebin
DL (Dave) Styris
H (Harvey) Tenny
RA (Ray) Warner

NL (Lois) Abbey
LA (Lee) Bond
***PD (Pat) Draze
DR (Don) Ells
RM (Rose Ann) Graves
RA (Robert) Kiddy
***LA (Laurie) McVey
RB (Roberta) Myers
MS (Mike) Rapids
DE (Donald) Rinehart
LW (Lena) Schock
CJ (Carol) Seaman
CA (Christie) Shields
SC (Shirley) Simpson

Technical Analysis
(7HA6)

LJ ("Rip") Kirby, Manager

AC (Art) Case

VC (Velma) Beard
JD (Jerry) Forsythe
DT (Dottie) Harless

Earth and Planetary Chemistry
(7HA7)

LA (Lou) Rancitelli, Manager
ES (Betty) Getchell, Secretary

KH (Keith) Abel
DP (Don) Brown
++EA (Eric) Crecelius
JC (John) Evans
JC (John) Fruchter
SR (Sammy) Garcia
JC (JC) Laul
EA (Elwood) Lepel
JD (Don) Ludwick
+++KB (Khris) Olsen
HG (George) Rieck, Jr.
DE (Dave) Robertson
WB (Wyatt) Silker
DS (Debbie) Skalrew
VW (Bill) Thomas, Jr.
CL (Connie) Wilkerson
JA (Jim) Young

LL (Lavern) Baker
EF (Ermel) Briggs
BG (Chris) Christensen
DA (Dave) Cochran
CL (Chuck) Nelson
++CW (Clay) Philbrick
JH (Jim) Reeves
WC (Wayne) Richey
RW (Ron) Sanders

Chemical Methods and Kinetics
(7HA8)

WD (Dale) Felix, Manager
CH (Cozette) Connally, Secretary

BA (Barbara) Bergstedt
RL (Ron) Brodzinski
JE (Jim) Burger
BA (Bruce) Bushaw
JA (Jim) Campbell
PO (Pete) Jackson
DR (Don) Kalkwarf
JC (John) Kutt
JC (Jim) Langford
ML (Mary Lou) Mauch
JR (John) Morrey
HL (Howard) Nielson
KK (Kirk) Nielson
MR (Mike) Petersen
DM (Don) Schoengold
RD (Dick) Smith
CW (Chuck) Thomas
WC (Wally) Weimer
TJ (Tom) Whitaker
NA (Ned) Wogman

GG (Gwen) Brodaczynski
RM (Rush) Campbell
DR (Don) Edwards
JG (Grant) Pratt
C (Chuck) Veverka, Jr.

LEGEND:
*Part-time employee, included in total.
***Hourly employee included in total.
+S&E Program, not included in total.
#Assigned from another organization, not included in total.
++Offsite, Marine Research Lab., Sequim, Washington.
+++Offsite, Colstrip, Montana.

Total Number of Exempt	= 72
Total Number of Non-Exempt	= 41
TOTAL	= 113

DISTRIBUTION

OFFSITE

A. A. Churm, Director
Patent Division
DOE - Chicago Operations
Office
9800 South Cass Ave.
Argonne, IL 60439

Ruth C. Clusen (3)
Assistant Secretary
Department of Energy
Office of the Assistant
Secretary for Environment
Washington, DC 20545

J. L. Liverman
Deputy Assistant Secretary
Department of Energy
Office of the Assistant
Secretary for Environment
Washington, DC 20545

W. R. Albers
Department of Energy
Office of the Assistant
Secretary for Environment
Washington, DC 20545

R. W. Barber
Department of Energy
Office of the Assistant
Secretary for Environment
Washington, DC 20545

N. F. Barr
Department of Energy
Office of the Assistant
Secretary for Environment
Washington, DC 20545

J. W. Benson
Department of Energy
Office of the Assistant
Secretary for Environment
Washington, DC 20545

L. C. Brazley
Department of Energy
Office of the Assistant
Secretary for Environment
Washington, DC 20545

W. A. Brobst
Department of Energy
Office of the Assistant
Secretary for Environment
Washington, DC 20545

W. W. Burr, Jr.
Department of Energy
Office of the Assistant
Secretary for Environment
Washington, DC 20545

C. E. Carter
Department of Energy
Office of the Assistant
Secretary for Environment
Washington, DC 20545

R. J. Catlin
Department of Energy
Office of Assistant
Secretary for Environment
Washington, DC 20545

J. A. Coleman
Department of Energy
Office of the Assistant
Secretary for Environment
Washington, DC 20545

R. A. Conaway
Department of Energy
Office of the Assistant
Secretary for Environment
Washington, DC 20545

D. K. Craig
Department of Energy
Office of the Assistant
Secretary for Environment
Washington, DC 20545

L. J. Deal
Department of Energy
Office of the Assistant
Secretary for Environment
Washington, DC 20545

G. P. Dix
Department of Energy
Office of the Assistant
Secretary for Environment
Washington, DC 20545

C. W. Edington
Department of Energy
Office of the Assistant
Secretary for Environment
Washington, DC 20545

R. E. Grossman
Department of Energy
Office of the Assistant
Secretary for Environment
Washington, DC 20545

J. H. Harley
Environmental Measurements
Laboratory
376 Hudson St.
New York, NY 10014

J. Hock
Department of Energy
Office of the Assistant
Secretary for Environment
Washington, DC 20545

H. Hollister
Department of Energy
Office of the Assistant
Secretary for Environment
Washington, DC 20545

P. W. House
Secretary for Environment
Office of Technology Impacts
Washington, DC 20545

R. L. Leith
Department of Energy
Office of the Assistant
Secretary for Environment
Washington, DC 20545

F. A. Leone
Department of Energy
Office of the Assistant
Secretary for Environment
Washington, DC 20545

R. A. Lewis
Department of Energy
Office of the Assistant
Secretary for Environment
Washington, DC 20545

W. J. Little, Jr.
Department of Energy
Office of the Assistant
Secretary for Environment
Washington, DC 20545

K. E. Lockridge
Department of Energy
Office of the Assistant
Secretary for Environment
Washington, DC 20545

J. N. Maddox
Department of Energy
Office of the Assistant
Secretary for Environment
Washington, DC 20545

D. Mayhew
Department of Energy
Office of the Assistant
Secretary for Environment
Washington, DC 20545

W. J. McCool
Department of Energy
Office of the Assistant
Secretary for Environment
Washington, DC 20545

B. F. McCully
Department of Energy
Office of the Assistant
Secretary for Environment
Washington, DC 20545

M. L. Minthorn, Jr.
Department of Energy
Office of the Assistant
Secretary for Environment
Washington, DC 20545

D. Monti
Department of Energy
Office of the Assistant
Secretary for Environment
Washington, DC 20545

W. E. Mott
Department of Energy
Office of the Assistant
Secretary for Environment
Washington, DC 20545

W. H. Pennington
Department of Energy
Office of the Assistant
Secretary for Environment
Washington, DC 20545

R. W. Ramsey, Jr.
Department of Energy
Office of the Assistant
Secretary for Environment
Washington, DC 20545

D. M. Ross
Department of Energy
Office of the Assistant
Secretary for Environment
Washington, DC 20545

D. E. Shaw
Department of Energy
Office of the Assistant
Secretary for Environment
Washington, DC 20545

G. Shepherd
Department of Energy
Office of the Assistant
Secretary for Environment
Washington, DC 20545

R. D. Shull
Department of Energy
Office of the Assistant
Secretary for Environment
Washington, DC 20545

M. Shulman
Department of Energy
Office of the Assistant
Secretary for Environment
Washington, DC 20545

N. F. Simpson
Department of Energy
Office of the Assistant
Secretary for Environment
Washington, DC 20545

D. H. Slade
Department of Energy
Office of the Assistant
Secretary for Environment
Washington, DC 20545

J. Snyder
Department of Energy
Office of the Assistant
Secretary for Environment
Washington, DC 20545

R. J. Stern
Department of Energy
Office of the Assistant
Secretary for Environment
Washington, DC 20545

J. Swinebroad
Department of Energy
Office of the Assistant
Secretary for Environment
Washington, DC 20545

A. R. Vincent
Department of Energy
Office of the Assistant
Secretary for Environment
Washington, DC 20545

B. W. Wachholz
Department of Energy
Office of the Assistant
Secretary for Environment
Washington, DC 20545

S. Weinstein
Department of Energy
Office of the Assistant
Secretary for Environment
Washington, DC 20545

W. W. Weyzen
Department of Energy
Office of the Assistant
Secretary for Environment
Washington, DC 20545

J. C. Whitnah
Department of Energy
Office of the Assistant
Secretary for Environment
Washington, DC 20545

T. Williams
Department of Energy
Office of the Assistant
Secretary for Environment
Washington, DC 20545

R. W. Wood
Department of Energy
Office of the Assistant
Secretary for Environment
Washington, DC 20545

C. W. Fischer
Department of Energy
Office of Assistant Secretary
for Energy Information
Administration
Washington, DC 20545

G. C. Facer
Department of Energy
Office of the Assistant
Secretary for Defense
Programs
Washington, DC 20545

C. B. Curtis
Department of Energy
Office of the Assistant
Secretary for Federal
Energy Regulatory
Commission
Washington, DC 20545

T. J. Dobry
Department of Energy
Office of the Assistant
Secretary for Energy
Technology
Washington, DC 20545

F. A. Koomanoff
Department of Energy
Office of the Assistant
Secretary for Energy
Technology
Washington, DC 20545

C. Kuhlman
Department of Energy
Office of the Assistant
Secretary for Energy
Technology
Washington, DC 20545

W. E. Lotz
Department of Energy
Office of the Assistant
Secretary for Energy
Technology
Washington, DC 20545

H. F. Soule
Department of Energy
Office of the Assistant
Secretary for Energy
Technology
Washington, DC 20545

J. M. Deutch
Department of Energy
Office of the Assistant
Secretary for Energy
Research
Washington, DC 20545

J. S. Kane
Department of Energy
Office of the Assistant
Secretary for Energy
Research
Washington, DC 20545

R. L. Butenhoff
Department of Energy
Office of Biomedical and
Environmental Research
Washington, DC 20545

R. P. Blaunstein
Department of Energy
Office of Biomedical and
Environmental Research
Washington, DC 20545

G. Goldstein
Department of Energy
Office of Biomedical and
Environmental Research
Washington, DC 20545

F. Hudson
Department of Energy
Office of Biomedical and
Environmental Research
Washington, DC 20545

D. W. Cole, Jr.
Department of Energy
Office of Biomedical and
Environmental Research
Washington, DC 20545

J. R. Maher
Department of Energy
Office of Technology
Overview
Washington, DC 20545

G. Hagey
Department of Energy
Office of Technology
Overview
Washington, DC 20545

E. J. Vallario
Department of Energy
Office of Safety, Standards
and Compliance
Washington, DC 20545

A. A. Schoen
Department of Energy
Office of Safety, Standards
and Compliance
Washington, DC 20545

F. R. Zintz
Department of Energy
Office of Safety, Standards
and Compliance
Washington, DC 20545

C. I. York
Department of Energy
Office of Safety, Standards
and Compliance
Washington, DC 20545

D. E. Patterson
Department of Energy
Office of Safety, Standards
and Compliance
Washington, DC 20545

E. K. Loop
Department of Energy
Office of Safety, Standards
and Compliance
Washington, DC 20545

M. A. Bell
Department of Energy
Office of Safety, Standards
and Compliance
Washington, DC 20545

J. D. Griffith
Department of Energy
Development and Demonstration
Branch
Washington, DC 20555

E. E. Held
Office of Standards
Development
U. S. Nuclear Regulatory
Commission
Washington, DC 20555

J. O'Toole
Ames Laboratory
Iowa State University
Ames, IA 50010

P. F. Gustafson
Argonne National Laboratory
9700 South Cass Ave.
Argonne, IL 60439

J. Sedlet
Argonne National Laboratory
9700 Cass Ave.
Argonne, IL 60439

C. Jackson
DOE - San Francisco
Operations Office
133 Broadway
Wells Fargo Building
Oakland, CA 94616

C. W. Sill
Department of Energy
Idaho Operations Office
P. O. Box 2108
Idaho Falls, ID 83401

J. H. Spickard
Department of Energy
Idaho Operations
Commission
550 Second Street
Idaho Falls, ID 83401

D. M. Gardiner
Department of Energy
Chicago Operations Office
9800 South Cass Ave.
Argonne, IL 60439

M. E. Gates
Department of Energy
Nevada Operations Office
P. O. Box 14100
Las Vegas, NV 89114

R. Ray
Department of Energy
Nevada Operations Office
P.O. Box 14100
Las Vegas, NV 89114

P. B. Dunnaway
Department of Energy
Nevada Operations Office
P.O. Box 14100
Las Vegas, NV 89114

J. R. Roeder
Department of Energy
Albuquerque Operations Office
P.O. Box 5400
Albuquerque, NM 87115

E. W. Bean
Rocky Flats Area Office
Department of Energy
Albuquerque Operations Office
P.O. Box 928
Golden, CO 80401

J. F. Stevens
Dayton Area Office
Department of Energy
Albuquerque Operations Office
P.O. Box 66
Miamisburg, OH 45342

W. Reese
Department of Energy
Savannah River Operations
Office
P.O. Box A
Aiken, SC 29801

J. A. Lenhard
Department of Energy
Oak Ridge Operations
Office
P.O. Box E
Oak Ridge, TN 37830

J. S. Ball
Bartlesville Energy Technology
Center
Department of Energy
P.O. Box 1398
Bartlesville, OK 74003

G. H. Gronhovd
Grand Forks Energy Technology
Center
Department of Energy
Box 8213, University Station
Grand Forks, ND 58202

A. W. Decora
Laramie Energy Technology Center
Department of Energy
P.O. Box 3395
University Station
Laramie, WY 82071

D. Farrier
Laramie Energy Technology Center
Department of Energy
P.O. Box 3395
University Station
Laramie, WY 82071

A. A. Pitrolo
Morgantown Energy Technology
Center
Department of Energy
P.O. Box 880
Morgantown, WV 26505

H. Jensen
Laramie Energy Research
Center
Department of Energy
P.O. Box 3395
University Station
Laramie, WY 82701

I. Wender
Pittsburgh Energy Technology
Center
Department of Energy
4800 Forbes Avenue
Pittsburgh, PA 15213

B. M. Erickson
Department of Energy
Schenectady Naval
Reactors Office
P.O. Box 1069
Schenectady, NY 12301

NRC Advisory Committee on
Reactor Safeguards
Washington, DC 20555

W. Cool
Nuclear Regulatory Commission
Washington, DC 20545

R. Alexander
Nuclear Regulatory Commission
Washington, DC 20545

J. J. Davis (2)
Assistant Director of Research
Nuclear Regulatory Commission
Washington, DC 20545

D. D. Dominick
Office of Categorical
Programs
Environmental Protection
Agency
Washington, DC 20460

S. M. Greenfield
Environmental Protection
Agency
Washington, DC 20460

D. Smith
Environmental Protection
Agency
Washington, DC 20460

W. A. Mills
Director
Division of Criteria and Standards
Office of Radiation Program
Environmental Protection Agency
Rockville, MD 20852

M. K. Hubbert
Department of the Interior
U.S. Geological Survey
Water Resources Division
Washington, DC 20242

D. N. Breiter
National Bureau of Standards
A121, Building 222
Washington, DC 20234

J. R. DeVoe
National Bureau of Standards
A121, Building 222
Washington, DC 20234

J. W. McCaslin
INEL, Aerojet Nuclear
550 Second Street
Idaho Falls, ID 83401

R. C. Yoder
Rockwell International
P.O. Box 888
Golden, CO 80401

A. R. Boulogne
E. I. DuPont de Nemours
and Company, Aiken
Savannah River Laboratory
Technical Information
Service
Room 773A
Aiken, SC 29801

K. MacMurdo
E. I. DuPont de Nemours
and Company, Aiken
Savannah River Laboratory
Technical Information
Service
Room 773A
Aiken, SC 29801

C. M. Patterson
E.I. DuPont de Nemours
and Company
Savannah River Plant
Aiken, SC 29801

B. C. Rusche
E.I. DuPont de Nemours
and Company, Aiken
Savannah River Laboratory
Technical Information
Service
Room 773A
Aiken, SC 29801

W. B. Scott
E.I. DuPont de Nemours
and Company, Aiken
Savannah River Laboratory
Technical Information
Service
Room 773A
Aiken, SC 29801

Technical Information
Service
Room 773A
Savannah River Laboratory
E.I. DuPont de Nemours
and Company
Aiken, SC 29801

R. J. Beyers
Savannah River Ecology
Laboratory
University of Georgia
Savannah River Plant
P.O. Box A
Aiken, SC 29801

C. L. Karl
National Lead Company
of Ohio
P.O. Box 39158
Cincinnati, OH 45239

V. P. Bond
Brookhaven National
Laboratory
Upton, Long Island, NY 11973

L. P. Hatch
Brookhaven National
Laboratory
Research Library
Reference Section
Information Division
Upton, Long Island, NY 11973

C. B. Meinhold
Brookhaven National
Laboratory
Upton, Long Island, NY 11973

Librarian
Research Library, Reference
Brookhaven National
Laboratory
Upton, Long Island, NY 11973

B. Manowitz
Radiation Division
Brookhaven National
Laboratory
Upton, Long Island, NY 11973

G. M. Woodwell
Brookhaven National
Laboratory
Research Library
Reference Section
Information Division
Upton, Long Island, NY 11973

C. R. Richmond
Oak Ridge National
Laboratory
P.O. Box X
Oak Ridge, TN 37830

S. I. Auerbach
Oak Ridge National
Laboratory
Oak Ridge Operations
Office
P.O. Box X
Oak Ridge, TN 37830

J. A. Auxier
Oak Ridge National
Laboratory
P.O. Box X
Oak Ridge, TN 37830

G. D. O'Kelley
Oak Ridge National
Laboratory
Oak Ridge Operations
Office
P.O. Box X
Oak Ridge, TN 37830

E. G. Struxness
Oak Ridge National
Laboratory
Oak Ridge Operations
Office
P.O. Box X
Oak Ridge, TN 37830

J. E. Turner
Oak Ridge National
Laboratory
Oak Ridge Operations
Office
P.O. Box X
Oak Ridge, TN 37830

W. K. Sinclair
Argonne National
Laboratory
9700 South Cass Ave.
Argonne, IL 60439

E. L. Alpen
Lawrence Berkeley Laboratory
University of California
Building 90, Room 2056
No. 1 Cyclotron Road
Berkeley, CA 94720

R. E. Heft
Lawrence Radiation
Laboratory
University of California
Lawrence Livermore
Laboratory
Technical Information
Department, L-3
P.O. Box 808
Livermore, CA 94550

G. H. Higgins
Lawrence Radiation
Laboratory
University of California
Lawrence Livermore
Laboratory
Technical Information
Department, L-3
P.O. Box 808
Livermore, CA 94550

J. B. Knox
Lawrence Radiation
Laboratory
University of California
Lawrence Livermore
Laboratory
Technical Information
Department, L-3
P.O. Box 808
Livermore, CA 94550

M. L. Mendelsohn
University of California
Lawrence Livermore
Laboratory
P.O. Box 808
Livermore, CA 94550

P. Phelps
Lawrence Radiation
Laboratory
University of California
Lawrence Livermore
Laboratory
Technical Information
Department, L-3
P.O. Box 808
Livermore, CA 94550

Librarian
Lawrence Radiation
Laboratory
University of California
Technical Information
Department, L-3
P.O. Box 808
Livermore, Ca 94550

G. L. Voelz
University of California
Los Alamos Scientific
Laboratory
P.O. Box 1663
Los Alamos, NM 87545

Librarian
Los Alamos Scientific
Laboratory
P.O. Box 1663
Los Alamos, NM 87545

J. W. Healy
Los Alamos Scientific
Laboratory
University of California
P.O. Box 1663
Los Alamos, NM 87545

R. O. McClellan
Inhalation Toxicology
Research Institute
Lovelace Foundation for
Medical Education and
Research
P.O. Box 5890
Albuquerque, NM 87115

K. A. Smith
Sandia Laboratories
P.O. Box 5800
Albuquerque, NM 87115

Librarian
Battelle Memorial Institute
Columbus Laboratories
505 King Avenue
Columbus, OH 43201

E. W. Ungar
Director, Columbus Laboratories
Battelle Memorial Institute
505 King Avenue
Columbus, OH 43201

R. S. Paul
Vice President
Battelle Memorial Institute
Columbus Laboratories
505 King Avenue
Columbus, OH 43201

Librarian, Building 465
Atomic Energy Research
Establishment
Harwell, Didcot
OXON OXII ORD, ENGLAND

H. Daw
Director, Division of
Health, Safety and Waste
Management
International Atomic Energy
Agency
Kärtner Ring 11
P.O. Box 590
A 1011 VIENNA, AUSTRIA

Director, Office of Nuclear
Safety and Environmental
Protection
International Atomic Energy
Agency
Kärtner Ring 11
P.O. Box 590
A 1011 VIENNA, AUSTRIA

J. Z. Minczewski
International Atomic Energy
Agency
Kärtner Ring 11
P.O. Box 590
A 1011 VIENNA, AUSTRIA

David Rall, Director
NIEHS
P.O. Box 12233
Research Triangle
Park, NC 27709

D. Beirman
Chief, Document Service
Branch
Central Intelligence
Agency
Attn: CRS/DPSD/DSB/IAS/
409779/DB
Washington, DC 20505

Council on Environmental
Quality
72 Jackson Place, N.W.
Washington, DC 20006

A. Barbreau
Centre d'Etudes
Nucléaires de Saclay
P.O. Box 2, Saclay
Gif-sur-Yvette
(S & O)
FRANCE

F. Duhamel
Centre d'Etudes
Nucléaires de Saclay
P.O. Box 2, Saclay
Gif-sur-Yvette
(S & O)
FRANCE

Librarian
Centre d'Etudes
Nucléaires de Saclay
P.O. Box 2, Saclay
Gif-sur-Yvette
(S & O)
FRANCE

P. Slizewicz
Centre d'Etudes
Nucléaires de Saclay
P.O. Box 2, Saclay
Gif-sur-Yvette
(S & O)
FRANCE

A. M. Menoux
Commissariat à l'Energie
Atomique
Centre d'Etudes
Nucléaires Fontenay-aux-
Roses,
BP n°, 6-9226 Fontenay-aux-
Roses,
FRANCE

M Rzekiecki
Commissariat à l'Energie
Atomique
Centre d'Etudes
Nucléaires de Cadarache
BP n°, 3-St. Paul
Les Durance
FRANCE

Director
Comissariat à l 'Energie
Atomique
Center d'Etudes
Nucléaires de Fontenay-aux-
Roses (Seine)
FRANCE

Librarian
Commonwealth Scientific and Industrial Research Organization
314 Albert Street
P.O. Box 89
East Melbourne, Victoria
AUSTRALIA

Director
Commonwealth Scientific and Industrial Research Organization,
Aspendal, Victoria
AUSTRALIA

B. B. Hicks
Commonwealth Scientific and Industrial Research Organization
Aspendal, Victoria
AUSTRALIA

E. Wallauschek
ENEA (OECD) Health and Safety Office
38, Blvd. Suchet
Paris IVI,
FRANCE

M. Saiki
National Institute of Radiological Sciences
Environmental Hygiene Division
4-9-1, Anagawa
Chiba-shi
JAPAN

M. Suzuki
National Institute of Radiological Sciences
Environmental Hygiene Division
4-9-1, Anagawa
Chiba-shi
JAPAN

Director
National Institute of Radiological Sciences
4-9-1, Anagawa
Chiba-shi
JAPAN

Librarian
Australian AEC
Riverina Laboratory
P.O. Box 226
Deniliquin
New South Wales
AUSTRALIA 2710

A. M. Marko
Director
Atomic Energy of Canada Ltd.
Biology and Health Physics Division
Chalk River Nuclear Laboratories
Chalk River, Ontario
KOJ IJO
CANADA

C. A. Mawson
Atomic Energy of Canada Ltd.
Chalk River, Ontario
CANADA

I. Ophel
Atomic Energy of Canada Ltd.
Chalk River, Ontario
CANADA

F. D. Sowby
International Commission on Radiological Protection
Clifton Avenue
Sutton, Surrey
ENGLAND

W. R. Ney
Executive Director
National Council on Radiation Protection and Measurements
7910 Woodmont Ave.
Suite 1061
Washington, DC 20014

L. Bustad, Dean
College of Veterinary Medicine
Washington State University
Pullman, WA 99163

R. H. Filby
Director
Nuclear Radiation Center
Washington State University
Pullman, WA 99163

G. W. Dolphin
National Radiological Protection Board
Harwell, Didcot
Oxfordshire OXII ORQ
ENGLAND

A. K. Ganguly
Atomic Energy Establishment
Trombay, Bombay 73
INDIA

Librarian
Atomic Energy Research Establishment
Harwell, Berks.
ENGLAND

A. W. R. Wilson
Australian AEC
Post Office Coogee
New South Wales
AUSTRALIA

D. J. Benison
Comision Nacional de Energia Atomica
Buenos Aires
ARGENTINA

E. Vander Elst
Comision Nacional de Energia Atomica
Buenos Aires
ARGENTINA

V. R. Thayer
E.I. DuPont de Nemours and Company
Polymer Intermediate Department
Department of Energy
Wilmington, DE 19898

Librarian
Eurochemic Library
B 2400
MOL
BELGIUM

W. B. Heroy
Geotechnical Corporation
Box 28277
Dallas, TX 75228

H. Krause
Gelleschaft für Kernforschung mbH
Postfach 3640
D-7500 Kärlsruhe
WEST GERMANY

Librarian (5)
Ministry of Agriculture Fisheries and Food
Laboratory
Lowestoft, Suffolk
ENGLAND

J. J. Rasmussen
Montana Energy Research Center
P.O. Box 3809
Butte, MT 59701

M. Haworth
Montana Power
(Colstrip)
P.O. Box 419
Colstrip, MT 59323

Library
Ontario Hydro
620 University Ave.
Toronto, Ontario
CANADA

A. G. Sharkey
Pittsburgh Energy Research
Center
4800 Forbes Ave.
Pittsburgh, PA 15213

E. D. Goldberg
Scripps Institute of
Oceanography
University of California
La Jolla, CA 92093

D. Lal
Scripps Institute of
Oceanography
University of California
La Jolla, CA 92093

Librarian
World Meteorological
Organization
Geneva
SWITZERLAND

J. R. Arnold
Chemistry Department
University of California
San Diego
La Jolla, CA 92037

W. Broecker
Lamont Geological
Observatory
Columbia University
Palisades, NY 10964

Education and Information
Section
Health Physics Division
Oak Ridge National
Laboratory
Oak Ridge, TN 37830

M. C. Gaske
Assistant to Executive
Secretary
Advisory Committee on
Reactor Safeguards
U.S. Nuclear Regulatory
Commission
Washington, DC 20555

C. Gordon
Department of Botany
University of Montana
Missoula, MT 59801

N. Harley
New York University
Medical Center
550 First Ave.
New York, NY 10016

D. P. Kharkar
LFE Corporation
Environmental Analysis
Laboratories
2030 Wright Ave.
Richmond, CA 94804

H. W. Kirby
Monsanto Research
Corporation
Mound Laboratory
Miamisburg, OH 45342

P. K. Kuroda
Department of Chemistry
University of Arkansas
Fayetteville, AR 72701

P. LaFluer
Nuclear Reactor Laboratory
National Bureau of Standards
Gaithersburg, MD 20760

D. G. McCauley
Code 304, Michelson Lab.
Department of the Navy
Naval Weapons Center
China Lake, CA 93555

C. Menninga
Physics Department
Calvin College
1331 Franklin St. S.E.
Grand Rapids, MI 49506

D. Montgomery
Environmental Protection
Agency
26 W. St. Clair St
Cincinnati, OH 45219

A. Seymour
Laboratory of Radiation
Ecology
University of Washington
College of Fisheries
Seattle, WA 98105

W. Singlevich
Air Force Technical
Applications Center/TD-4
Patrick AFB, FL 32925

C. V. Theis
U.S. Geological Survey
P.O. Box 436
Albuquerque, NM 87106

D. Uhl
Nuclear Engineering and
Operations Department
Electric Power Research
Institute
3412 Hillview Ave.
P.O. Box 10412
Palo Alto, CA 94303

J. C. Dalton
U.K. Atomic Energy
Authority
Windscale Works, P.G.
Sellafield, Seascale,
Cumberland
ENGLAND

K. Edvarson
Forsvarets Forskningsanstalt
Res. Institute of National
Defence
Avdelning 4,
Stockholm 80
SWEDEN

F. Girardi
C.C.R. EURATOM-ISPRA
(VERESE)
ITALY

S. Jackson
U.K. Atomic Energy
Authority
Harwell, Didcot
Berkshire
ENGLAND

A. Malvicini
Chief, Protection Service
C.C.R. EURATOM-ISPRA
(VERESE)
ITALY

D. P. Meyerhoff
Environmental Radioactivity
Section
Nuclear Safety Division
Radiation Protection Bureau
Brookfield Road
Ottawa, Ontario
K1A1C1
CANADA

DOE Technical Information
Center (27)

J. K. Miettinen
University of Helsinki
Department of
Radiochemistry
Unionkatu 35, Helsinki
FINLAND

R. V. Osborne
Atomic Energy of
Canada, Ltd.
Chalk River, Ontario
CANADA

D. H. Peirson
AERE (Atomic Energy
Research Establishment)
Health Physics and
Medical Division
B. 364
Harwell, Didcot, Berkshire
ENGLAND

ONSITE

DOE Richland Operations Office (8)

R. E. Austin
P. F. Dunigan
J. L. Landon
H. E. Ransom
P. R. Rhodes
F. R. Standerfer
M. W. Tiernan
J. D. White

Joint Center for Graduate Study (2)

Director
Librarian

Hanford Environmental Health Foundation (4)

Medical Library (2)
B. D. Breitenstein
P. A. Fuqua

Pacific Northwest Laboratory (138)

T. W. Ambrose
W. J. Bair (20)
N. E. Ballou
J. S. Burlison
N. E. Carter
D. B. Cearlock
J. R. Corley
J. M. Davidson
H. Drucker
C. E. Elderkin
S. J. Farmer
W. D. Felix (15)
J. W. Finnigan
R. F. Foster
J. C. Fox (5)
J. J. Fuquay
C. I. Gibson
W. A. Glass (10)
A. J. Haverfield (5)
D. L. Hessel
R. L. Hooper
V. G. Horstman
L. J. Kirby

Pacific Northwest Laboratory (contd)

H. V. Larson
R. C. Liikala
S. Marks
R. P. Marshall
I. C. Nelson (5)
J. M. Nielsen (10)
R. E. Nightingale
D. E. Olesen
J. F. Park
R. W. Perkins (5)
L. A. Rancitelli (15)
W. D. Richmond
C. L. Simpson
W. H. Swift
W. L. Templeton
C. M. Unruh
B. E. Vaughan
W. R. Wiley
Biology Library (2)
Technical Information (5)
Publishing Coordination (2)

Battelle Seattle (5)

G. W. Duncan
J. Hebert
S. Nealey
J. O'Toole
J. E. Rasmussen